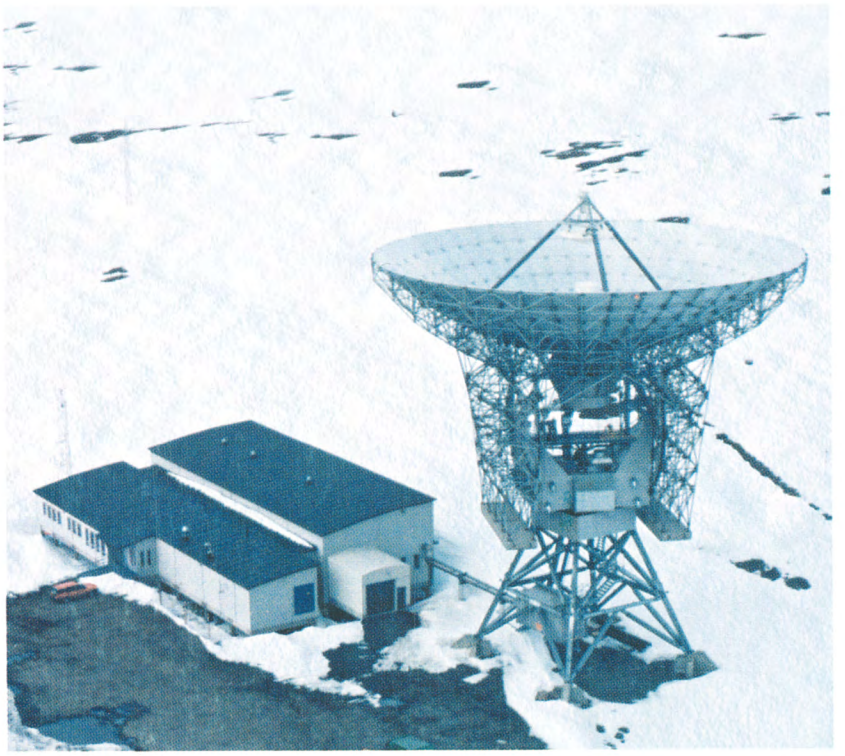

EISCAT

EUROPEAN INCOHERENT SCATTER SCIENTIFIC ASSOCIATION

ANNUAL REPORT 1994 – 1995

S-981 28 KIRUNA, SWEDEN

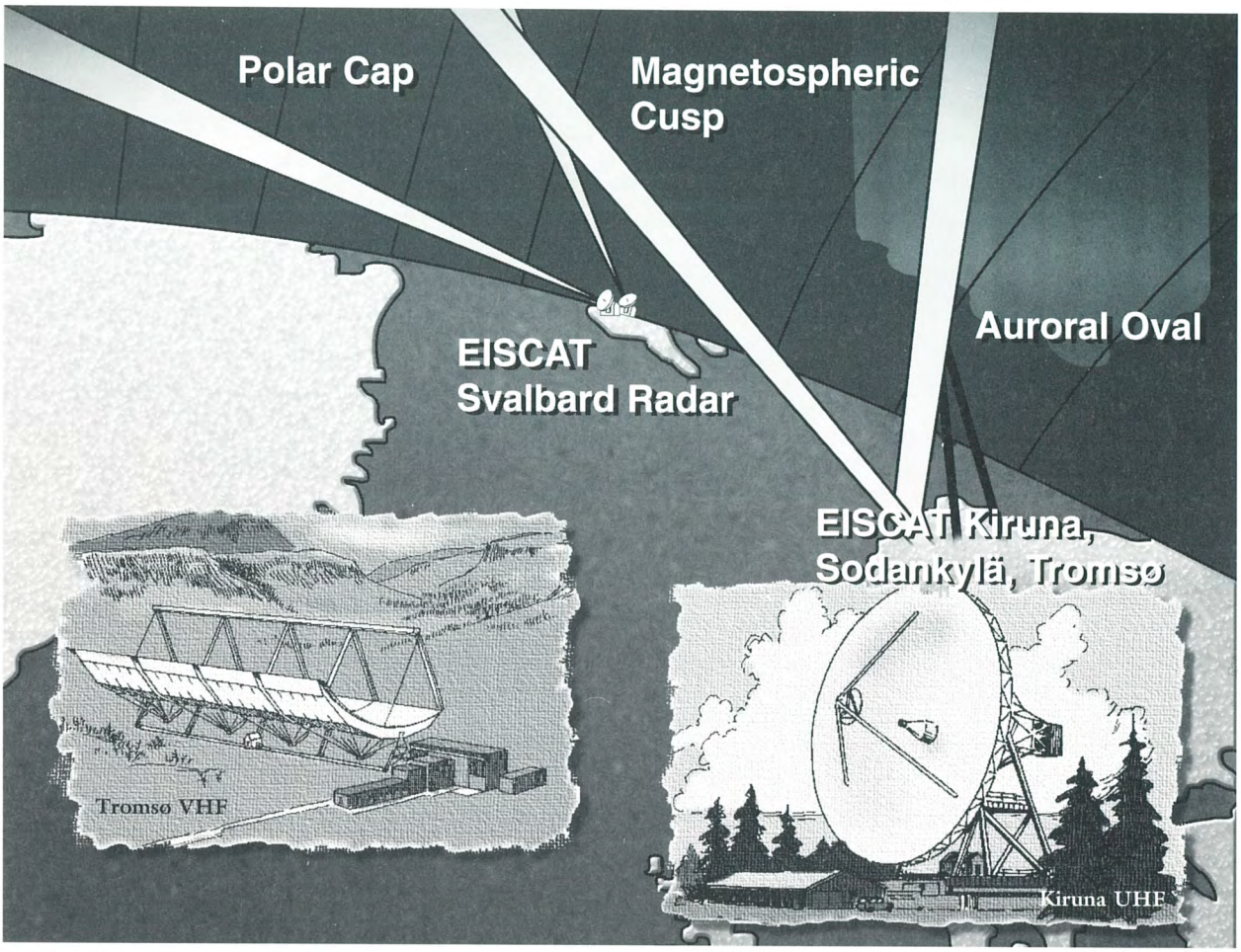

EISCAT Radar Systems

Location		Tromsø	Kiruna	Sodankylä	Longyearbyen
Geograph. coordinates		69°35°N 19°14°E	67°52°N 20°26°E	67°22°N 26°38°E	78°09°N 16°03°E
Geomagn. inclination		77°30°N	76°48°N	76°43°N	82°06°N
Invariant latitude		66°12°N	64°27°N	63°34°N	75°18°N
Band	VHF	UHF	UHF	UHF	UHF
Frequency (MHz)	224	931	931	931	500
Max. bandwidth (MHz)	3	8	8	8	10
Transmitter	2 klystr	1 klystr	-	-	8 klystr
Channels	8	8	8	8	6
Peak power (MW)	2x1.5	1.5	-	-	0,5
Average power (MW)	2x0.15	0.15	-	-	0.125
Pulse duration (msec)	.001-2.0	.001-1.0	-	-	<.001-2.0
Phase coding	binary	binary	binary	binary	binary
Min. interpulse (msec)	1.0	1.0	-	-	0.1
Receiver	analog	analog	analog	analog	anal.-digit
System temperature (K)	250-350	90-110	30-35	30-35	80-85
Digital processing	8bit ADC	32 bit complex	autocorrelation functions, parallel channels		12bit ADC lag profiles 32 bit complex
Antenna	4 parab.cylinders	parab.dish	parab.dish	parababol dish	parabol dish
Feed system	line feed 128 crossed dipoles	Cassegrain	Cassegrain	Cassegrain	Cassegrain optim Potterhorn
Gain (dBi)	46	48	48	48	42.5
Polarization	circular	circular	any	any	circular
System figure of merit ($MW\ m^2\ K^{-1}$)	30	8	-	-	3

EISCAT Heating Facility in Tromsø

Frequency range: 4-8 MHz, Maximum transmitter power: 12 x 0.1 MW, Antennas: two arrays (4-8 MHz): 24 dBi, one array (5.4-8 MHz): 30 dBi. Additionally a Dynasonde is operated at the Heating facility.

ANNUAL REPORT 1994-1995

EISCAT, the European Incoherent Scatter Scientific Association, is established to conduct research on the lower, middle and upper atmosphere and ionosphere using the incoherent scatter radar technique. This technique is the most powerful ground-based tool for these research applications. EISCAT is also being used as a coherent scatter radar for studying instabilities in the ionosphere, as well as for investigating the structure and dynamics of the middle atmosphere and as a diagnostic instrument in ionospheric modification experiments with the Heating facility.

There are eight incoherent scatter radars in the world, and EISCAT operates three of the highest-standard facilities. The experimental sites of EISCAT are located in the Scandinavian sector, north of the Arctic circle. They consist of two independent radar systems on the mainland, together with a new radar constructed on the island of Spitzbergen in the Svalbard archipelago - the EISCAT Svalbard Radar. Scandinavia (see schematic and operating parameters on the inside of the front cover).

The EISCAT UHF radar operates in the 931 MHz band with a peak transmitter power of 1.5 MW and 32 m, fully steerable parabolic dish antennas. The transmitter and one receiver are in Tromsø (Norway). Receiving sites are also located near Kiruna (Sweden) and Sodankylä (Finland), allowing continuous tristatic measurements to be made.

The monostatic VHF radar in Tromsø operates in the 224 MHz band with a peak transmitter power of 2 x 1.5 MW and a 120 m x 40 m parabolic cylinder antenna, which is subdivided into four sectors. It can be steered mechanically in the meridional plane from vertical to 60° north of the zenith; limited east-west steering is also possible using alternative phasing cables.

The EISCAT Svalbard radar (ESR), located near Longyearbyen, operates in the 500 MHz band with a peak transmitter power of 0.5 MW (modular design allows this to be raised in future) and a fully steerable parabolic dish antenna of 32 m diameter (another antenna is being added). The high latitude location of this facility is particularly aimed at studies of the cusp and polar cap region.

The basic data measured with the incoherent scatter radar technique are profiles of electron density, electron and ion temperature and ion velocity. Subsequent processing allows a wealth of further parameters, describing the ionosphere and neutral atmosphere, to be derived. A selection of well-designed radar pulse schemes are available to adapt the data-taking routines to many particular phenomena, occurring at altitudes between about 5 km and more than 2000 km. Depending on geophysical conditions, a best time resolution of less than one second and an altitude resolution of a few hundred meters can be achieved.

Operations of approximately 1500 hours each year are distributed equally between Common Programmes (CP) and Special Programmes (SP). At present, six well-defined Common Programmes are run regularly, for between one and three days, typically about once per month, to provide a data base for long term synoptic studies. A large number of Special Programmes, defined individually by Associate scientists, are run to support national and international studies of both specific and global geophysical phenomena.

The Annual Reports present a summary of EISCAT's operations, developments, scientific results, publications, budget and Council and committee structure for each year. Further details of the EISCAT system and operation can be found in various EISCAT reports, including illustrated brochures, which can be obtained from EISCAT Headquarters in Kiruna, Sweden.

The investments and operational costs of EISCAT are shared between:

Suomen Akatemia, Finland
Centre National de la Recherche Scientifique, France
Max-Planck-Gesellschaft, Federal Republic of Germany
Norges forskningsråd, Norway
Naturvetenskapliga forskningsrådet, Sweden
Particle Physics and Astronomy Research Council, United Kingdom
[on 1 April, 1996, Japan (National Institute of Polar Research)
became a member of the EISCAT Scientific Association]

EISCAT ANNUAL REPORT 1994-1995

CONTENTS

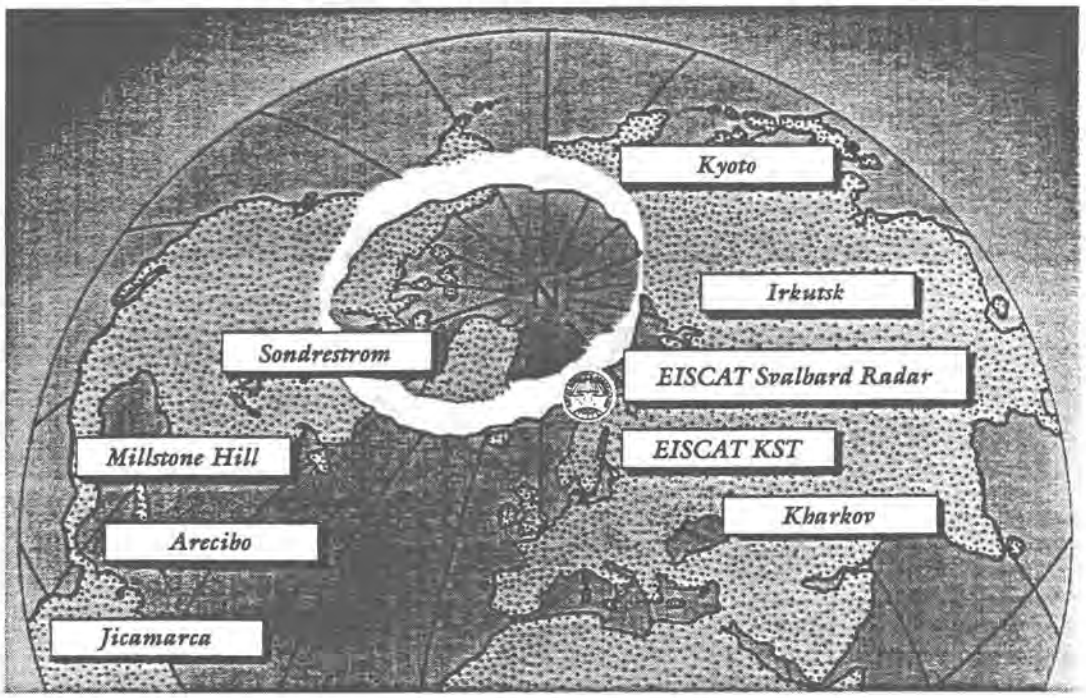

There are several radar facilities using the incoherent scatter technique for studies of the ionosphere and upper atmosphere. Three of these are located close to or in the auroral oval. Two of these are the EISCAT facilities on the northern Scandinavian mainland in Kiruna, Sodankylä and Tromsø (the **KST** system) and the EISCAT Svalbard Radar (**ESR**).

The EISCAT Scientific Association was founded by six European research councils when signing the EISCAT Agreement in December 1975.

At the end of the period covered by this Annual Report, on 31 December 1995, the EISCAT Scientific Association passed its 20th anniversary, looking back on 25000 experiment hours within 15 years of operation and almost 600 publications in scientific journals, and looking ahead to operate the ESR, which concluded its main construction period at the end of 1995.

It was also decided at the end of 1995 that Japan will join as the seventh member of the EISCAT Scientific Association in the beginning of 1996.

Council Chairmen's Page

As this report is a biennial one which straddles the terms of two chairmen, the chairman's page is jointly written by the past and the present chairs.

The 1994/1995 period was a very busy one for the EISCAT organization. The construction and installation of the EISCAT Svalbard radar was progressing with amazing speed, and the deadlines were held quite faithfully. In spite of the load on the staff caused by the heavy involvement with the construction of the Svalbard radar system, the "old" EISCAT facilities were kept running, and an active research programme successfully maintained. At the end of the period it was quite clear that the Svalbard radar would be operational during 1996, and ready for the planned cooperation with the Cluster mission, which, it turned out, tragically failed.

The organization has been blessed with a stable staff for a number of years, and a high level of skill and know-how has been built up. The problems which arose as a result of the decision by the Research Council of Norway to relinquish the employer responsibility for the Tromsø personnel and transfer the staff to another organization caused some unfortunate turbulence. By the end of 1995 a transfer of the local staff to the University of Tromsø was agreed, bringing it into the same relation with the local host as the staffs in Kiruna and Sodankylä. The details of this staff transfer were worked out during the first half of 1996. With this accomplished we believe that the competent and dedicated staff can be kept intact and the high level of professional competence retained.

The revision of the EISCAT Agreement, Statutes and Financial rules, essentially to include the Svalbard radar operation, had been finished and the documents were signed by the Associates in the period covered by this report.

For some time there has been an interest in Japan, particularly at the University of Nagoya, to start incoherent scatter observations on Svalbard, where Japanese scientists have conducted upper atmosphere and ionosphere studies for some time. During the 1994/1995 period it was decided by the Japanese that their scientific aims were best served by joining EISCAT, contributing to the organization a second antenna, which would allow dual beam operation which enhances the ability to observe dynamic phenomena and measure ionospheric motion with high time resolution.

In preparation for joining EISCAT, a joint Japanese EISCAT Symposium was arranged in Toba, Japan, at the end of August, 1994. This symposium was attended by some 60 scientists, 15 of whom came from EISCAT countries. Selected papers from this symposium were published in the Journal of Geomagnetism and Geoelectricity, and all the published papers were collected into a single volume under the title "Structure and Dynamics of the Polar Ionosphere". This volume represents a significant contribution to the field, and will receive wide distribution.

The Japanese, represented by the National Institute of Polar Research, became full members of EISCAT from 1996 on. The original members of EISCAT now look forward to the cooperation and exchange of ideas with the scientists from the new member country. There is little doubt that the infusion of resources and ideas which goes with the expanded membership will have an invigorating effect on the organization.

The plans for the new antenna at Svalbard are being developed, investigations are under way to double the transmitter power in Svalbard, a number of coordinated experiments with both ground and space-borne experiments are either under way or in the planning stages. The number of users and their publication rate are high, and the promise for significant contributions to the field of ionosphere-magnetosphere research in the next few years is excellent. The director and his staff are highly recommended for their effort in providing the ground work for this promising future.

Professor Asgeir Brekke
Chairman 1993-1994

Professor Tor Hagfors
Chairman 1995-1996

Director's Summary of Highlights during the Years 1994 and 1995

Since the EISCAT Svalbard Radar construction project had overrun the resources of EISCAT staff during the recent years, it had to be decided to combine the annual reports 1994 and 1995 into a biennial report. The projected milestone of the first test operation of the EISCAT Svalbard Radar (ESR) had been achieved as planned very close to the end of 1995. It is therefore justified to devote a special section of this biennial report to a description of the ESR project development. It follows on pages 19 to 39 after this summary of some highlights of the general EISCAT operations development.

The operations of the EISCAT systems, which include the Radar and the Heating facilities, was without major interruptions, except at the end of 1994 due to transmitter problems. The accounted operating hours are shown in the adjacent table and the following graph. Due to dual Radar and Heating operation, the real operating time is larger than the accounted time.

Common Programmes CP

	1994	**1995**
CP-1	61	135
CP-2	74	55
CP-3	111	92
CP-4	111	106
CP-6	112	141
CP-7	149	136
Total:	**618**	**665**

Special Programmes SP

	1994	**1995**
Finland	27	43
France	123	162
Germany	90	175
Norway	56	84
Sweden	39	87
United Kingdom	241	275
EISCAT	38	38
Third Party	-	20
Total:	**614**	**884**

A detailed break-up of the EISCAT operations is given on pages 41-44 of this biennial report.

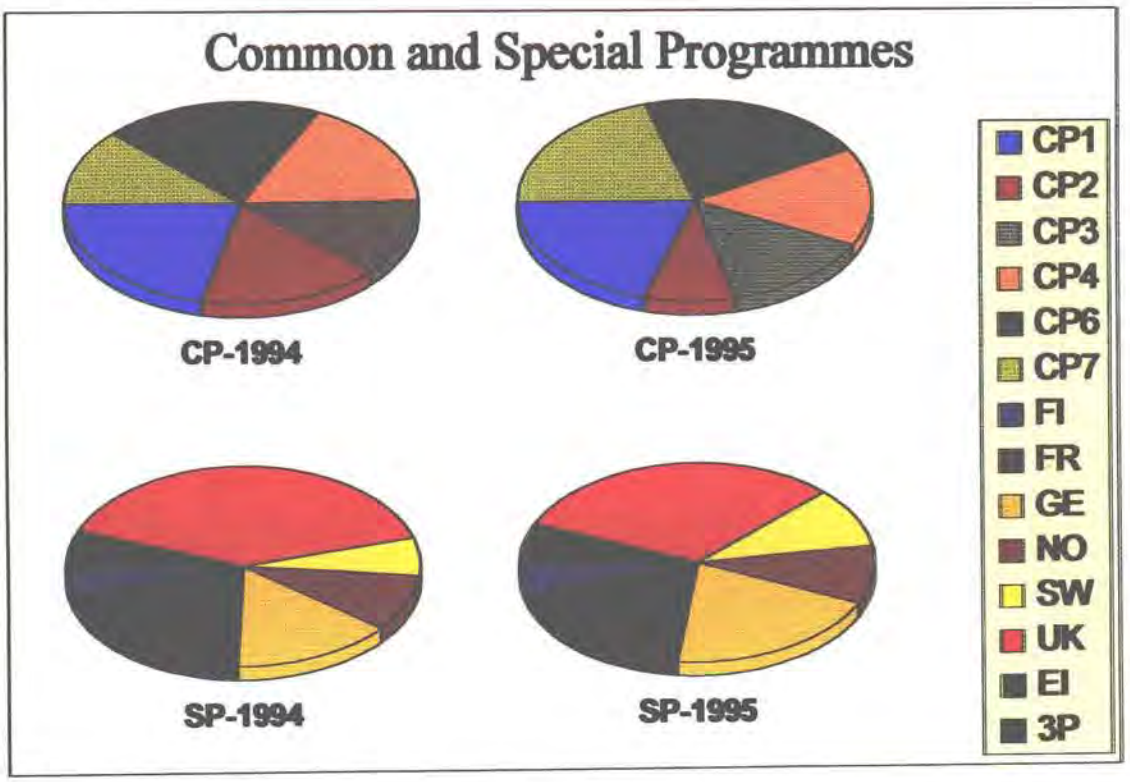

Operations were partially interrupted for shorter periods. One such event occurred when the sub-reflector of the Tromsø UHF antenna had to be repaired, since part of its surface was destroyed. Similar problems were not observed at the receiving sites Kiruna and Sodankylä and it is assumed that the high power density during transmission was the cause of these surface perforations. The subreflector had to be removed from the antenna (see photo) and was repaired by the site staff.

In early January 1994, the refurbished UHF klystron was delivered to the Tromsø site, where it yielded a peak power of 1.8 MW during tests. That brought the number of UHF klystrons at the site back to two. It turned out, however, that the corresponding high voltage to operate the new klystron at this high power was in excess of 92 kV, which could not be handled reliably by all the modulator tubes. Thus, a careful selection of the tubes in the UHF and VHF transmitter modulator needed to be undertaken. A stable UHF transmitter operation at 1.2-1.5 MW could be achieved this way. It is to be noted, however, that a modulator redesign or a completely new design will become necessary in future, since the present tubes are no longer on the market and cannot be refurbished too many times. Although the number of disruptions to UHF operations was relatively small, the critical modulator stability caused most of these, such as the one at the end of 1994. In October 1995, the filament of the refurbished UHF klystron broke and it had to be returned for warranty repair to the supplier, leaving EISCAT with only one UHF klystron for another period of eight months. Since this break was not a result of the operation by EISCAT a reduced pro-rata warranty payment was negotiated with the supplier. The high-voltage switch gear, interlocks, monitors and other parts of the transmitter systems had to be rebuilt, adjusted or improved.

The regular quadri-annual bolt tightening of the UHF antennas took place at all sites in 1995. Events which caused shorter, but not critical, UHF operation interruptions were the repairs of an elevation motor, rail undercast, pintle bearing, fixing of leakages in the foundation roof, and elevation rotary joint restoration.

The VHF transmitter operation was relatively stable, despite some sporadic failures of transmitter and antenna, and some defocusing problems in one of the VHF klystrons. Usually the VHF operation was reliable at 2 x 1.2-1.4 MW power.

The Heating facility experienced no critical interruptions. The usual overhaul of the antenna system after the winter season was performed without major problems. The Dynasonde, operated at the Heating facility, provided regular ionograms during many CP and SP experiments. Dynasonde records are also used for checks of the radar calibration.

Some interference problems continue to occur on 931 MHz in Kiruna and 224 MHz in Tromsø. Occasional reports from neighbours of the Tromsø site on interference to their home equipment or telephones were, as usual, properly dealt with. We are now, however, particularly concerned about the tests and introduction of digital audio broadcasting in the frequency band used by the EISCAT VHF radar.

In Sodankylä the compressor for the cryogenic cooling of the UHF pre-amplifier had to be replaced. Extensive tests of the time and frequency standards using the Cesium tube and GPS (Global Positioning System using satellites) synchronized instrumentation proved that we can replace the Cesium devices, which are inevitably aging, by GPS-receivers. A comparison is shown in the graph, which proves that the relative deviations between these two systems are within $\pm\ 1{\cdot}10^{-11}$. Upgrading to these GPS systems is now being implemented at all sites.

Communications on scheduling, system status and the annual operation planning has been improved and is also available in the Tromsö WWW homepage http://seldon.eiscat.no/.

The operation of the EISCAT sites Kiruna, Sodankylä and Tromsø (KST) was developed further by connecting the SUN Sparc computers to the radar system and ND computers. All sites and Headquarters are internally linked via local area networks and also to the Internet, which has significantly increased the internal and external contacts.

Major progress to optimize costs was achieved by replacing the inter-site communication, which was through leased lines, by connections via the Internet. Common programme analysis was performed regularly on-line (see summary on pages 41-42), and SUN workstations are used in addition to the aging ND computers. Analysed data of international World-Day operations are as usual supplied to the NCAR data base and are also accessible as color plots on the World Wide Web.

The data tape archiving at Headquarters has been continuously revised to copy all data existing on the old 6250 bpi tapes onto Exabyte for reduced storage space. Information on the data archive of SP, CP and UP data are available on the EISCAT Headquarters WWW homepage http://snowflake.irf.se/.

GPS to Cesium comparison September / October 1993
Units * E-11

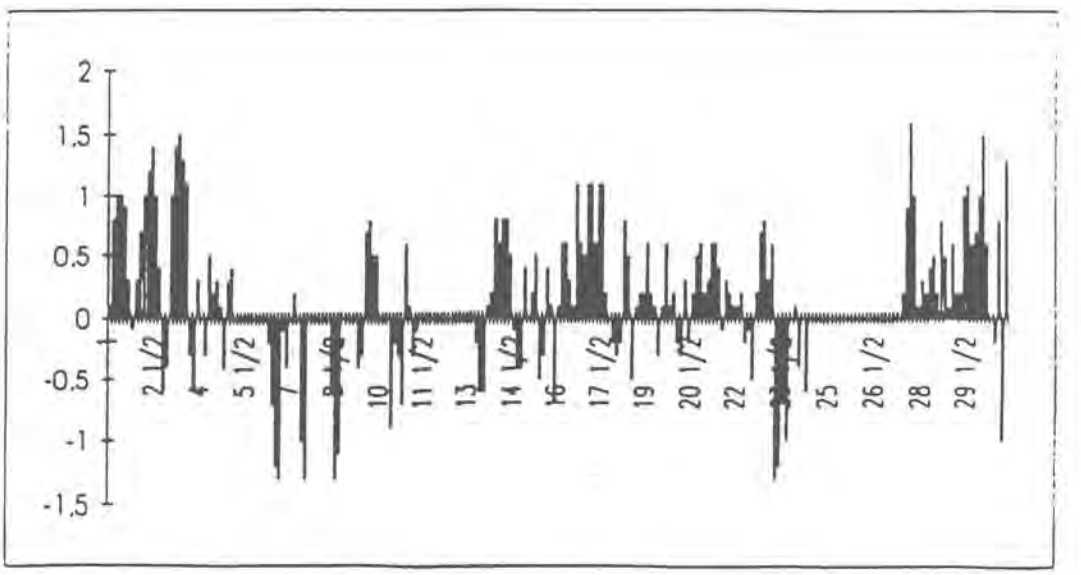

AGREEMENT

between

Centre National de la Recherche Scientifique *(France)*,
Max-Planck-Gesellschaft *(Germany)*,
Naturvetenskapliga forskningsrådet *(Sweden)*,
Norges forskningsråd *(Norway)*,
Particle Physics and Astronomy Research Council
(United Kingdom of Great Britain and Northern Ireland),
Suomen Akatemia *(Finland)*

concerning the development and operation of radar facilities at high latitudes, called EISCAT.

Taking into account the development of atmospheric, ionospheric and magnetospheric research and the quality and range of the work carried out in universities and specialized research centres,

Having regard to the necessity of possessing facilities at the highest standard meeting the requirements of research workers in this field,

Having regard to the basic scientific value of the study of high latitude regions and the considerable possibilities of radar techniques for studies of the atmosphere and ionosphere,

Having regard to the specially favourable geographical position of the countries of Northern Europe, and the existence in these countries of observatories suitable for studies of solar-terrestrial physics,

Having regard to the value of international cooperation when large scale facilities are needed for scientific use,

The Centre National de la Recherche Scientifique of France, the Max-Planck-Gesellschaft of the Federal Republic of Germany, the Naturvetenskapliga forskningsrådet of Sweden, the Norges forskningsråd of Norway, the Particle Physics and Astronomy Research Council of the United Kingdom of Great Britain and Northern Ireland, and the Suomen Akatemia of Finland have reached agreement on the following provisions:

The Centre National de la Recherche Scientifique, the Max-Planck-Gesellschaft, the Naturvetenskapliga forskningsrådet, the Norges forskningsråd, the Particle Physics and Astronomy Research Council, and the Suomen Akatemia have established an educational and scientific association with the view to the development and operation of radar facilities in high latitudes, comprising so far a system of stations at Tromsö (Norway), Kiruna (Sweden), Sodankylä (Finland), and Longyearbyen (Svalbard), called the "EISCAT Scientific Association".

At its 45th Meeting of the EISCAT Council in Paris, France, on 28/29 November 1995 the EISCAT Associates agreed unanimously that* Japan, represented by the National Institute of Polar Research, *joins the EISCAT Scientific Association as full member on 1 April 1996.

At the 42nd meeting of the EISCAT Council in Copenhagen on 19-20 May, 1994, the unceasing services of the Assistant to the Director, Mrs. Gurli Hultqvist, were honoured before her retirement in the autumn of that year. The photo shows (l.t.r.) Prof. T. Hagfors, Prof. B. Hultqvist, Mrs. G. Hultqvist, Prof. A. Brekke, Dr. J. Röttger and Mr. M. Meinecke.

During the same Council meeting Prof. Bengt Hultqvist was elected an Honorary Member of EISCAT in recognition of his long and distinguished contributions to the EISCAT Scientific Association. He was handed a booklet with photographs showing the development of the EISCAT systems and in particular the EISCAT Svalbard Radar. At the same meeting the Council approved final adjustments of the Agreement and Statutes of the Association, which had been revised during recent years to allow for the inclusion of the EISCAT Svalbard Radar into the EISCAT operation. A new calculus had to be developed to determine the percentage observing time per Associate. This is included in the new Agreement, The Agreement and Statutes were approved at the 43rd Council meeting, 28-29 Nov. 1994 in Windsor, and an English and French version was signed by the Associates' research councils in 1995 to become effective on 1 January 1996. Also the EISCAT Financial Rules and the Rules for Scientific Programs and Use of Data were revised accordingly.

The participants of the Japan-EISCAT Symposium on the Polar Ionosphere, JESPI, in Toba, Ise-Shima, Japan, 31 Aug. - 3 Sept. 1994.

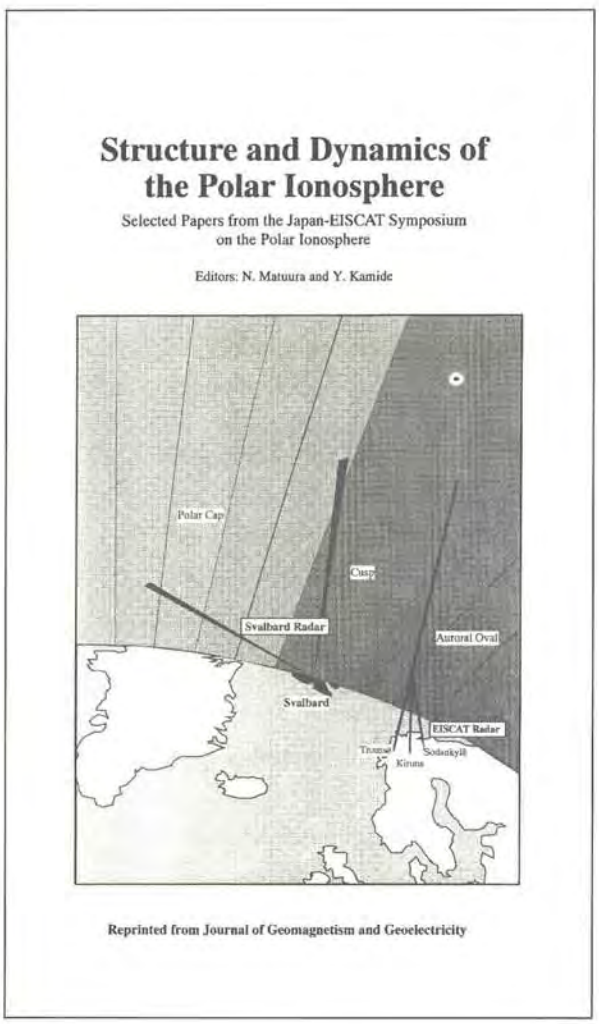

The Solar Terrestrial Environment Laboratory (STEL) of Nagoya University in Japan and EISCAT arranged the JESPI symposium in order to encourage further collaboration between scientists in Japan and the EISCAT Associates. About one quarter of the 60 participants were from Europe. Besides some 60 presented papers and a dedicated panel discussion, a resolution was adopted determining the basis for Japan to become a full Associate of EISCAT by providing funds for a second antenna of the EISCAT Svalbard Radar. Selected papers of JESPI were published in 1995 in a special issue of the Journal of Geomagnetism and Geoelectricity, and are reprinted in an exclusive booklet (see cover on left).

In 1994, delegations from Japan visited the EISCAT sites and the EISCAT Svalbard Radar, and detailed consultations were held between the delegation members and the EISCAT executives to explain the EISCAT structure and administration.

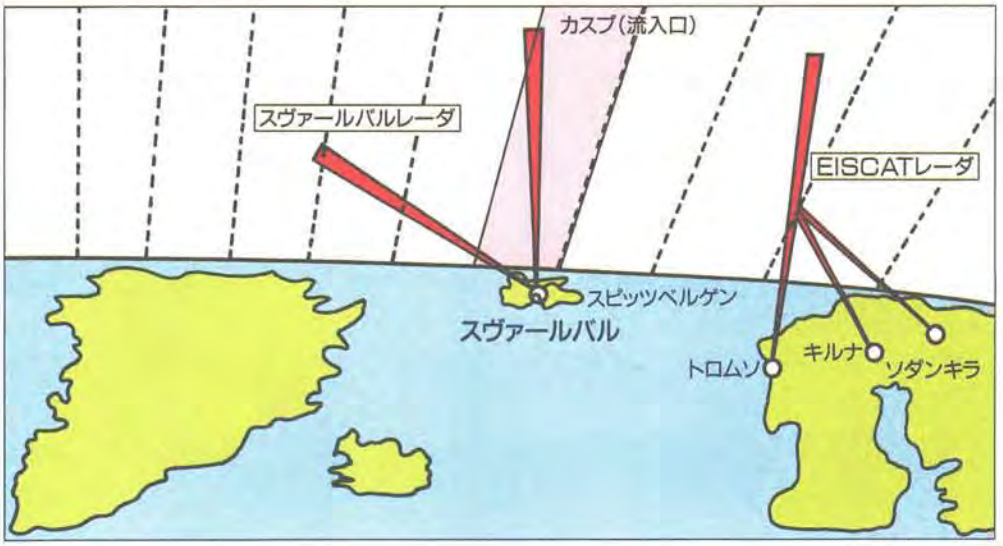

EISCAT(欧州ISレーダ)科学協会

欧州6か国の研究機関は北欧に設置するISレーダを用いて高緯度高層大気圏の研究を行うためEISCAT (European Incoherent Scatter Radar)科学協会を1975年に設立した。

Great efforts were undertaken in Japan to promote the proposal for funding support for the ESR. The upper figure is from one of the brochures published for this purpose by STEL in Japan. In May 1995, funds were released by the Japanese ministry Monbusho, followed immediately by further executive meetings of EISCAT, the National Institute of Polar Research of Japan (NIPR) and STEL, leading to the EISCAT Council approving the signature of a Memorandum of Understanding after the 44th EISCAT Council meeting on 23 May 1995. The centre photo shows delegates of Council, Japan and EISCAT executives before signing the memorandum.

Plans for the provision of an additional antenna were discussed with the Japanese counterparts. Further communications between the EISCAT executive and the NIPR administration were necessary to analyze the situation after the funding approval to secure consistency of the Japanese administrative requirements and the Agreement, Statutes and Financial Rules of EISCAT. Additional extensive communications and another meeting at the NIPR in Tokyo were required. The photo on the bottom of the preceding page shows the participants of this meeting on 10-12 August 1995. The EISCAT Associates, which had been regularly informed about the negotiations, finally came to an agreement on the arrangements and in Paris, on 27-28 November 1995, decided that Japan would become the seventh full member of the EISCAT Scientific Association. Further administrative actions had to be executed thereafter before the admission date of 1 April 1996. On joining EISCAT the NIPR paid 42 million SEK for an ESR antenna and assured 7% contribution to the total annual operating budget of EISCAT.

During the same period, when the negotiations with NIPR were in steady progress, the 7th EISCAT Scientific Workshop was held in Cargese, Corsica, on 2-6 October 1995. It was preceded by a 2-day EISCAT course with lectures by radar and science experts to introduce students and newcomers to EISCAT research and the radar system. The course and the workshop were very well organized by our French colleagues. More than 100 participants attended the workshop, representing 10 countries. Selected papers from the total of 66 oral and 20 poster papers presented at the workshop will be published in the journal Annales Geophysicae. Publication of 39 papers resulting from the 6th EISCAT Workshop held in autumn 1993 in Andenes, Norway, were in press at this time with the Journal of Atmospheric and Terrestrial Physics.

The EISCAT Scientific Advisory Committee met after the 7th Workshop in Corsica (see photo on next page) and expressed its satisfaction with the vital interest signified by the EISCAT workshop and the course activities. The SAC received reports from the executives on the development of the ESR, which was on time to meet the expected launch of the Cluster satellites. Particular attention was on the design of the analysis program GUISDAP as well as the level-2 user software to operate the ESR. The GUISDAP analysis program, which is provided by Finnish scientists as in-kind contribution to EISCAT, is being used more frequently by many Associates and is also needed for the analysis of the ESR data. Groups in the UK are in charge of designing parts of the special user software packages, which the SAC had to approve. The SAC also considered in depth the different solutions for the extension of the ESR due to the possibility of obtaining a further antenna for the EISCAT Svalbard Radar as well as other ground-based observations to supplement the EISCAT KST and ESR observations. The importance of the Announcement of Opportunity, which EISCAT had issued for external users of the EISCAT systems, was also credited with satisfaction by the Scientific Advisory Committee.

49th SAC meeting on 6/7 October 1995 in Cargese, Corsica: First row (l.t.r): M. Lockwood, M. Lehtinen, J. Röttger, A.P. van Eyken; second row: S. Kirkwood, D. Fontaine, K. Rinnert, C. La Hoz, D. Alcaydé; third row: M.T. Rietveld, Y. Kamide, P.J.S. Williams, A. Richmond, W. Baumjohann.

45th AFC meeting on 18/19 October 1995 in Sodankylä: (l.t.r.) G. Brooks, A. Röhr, H. Andersson, G. Leliévre, J. Röttger, O.J. Marttila (secretary), E. Ikonen, F. Karlsson, A. Andersen.

The total budgets for the KST operations were 25.819 million SEK in 1994 and 26.187 million SEK in 1995. These were distributed in 1994 (1995 in brackets) as 45.2% (46.5%) for personnel, 20.0% (20.3%) for administration (incl. Council and Committees), 16.6% (15.3%) for operation and 18.1% (17.9%) for capital operations. The chart at the bottom of the page shows the total budget development for the different sites and the ESR project. The recurrent costs for the ESR construction of 5.257 million SEK in 1994 and 5.902 million SEK in 1995 were distributed as 39.6% (36.24%) for personnel, 29.5% (32,1%) for administration (mainly travel costs between sites and to Svalbard) and 30.8% (32.1%) for operational site preparations. The investments for the ESR were accounted separately (see page 38).

The Sodankylä site enjoyed a major building extension as part of the renovation of the Sodankylä Geophysical Observatory and now has enlarged laboratory and office space. A sketch of the new site lay-out is shown, where Laajennus is the new part of the site building.

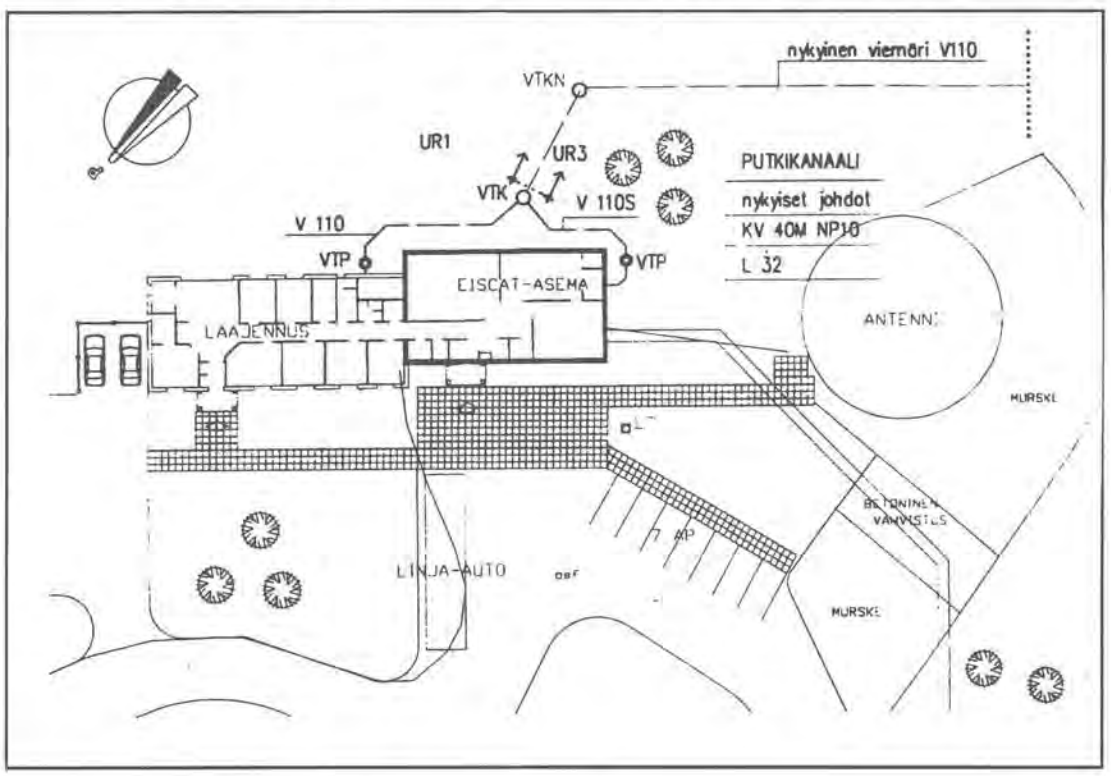

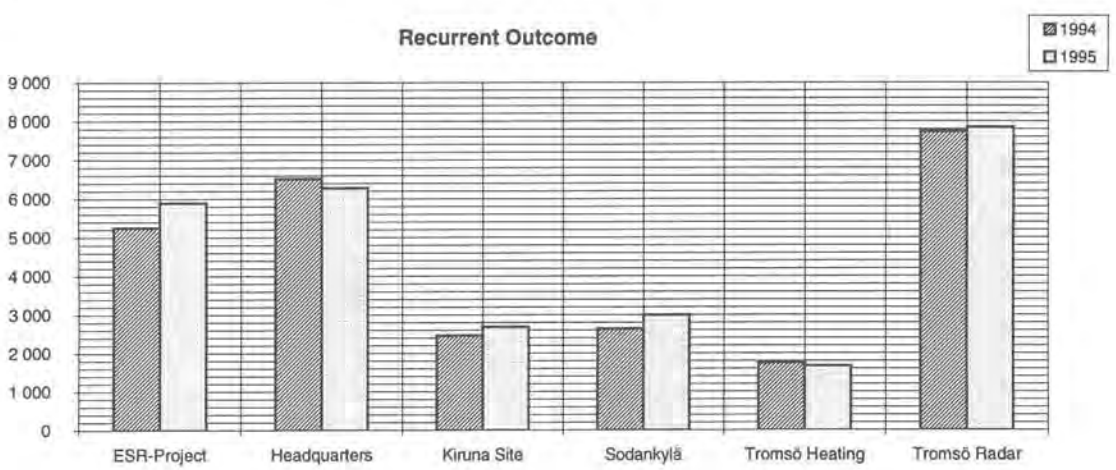

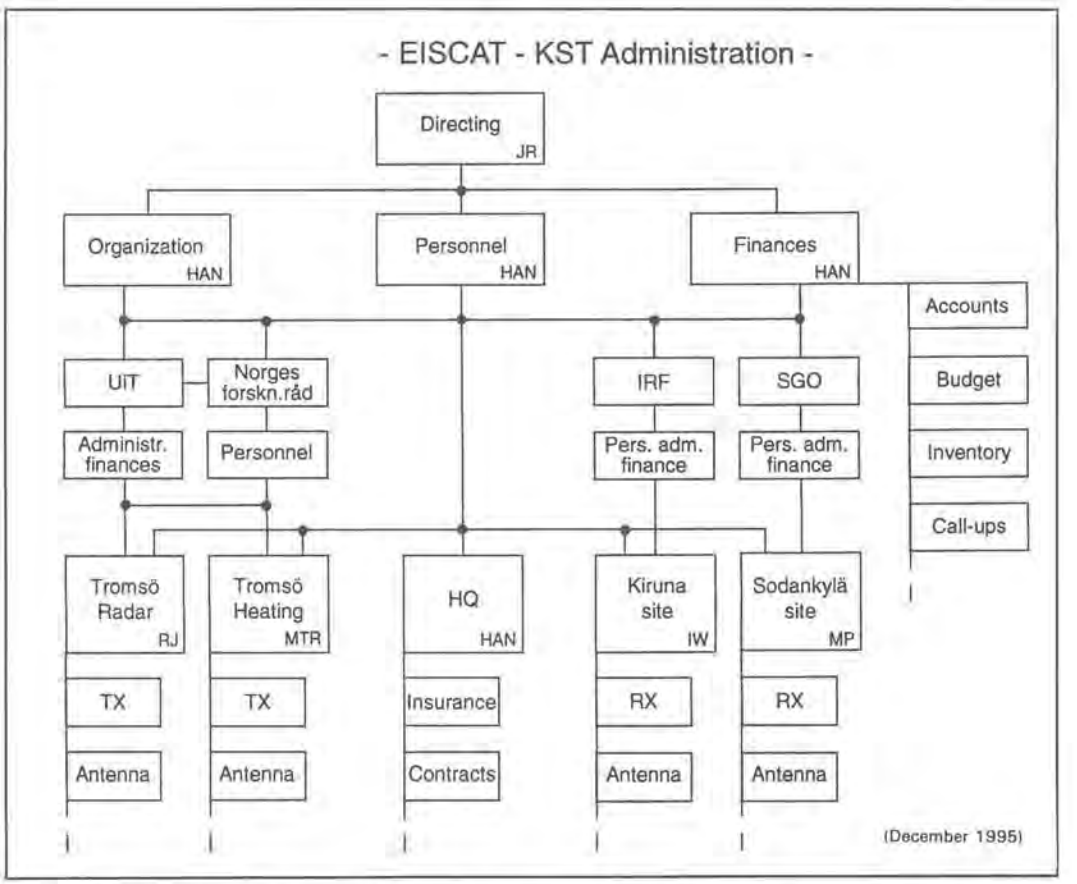

The introduction of the EISCAT Svalbard Radar into the operation of EISCAT is planned to take place after 1 January 1997. It was recognized by the Council that it was necessary to identify sources of additional funds and to suggest plans for operations within the available budget. For this purpose the Council re-established the Long-Term-Planning Group (LTPG). Members of this group were from all Associates, together with the Director. In two meetings in spring 1995 the LTPG came to conclusions on flexible working arrangements by optimizing staff resources between the KST and ESR sites, possibilities for more remotely controlled operations and re-examination of site overheads. The Director was asked by the Council to implement these items.

The Council also formed a sub-committee on re-organization of the EISCAT structure, which consisted of three Council members, a representative of the Research Council of Norway and the Director. This sub-committee had a meeting in September and recommended a revised formation of technical operations, science support and administration. This was noted by the Council at its meeting in November 1995.

The administrative structure of EISCAT, as applied from the outset, is shown in the organogram above, where IRF, SGO and UiT are the host organizations providing the staff for the KST site operations. Norges forskningsråd decided in 1993 to transfer the employment responsibilities for the Tromsø staff completely to the University of Tromsø (UiT). There were various endeavors to introduce a transfer in 1994 and 1995, all of which turned out to be rather complicated. Although it was finally resolved, this process caused discontent and some disruption for the EISCAT executives and staff during the time of the dual work obligations for the KST operation and the ESR construction.

EISCAT Staff
(December 1995)

Ernst-Rolf Albrigtsen (T)
Henrik Andersson (H)
Birger Benjaminsen (T)
Thorstein Blomstrand (T)
Halvard Boholm (T)
Peter Collis (H)
Stein Eliassen (T)
Tony van Eyken (T)
Jim-Arne Hansen (T)
Kjell Hauglann (T)
Stefan Heck (E)
André Hellvig (T)
Knut Hellvig (T)
Reinhard Hund (E)
Toivo Iinatti (S)
Gunnar Isberg (H)
Roger Jacobsen (T)
Kent-Ove Johansson (K)
Magnhild Johansen (T)
Ingvar Keskitalo (H)
Ester Kjeldsen (T)
Knut Koskenniemi (K)
Carmen Kroll (H)
Ingela Kyrö (H)
Tarmo Laakso (S)
Ralf Larsen (T)
Unni Pia Løvhaug (T)*
Jussi Markkanen (S)
Inge Marttala (K)
Anna-Liisa Piippo (S)
Markku Postila (S)
Michael Rietveld (T)
Jürgen Röttger (H)
Misha Savitski (E)
Anette Snällfot (H)
Arild Stenberg (T)
Ingrid Storhaug (T)
David Tetenbaum (T)
Lars-Göran Vanhainen (K)
Gudmund Wannberg (H)
Ingemar Wolf (K)

(* leave of absence)

At the end of 1995 EISCAT had 41 staff members. Their names are shown in the box to the left. Three staff members working on project positions for the EISCAT Svalbard Radar are indicated by (E). The work place of other staff members is indicated by (H) = Headquarters, (K) = Kiruna site, (S) = Sodankylä site and (T) = Tromsø site; three of the Tromsø staff were working at the Heating facility. There were a total of 3 management, 5 administrative, 20 technical, 5 scientific, 6 computing and 2 other positions in the corresponding staff complement. Some of these positions were part-time. Most of the staff had to perform the usual duties for the Kiruna-Sodankylä-Tromsø (KST) operation and administration as well as the tasks for design and construction of the EISCAT Svalbard Radar (ESR).

Frequent commuting of several staff members between the KST sites, Headquarters and to Svalbard was necessary. The latter was particularly pronounced during the recent years, since expert staff were needed on Svalbard for the ESR installation. Besides the management meetings for the ESR project there were the routine executive and budget meetings. These meetings were usually combined, since the ESR project was executed as part of the EISCAT organization. Only one Annual Review Meeting was held in these two years, on 4-7 March 1994, being combined with the ESR Progress Analysis Meeting. This meeting in Longyearbyen also allowed the staff to see the ESR location and to experience the environment of this new EISCAT site.

I owe all the staff, involved in the dual work for the KST operation and for the ESR preparation, my highest appreciation for the perfect technical, administrative and logistic performance of these highly demanding tasks.

Jürgen Röttger

The EISCAT Svalbard Radar Project

A Summary 1989 - 1995 -

The EISCAT Svalbard Radar (ESR) project culminated in 1994-1995 when the main on-site construction and the instrument design and tests were accomplished. It is, thus, worthwhile to summarize the development of the ESR project, i.e. its main design and construction period, in this Annual Report.

The project was unique from the outset. The idea was already formulated in the second half of the 1980's when the motion was pioneered to build a three antenna system with three-megawatt transmitter power on Spitsbergen. The present system has a power-aperture product more than one order of magnitude smaller than the originally perceived one. Yet, as proved in estimates and in the first tests, it yields significant results.

The Cluster satellite project strongly stimulated the radar venture on Svalbard, and in 1990 the EISCAT Associates decided to study the feasibility of such a radar. It was resolved that the EISCAT Svalbard Radar (ESR) should be operational at the launch of the Cluster satellites in December 1995. At the end of 1992 it was decided to begin the construction of the ESR. However, the funds available at that time were sufficient only for a 0.5-megawatt transmitter and one antenna. Expansion, however, is planned.

Two design strategies, a hardware-driven one and a software-driven one, were considered, and the former was adopted by the project executives.

The staff was temporarily increased by 10% during the ESR construction period. EISCAT's limited manpower resources, employed for the maintenance and operation of the mainland EISCAT systems, had thus to be utilized, regardless of the fact that operation had to continue. Executive and staff were additionally obliged during this period to finish the agreements and contracts for the Heating facility take-over and begin its operation as part of EISCAT, as well as had to deal with complex radio frequency interference, electromagnetic compatibility and apparent radiation hazard threats in Tromsø, etc.

As a consequence, EISCAT had to perform a dual assignment during this ESR construction phase. The development and construction of instrumentation had to be done at three locations, namely Kiruna, Sodankylä and Tromsø, all separated by several 100 km. This made the necessary intercommunication between the project designers much more tedious and less practical than in other comparable projects. More than 20 companies in six countries were additionally involved in the ESR project. Some complex contract negotiations had to be accomplished successfully with one of the main contractors.

Committees, representing research councils' administrations and a large international scientific user community had to be consulted and the Council had to approve many project procedures.

In the main phase of the ESR project, the employment structure had to be changed at EISCAT in Norway. For several years EISCAT had no leading administrator, and the entire project management had to be in the hands of the EISCAT chief executive. The project funds were fixed in currency values of the six Associates and had to be spent for fixed-price contracts in several currencies and then accounted in Swedish Crowns.

Finally, the equipment had to be installed and tested on the Svalbard archipelago, high in the Arctic, almost one thousand kilometers north of mainland Europe.

In parallel to these actions, communications and negotiations with the Japanese partners on joining EISCAT were carried through and the results of these negotiations, including provision of new funds, were assured to be in agreement to the routines of the six original EISCAT Associates.

In the following a summary of major milestones, events and facts of the ESR project is presented.

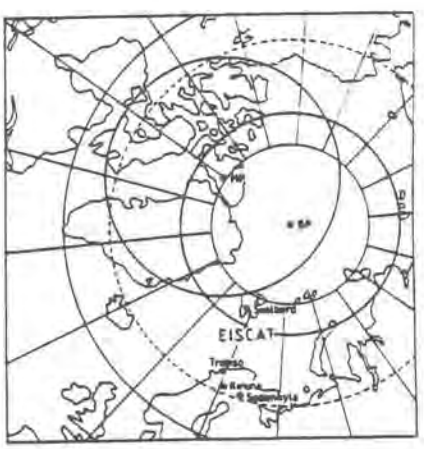

Some Major Milestones in the Development of the EISCAT Svalbard Radar (ESR) Project

1989: SERC Ground-Based Plan included a proposal for a major ionospheric and atmospheric radar in the polar cap. UK report on scientific and technical specifications for a radar on Svalbard and presentation of this plan to EISCAT.

Endorsement of this proposal by EISCAT SAC and Council.

1990: Installation of the Polar Cap Radar (PCR) Working Group during the EISCAT Council meeting on Svalbard: aim for three megawatts and three antennas. Monthly meetings of this EISCAT PCR Working Group. Antenna Pre-feasibility Study. Presentation of draft report to EISCAT Council on scientific goals and design specifications for an ionospheric and atmospheric radar facility on Svalbard. EISCAT Council agreement to continue planning in order to meet the Cluster mission in 1995.

1991: Continuation of organizational, administrative, management and technical preparations of an EISCAT radar system on Svalbard by EISCAT executives. Issue of the final version of the "Report on the design specifications for an ionospheric and atmospheric radar facility based on the archipelago of Svalbard" (White Report). Installation of first extra personnel for the planning of the new radar. Technical design specification meeting. Japanese plans for a radar on Svalbard. First meeting of the Long-Term Planning Group (LTPG) of the EISCAT Council. Council agreement on principal project management plan for the EISCAT Svalbard Radar "ESR". All EISCAT Associates agree meeting on the continuation of the ESR planning, using existing EISCAT and new resources.

1992: Meeting on the definition of data acquisition and digital signal processing (DSP). Executive meeting to explore further utilization of EISCAT resources for ESR development. Second meeting of LTP Group. AFC meeting agrees on transmitter amplifier tender action. Transmitter tender action, antenna studies. Preparations for site, infra-structure, frequency clearance, operating permits, etc. EISCAT Council memorandum on the intention to construct the ESR. Consensus to proceed with the preparations necessary to accomplish the phased development of the radar. Objective to reach an agreement to proceed with the construction of the initial phases of the radar at the Council meeting in November 1992 with the aim that the first two phases should be operational during the Cluster space mission.

Third meeting of LTP Group. Evaluation of expected funds would allow a minimum initial version of the ESR to be constructed. Receipt of transmitter bids. First formal ESR Management Meeting MM-01. Announcement of opportunity for antenna(s). Evaluation of transmitter bids, arrangements for site ground-work. Directions for DSP, control and monitor standards. Recommendation of SCOSTEP. SAC meeting investigates scientific merits of one-dish and two-dish systems and minimum power. ESR Design Review Meeting (DRM), Second Management Meeting MM-02. AFC meeting. Fourth LTPG meeting. Third ESR Management Meeting MM-03. Nov.: EISCAT Council decides to begin the construction of the initial phases of the EISCAT Svalbard Radar. Order of transmitter prototype module from Harris in UK. Request for Proposals of the antenna sent out. Fourth Management Meeting MM-04

The view along Adventdalen with the site location in the front on the day of the formal opening of the ESR site area on 22 May 1993.

1993: Fifth Management Meeting MM-05. Fifth LTPG Meeting, sixth Management Meeting MM-06. ESR Baseline Description Document issued. Design and construction of major system instrumentation etc.: Sodankylä: Digital signal acquisition and processing (DSP), based on definitions from particular ESR-DSP design meetings. Kiruna: Receiver, exciter, antenna supplements and supervision. Tromsø: Radar controller, air surveillance radar, transmitter tests. Headquarters: Administrative, technical and financial project management. On-site supervision in Longyearbyen: Project consultant. Beginning of ESR site construction following the opening by the Norwegian Minister for Research, Education and Church. Major companies involved in the construction of road, building, antenna foundation and electric power installation: SNSK, Barlindhaug, Veidekke, SSD. Agreement on a Svalbard Radar signed by all six EISCAT Associates. Signature of contract with the company Kvaerner-Kamfab, Karlstad, Sweden, for the design and construction of the ESR antenna. Management meeting MM-7a. Antenna design presentation by the Nordic Telescope Group NTG/NOTSA in Risø, Denmark. In-plant test of first transmitter module (250 kW). Management Meeting MM-7b. EISCAT Svalbard Radar Brochure released. Antenna foundation cast. Eighth Management Meeting MM-8. Order of second transmitter module. Final Design Review Meeting of the ESR antenna in Karlstad. Test installation of first transmitter module in Tromsø. Ninth Management Meeting MM-09. Presentation of the antenna design to the EISCAT Council meeting in Hamburg. Software layout adopted: Level 1 (engineering) and Level 2 (user-oriented). First EISCAT Svalbard Radar Software Project Group (ESPG) meeting in Hamburg; user software discussion group formed. Tenth Management Meeting MM-10.

1994

Jan.: Management Meeting MM-11.
Feb.: ESR System Description Document released.
Mar.: EISCAT Annual-Review Meeting and ESR Progress Analysis meeting in Longyearbyen. Adaption of the management structure to include on-site installation work.
Apr.: SAC adopts basic proposal for ESR software design, incl. in-kind contributions by Finland (GUISDAP), UK, Germany and France.
May : Second ESR Software Project Group (ESPG) Meeting in Abingdon, UK. In-plant inspection and review meeting on antenna construction at Kvaerner-Kamfab in Karlstad.
Jun.: ESR Midterm-Review Meeting (MRM) in Tromsø and Longyearbyen. Signature of final Agreement with SNSK for provision of land and services. Meetings with telecommunication authorities, clearance of ESR frequency bands etc.
ESR site building (incl. transformers, fire fighting and all supplies) and antenna foundations taken over by EISCAT. Emergency generator installation begins. Visit of Japanese delegations to Longyearbyen. Longyearbyen Scientific Workshop.
Jul.: Antenna shipment from Karlstad and erection begins at the ESR site.
Aug.: On-site installation team starts working regularly in ESR site building.
Instructions on Going-to-Svalbard issued.
Sep.: Japan-EISCAT Symposium on the Polar Ionosphere in Toba, Japan. Antenna erection on-site basically completed.
Oct.: Issue of initial operating permit to use the frequency 500 MHz for the EISCAT Svalbard Radar operation. First on-site ESR staff coordination meeting. Management Meeting MM-12 in Tromsö.
Nov.: Contract with DRAL, UK, for development of software components for the ESR.

1995

On-site work
Infrastructure and contracts

All site requirements under preparation/control. Permissions granted. Frequency clearance all right, EMC being tested. Airport communication being established. Local transportation functioning properly. Staff accommodation in Longyearbyen houses and flats, outside site-cleaning. Road access all right, further drainage placed. Personnel security on site, VHF radio communication, etc.

Building in full use:
Electric power fully connected and monitored. Emergency generator installed and tested under available load. Fresh water and sewage tank in use. Ventilation and heating system in operation. Fire fighting/alarm system installed and functional. Telephone, telefax, communication system functioning well. Workshop, laboratory, control room equipped and in use. Kitchen/living room in use.

Transmitter:
All modules, control and cooling units installed in transmitter hall. Power combiners and waveguides installed and tested, connected to dummy loads. 2x250 kW tests, final acceptance and commissioning performed.

Antenna:
Fully erected and tests basically successful. Run with full speed and acceleration, in stand-alone (ACU) and under EISCAT computer control. Panel alignment done, calibration underway. Vertex cabin being equipped, waveguide system being tested. Receiver protector principally tested. Weather station installed.

Antenna acceptance test:
First part in July 1995 and second part in Oct. 1995: Pattern, gain, antenna temperature yield mainly expected results. Problem with azimuth rotary joint occurred in autumn.

The ESR hardware and software preparations performed in Kiruna, Sodankylä and Tromsø (KST)

Receiver analog (Kiruna):
Preamplifier works in cryosystem at 8 Kelvin noise temp. Mixer ready and tested. 1st and 2nd IF stages finished and working. DDS prototype tested with PC and transmitter. Timing system (GPS) being tested.

Receiver digital (Sodankylä):
ADC/DSP hardware successfully tested. Channel board PCB layout ready, 6 units produced and tested. DSP software: digital filter, processor successfully tested.

Radar control (Tromsø): Functioning.

System software:
Software for access and control used in initial tests. VME crate installed and basically tested.

Main server (control console) delivered and installed at Kiruna site.

User software:
Specified and under design in-house and as in-kind projects by Finland, France, Germany and UK. Implementation at ESR site planned for end of 1996.

First hardware and system software integration test successfully took place in Kiruna end of August - middle Sept.

System integration took place in the beginning of November at Kiruna site:
First signals were received on 15 Nov. 1995 from Tromsø during these tests at the Kiruna site.
Final system integration test takes place in Kiruna in early March 1996, thereafter shipment to Svalbard and operational tests in middle of March 1996.

To allow proper planning, coordination, tracking and general management of the time critical project developments as well as providing a base-line for internal guidance of the project performance a Project Management Plan was implemented. This plan consisted initially of 17 work packages, which had been: (1) General management and organization, (2) System specifications, (3) RF generation and transmitter, (4) Antenna, analog receiver, (5) Hardware monitor and control, (6) Digital receiver, (7) Computing, system software and basic processing, (8) Data processing, analysis and user software, (9) Basic infra-structure, (10) Logistics, (11) Networking and communications, (12) Quality and reliability control, and system integration, (13) Financial and business matters, (14) On-site installation, (15) On-site performance analysis, (16) Transition into operation, (17) Operational maintenance.

The organogram shows part of the work break-down structure of the work package On-site installation.

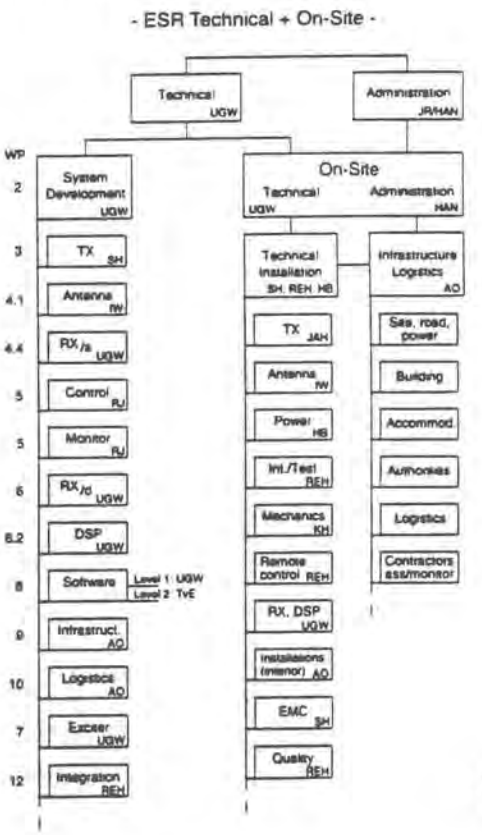

- EISCAT Scientific Association -

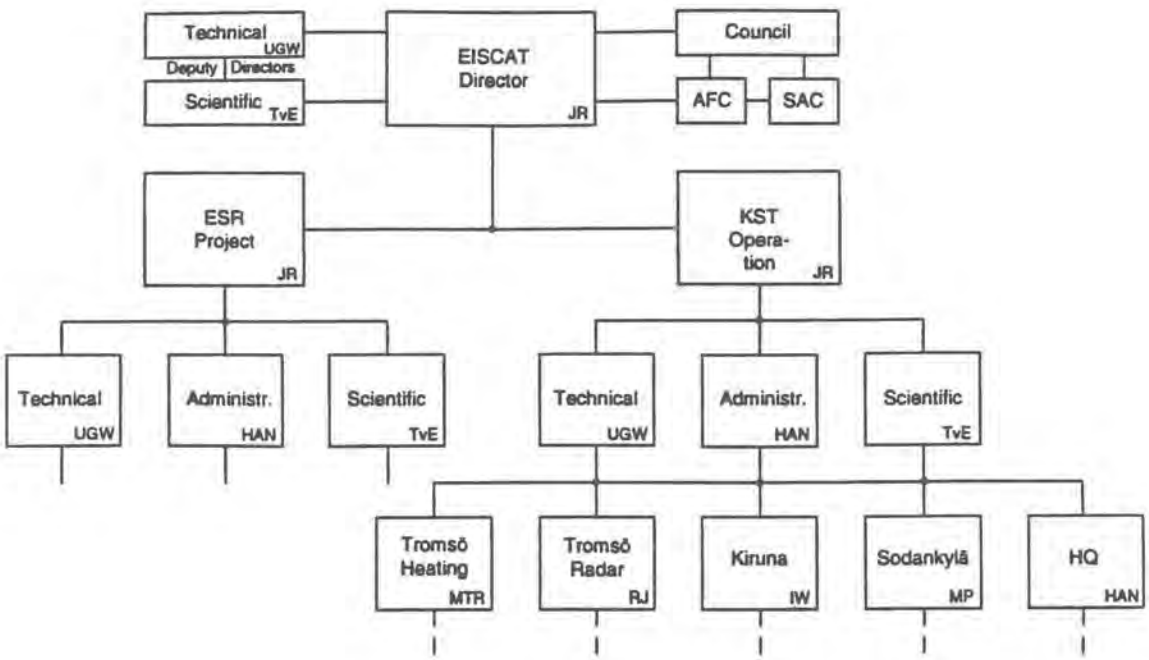

- EISCAT Svalbard Radar -

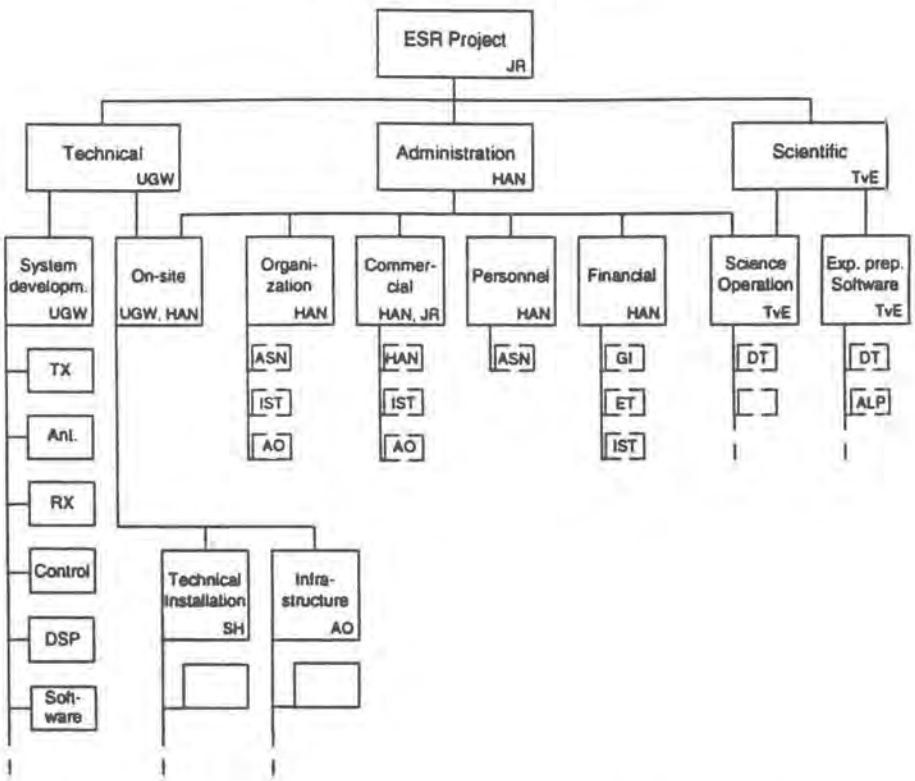

The dual structure of EISCAT during the period of the EISCAT Svalbard Radar construction, arranged in the two branches KST Operation and ESR Project (upper graph), and the basic structure of the ESR Project (lower graph). The organograms display the state at approximately the end of 1995.

Each of the work packages, which are summarized on page 23, was under one leader. The work packages were originally described in the Baseline Description Document and the tasks were adjusted as needed during the development of the project. Regular management meetings (in total 15), twice per year combined with the usual executive and budget meetings for the KST operation, were held to coordinate the tasks. This was particularly essential because the design and construction took place at separated locations. The day-to-day communication was by phone, fax and via the Internet.

Personnel plans and detailed project milestones were agreed upon for the work packages. These also included supervision of work and delivery of parts constructed or provided by companies.

The original personnel, budget and milestone plan was submitted to the EISCAT Council in 1990. It was updated in 1992 after the Council resolved the construction of the ESR. The milestone development was progressing closely to the originally planned one and at the end of 1995 there was a delay of three months with respect to the initial milestone plan of 1992. Some of the major milestones performed are shown in the right-hand-side graph.

The photo shows participants of the last Management Meeting, which took place on 16 November 1995 after the first successful tests of the ESR receiver, controller and DSP units in Kiruna. From left-to-right: J. Röttger, M. Postila, G. Wannberg, H. Andersson, R. Hund, S. Heck, I. Wolf, J. Markkannen and A.P. van Eyken; not participating at this meeting were A. Øvergård and R. Jacobsen.

The site, which was recommended for the EISCAT Svalbard Radar in 1990, is at a plateau above Mine No. 7 about 15 km south-east of Longyearbyen, the main community of Svalbard. The mine is operated by the Store Norske Spitsbergen Kulkompani (SNSK). Access to the mine is via a steep road with many hair-pin bends which climbs up from Adventdalen to the mine. A new road, which was built by SNSK for EISCAT, continues upwards a further kilometer across the slightly up-sloping plateau to the radar which is at 434 m above sea level. In order to reduce the effect on the fragile permafrost landscape and minimize environmental impact, every effort has been made to use existing tracks and roads as the foundation of the new access road to the radar site as well as the selection of the radar site itself. Meteorological parameters were measured, test drilling to analyze the soil at the plateau was done, the horizon profile was determined and the radio frequency spectrum was surveyed before it was finally decided to construct the radar at this site. The forceful antenna foundations are bolted to the bed rock, which is about six meters below the surface.

The site building contains all facilities to operate and maintain the radar. The building is thoroughly constructed for the harsh Arctic climate conditions. It consists of two elements, the transmitter hall (consisting of two parts to accommodate two 500 kW transmitter modules) and the operations compartment, such as technical rooms for ventilation, heating, sewage and fresh water tanks, transformer room, fire fighting system and emergency generator room, electronics workshop and laboratory, storage space, control and experimenters room, and personal facility rooms. For security reasons (harsh climate, dark winter period and remote location) accommodation at the site is not permitted, but precautions are done for emergency cases. The site staff lives in houses or flats in Longyearbyen and the transportation to the radar site is by EISCAT cars. An agreement exists between EISCAT and SNSK for provision of mechanical support for the site by the mine and snow cleaning of the road up to the radar site. The photo shows the leading civil engineer in charge of the site and foundation construction (by Barlindhaug and Veidekke) and the project consultant.

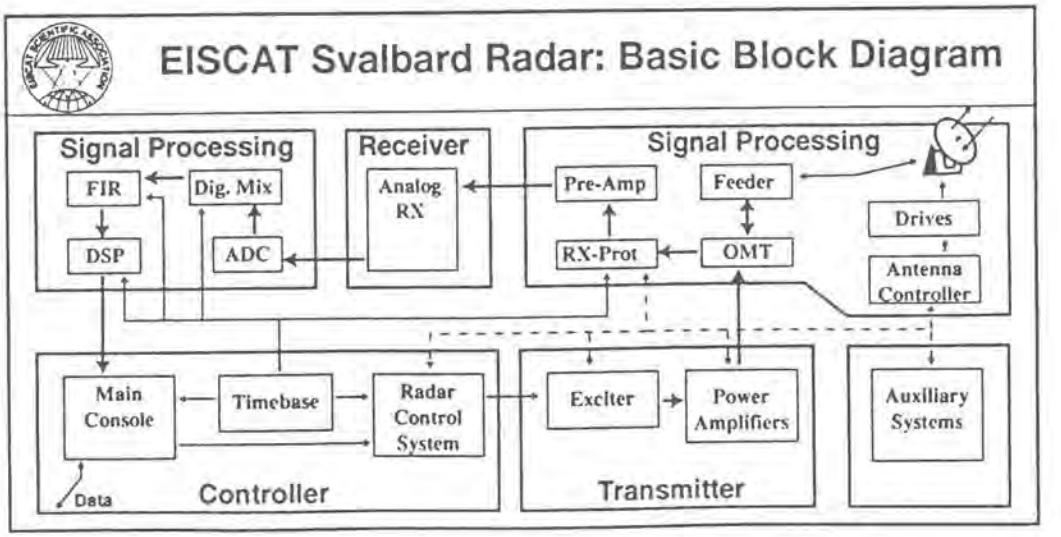

The block diagram shows the main instrument components of the ESR system, which had been set up at the site during the past three years. Controller, receiver, signal processing and other accessory equipment are located in the control room, the transmitter in the large transmitter hall, and the antenna just adjacent to the building.

The site is connected to the mains power line serving the Mine 7. Three transformers are installed in the site building for the antenna (1600 kVA), the transmitter (1000 kVA) and the house power (315 kVA). Since the antenna power consumption is very variable (see lower graph) and it also introduces significant reactive components, proper compensation was provided to prevent line mismatch.

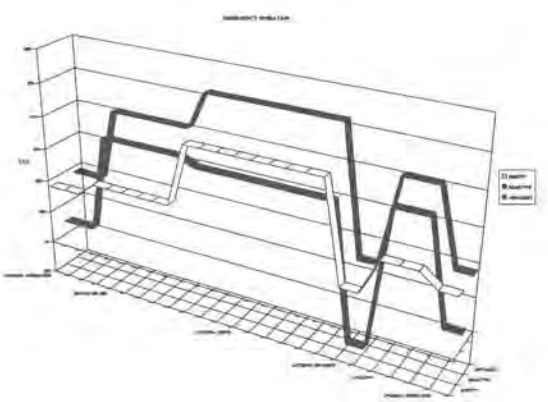

The emergency generator delivers 750 kVA power, which is sufficient to move the antenna into a safe stow position and provide the required house power in cases of longer power breaks. Very vital equipment, such as main computers, timing, safety and emergency communication systems, is further safe-guarded by an uninterrupted power supply.

Great care was taken for electromagnetic compatibility between the high power analog equipment and the sensitive digital systems, as well as for minimizing any critical radio frequency interference and potential radiation hazard.

Telephone, telefax and data communication lines (ISDN at 2x64 kb/s) as well as VHF communication is available the site. Increase of the data link capacity to 2 Mb/s is possible in future when the plans for the operations office in Longyearbyen will be implemented for remote monitoring and control of the ESR. From the operations office telescience connection to mainland institutions should be implemented in future.

The radar site is, thus, prepared for quite self-sufficient and partially unattended operation, which may eventually be adopted after the engineering and experimental tests have been completed successfully.

The initial configuration of the ESR system consists of one parabolic dish and a 500 kW peak power transmitter. The system is designed with the ability to add another antenna and for increasing the transmitter power to 1000 kW. The receiver, data acquisition and analysis applies state-of-the-art standards and devices and will be augmented by high-level software for experiment control and monitoring.

Major system components and elements were supplied by contractors, with whom EISCAT had close contacts during design, construction and commissioning phases.

Following a dedicated analysis of several offers for the ESR antenna, a contract for the antenna design and construction was signed with Kvaerner-Kamfab in July 1993 (see photo), who worked together with several sub-contractors. The design of the antenna was accomplished by the main sub-contractors NOTSA, the Nordic Optical Telescope Scientific Association, and TICRA in Denmark.

Resulting from a detailed design and feasibility study, EISCAT adopted a turning-head scheme, in view of the harsh Arctic environment in which the equipment needs to be operated and maintained. An antenna with a Cassegrain feed system was selected. The antenna main reflector of 32 m diameter, subreflector and feed horn are optimized to provide very low side-lobe emission. The antenna is movable over more than 360° and from 0°to 180° in elevation. The centre photo shows the extended elevation gear required for this purpose.

The antenna was constructed in-plant and transported by ship (see loading in the lower photo) to Svalbard, where erection commenced in early July 1994. The erection was finished in October 1994 and the antenna was placed into a safe stow position before the Arctic winter period.

On-site construction of antenna reflector support structures. The feed horn is seen in the centre.

The top of one of the four antenna foundations which is the base of a main support of the antenna tower.

The photos on the next page show several stages of the antenna erection. The antenna main structure consists of a four-leg steel truss tower which carries the tower head. The azimuth rotation is by using a large slewing ring bearing placed on the top of the tower. Two elevation bearings are situated on the sides of the fork arm, and there are two elevation motors on each side. The azimuth drive has six motors with reduction gears and pinions driving the antenna. The motors are thyristor controlled DC motors located in the tower head. Under wind conditions up to 27 m/s a maximum slewing speed of up to 3 degrees per second can be achieved and the maximum survival wind speed in stow position is larger than 50 m/s. The main reflector consists of 312 panels, each adjustable to match the optimum shape.

The antenna control system is computer-based and placed in a special cabin under the tower head. It can be controlled from a local terminal and from the main radar control system. Emergency stops and auto-stow are provided, as well as emergency motors to move the antenna in case of major motor or control unit failures.

The receiver front-end and receiver protector are in the vertex cabin, which is behind the centre of the main reflector. The feed is of Potter-horn type. The receiver front end has a noise temperature of 20 Kelvin, and the total system temperature is 85 Kelvin. The antenna gain is 42.5 dBi and sidelobes (> second) are lower than -30 dB (-40 dB at off-bore-site > 40°), which results from optimization of feed, sub- and main reflector.

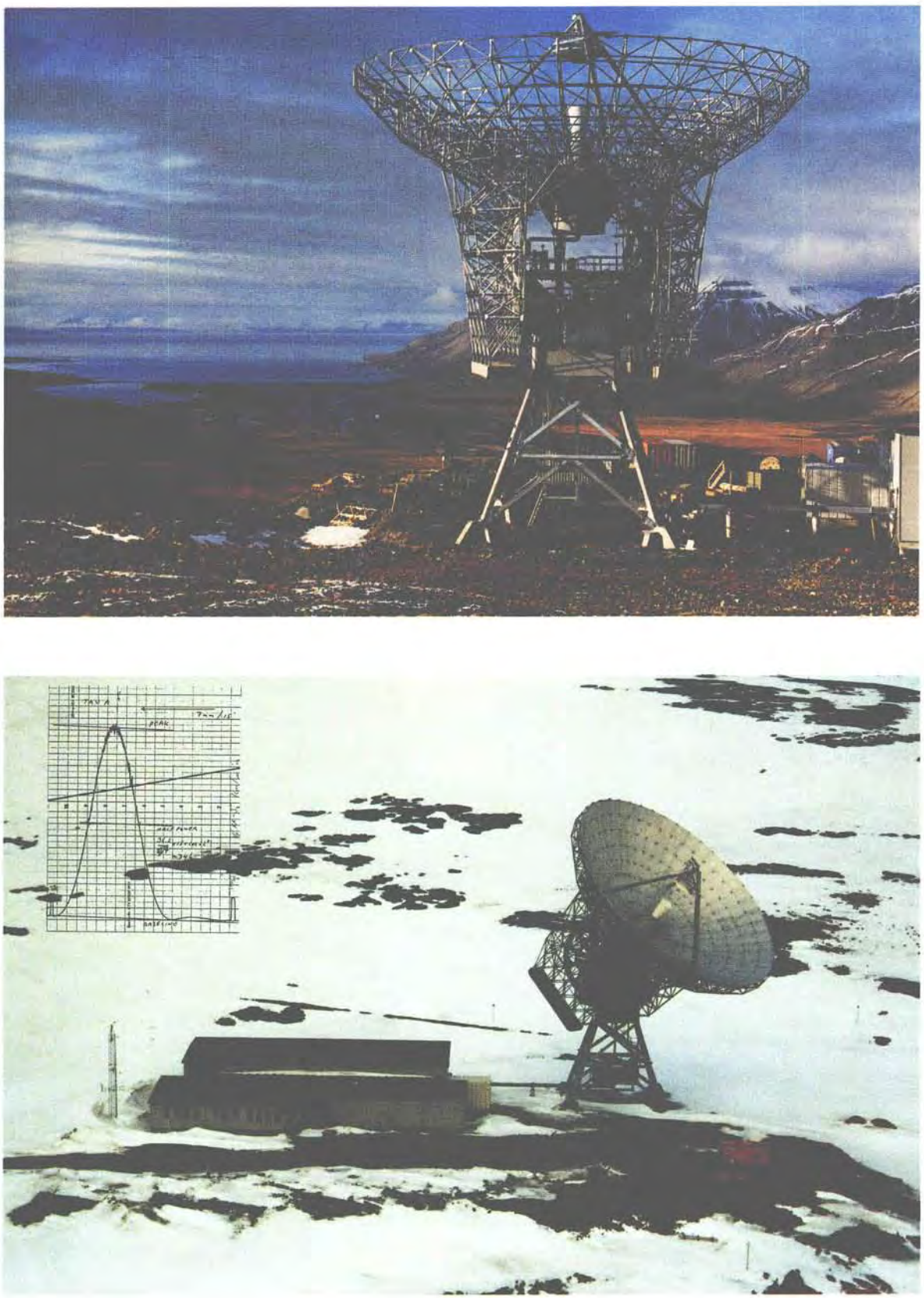

The ESR antenna after erection in September 1994 (upper photo) with the view towards the NW along Adventdalen. The lower photo shows the antenna and site building after completion. The insert shows the main lobe of the antenna pattern measured with Taurus-A drift scan.

The ESR operates on 500 MHz. This frequency is an optimum with respect to system noise and has the further advantage that standard klystrons, used for television applications, can be applied in the transmitter. The ESR transmitter is constructed (by Harris, UK) in modular form to increase system reliability and to improve maintenance. One single module of the transmitter uses standard external cavity vapor cooled klystron tubes rated at 64 kW peak output power. For radar applications a beam pulse modulator is added to the amplifier. Only 24 kV beam voltage is required, the power supplies are air-cooled, and neither crowbars nor oil-filled components are used. The application of television klystrons has another advantage, namely that these can be operated with a very large duty cycle. The ESR transmitter can be run at up to 25% duty cycle, which is most efficient for long-range (polar cap) and high altitude observations. The output of two modules, forming one amplifier unit, is fed through harmonic filters and combined in a switchless waveguide combiner to 125 kW. The total power of four amplifiers is combined further in waveguide combiners to yield 500 kW peak output power. The lower drawing shows eight amplifier units with the corresponding waveguides and combiners. This lay-out would finally yield 1000 kW output power; at this time only the four left-hand amplifier units are installed. The total area of the transmitter hall is 350 m^2.

The waveguide extends from the final combiner in the transmitter hall up to the antenna, where the power passes the azimuth (photo) and elevation rotary joint.

This photo shows one transmitter amplifier (125 kW), a waveguide part and a dummy load.

The photos on the next page show transmitter radar controller and part of the antenna control unit. The lower diagram displays the ESR system overview.

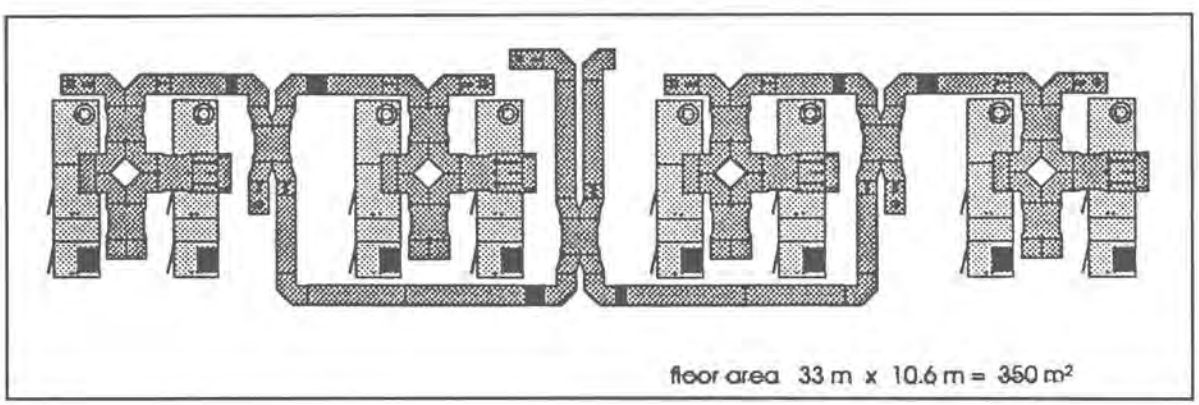

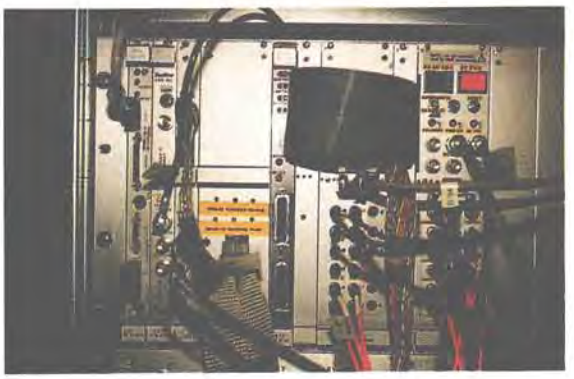

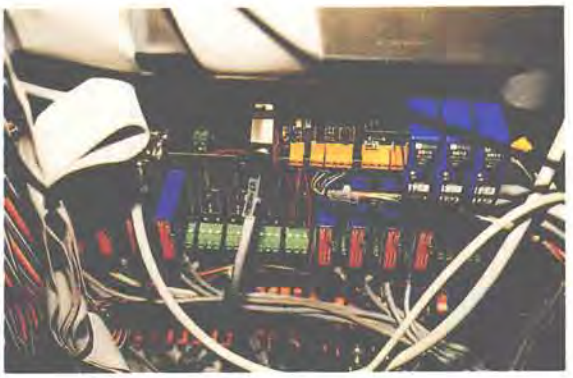

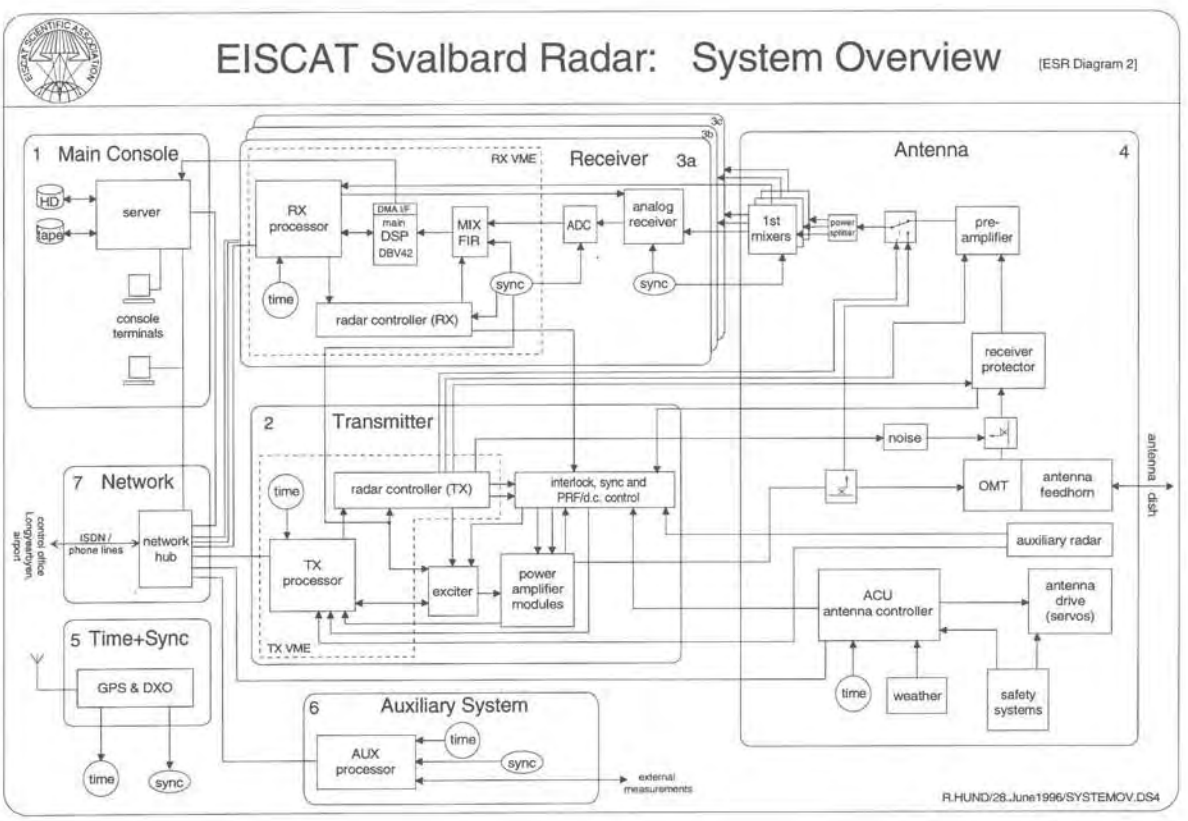
EISCAT Svalbard Radar: System Overview
[ESR Diagram 2]
1 Main Console
HD
tape
server
console terminals
RX VME
Receiver
3a
RX processor
DMA I/F
main DSP
DBV42
MIX FIR
ADC
analog receiver
time
sync
radar controller (RX)
Antenna
4
1st mixers
power splitter
pre-amplifier
receiver protector
noise
OMT
antenna feedhorn
antenna dish
auxiliary radar
2
Transmitter
time
radar controller (TX)
interlock, sync and PRF/d.c. control
TX processor
exciter
power amplifier modules
TX VME
ACU antenna controller
antenna drive (servos)
time
weather
safety systems
7 Network
ISDN / phone lines
network hub
5 Time+Sync
GPS & DXO
time
sync
6
Auxiliary System
AUX processor
time
sync
external measurements
R.HUND/28.June1996/SYSTEMOV.DS4

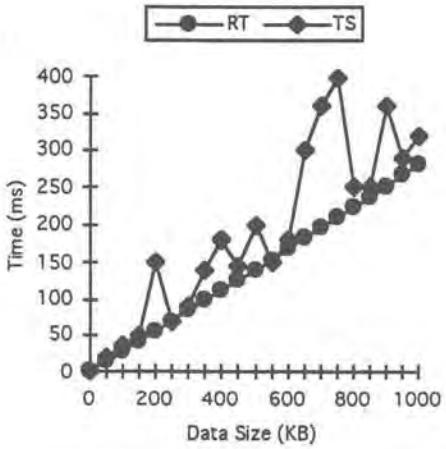

Data transfer tests for the DSP system, demonstrating the advantage of running real-time (RT) with respect to timesharing (TS). The lower block diagram shows the principle of the digital receiver and the photos some actual components.

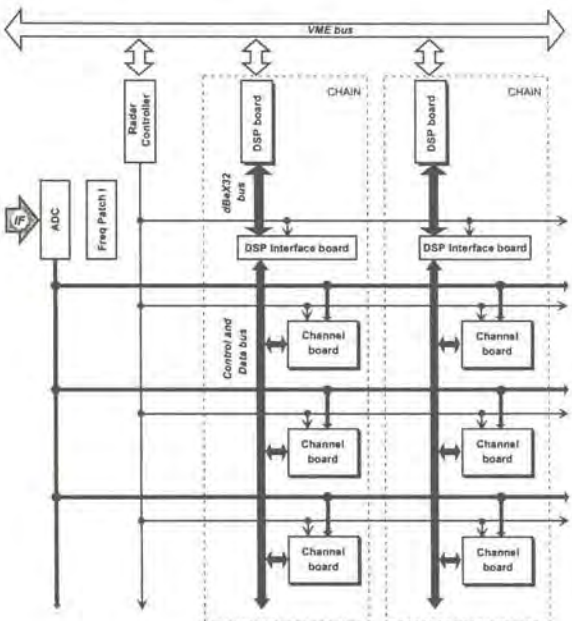

The ESR receiver accepts the 500 MHz analog signal at the preamplifier in the antenna vertex cabin. The receiver chain is configured as a dual-super-heterodyne with 1st IF at 70 MHz and 2nd IF at 7.5 MHz, which is sampled digitally at 10 MHz with 12-bit resolution. Further frequency translation, filtering, rate decimation and/or resampling is performed in the receiver digital backend before digital signal processing. In addition to the processed output, the 10 MHz digital raw data sample stream will be available for direct recording. The analog and digital receiver is fully phase coherent also to the transmitter exciter. The actual transmitter output waveform will be sampled in phase and amplitude for most accurate signal correction and calibration.

The digital signal processing (DSP) includes the on-line computation of both full autocorrelation lag profiles and frequency power spectra, handling all required modulations coded in amplitude and phase. The DSP system is designed and programmed using modified commercially produced DSP boards.

Specifications of the receiver and DSP are found in the total system specification shown on the next page.

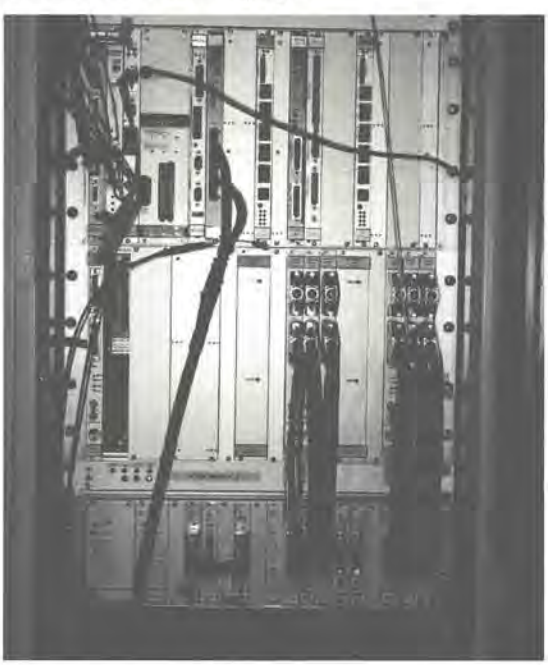

The EISCAT Svalbard Radar
System Parameters Dec. 1995

	Location: 78°09'N, 16°03'E	near Longyearbyen on Spitsbergen, Svalbard
Operating Frequency:		500 MHz
Bandwidth:	Transmitting: Receiving:	± 2 MHz ± 10 MHz
Antenna:	Parabolic dish: Gain: Aperture: Polarization: Steerability:	one (increased to two) 42.5 dBi ≈ 500 m² circular all azimuths, 0-180 degrees elevation
Transmitter:	Peak Power: Average Power: Tubes: Pulse Length: Modulation: Interpulse: Radar controller: Program memory:	0.5 (1.0) MW, modular system 0.125 MW (0.250 MW) TV-klystrons (8 (+8)) < 1 µs - 2 ms amplitude and phase coding min. 0.1 ms address space 20 bits 1 MW memory 32 bit control word with 100 ns resolution
Receiver:	Dual superheterodyne Noise temp.: System Temp.: 1st IF: Output channels: ADC: Complex digital mixer and filter: Digital multiplier: FIR filter:	≤ 20 K ≤ 85 K 70 MHz ± 5 MHz up to 6 10 MHz min. 12 bit min. 10 MHz bandwidth 10 MHz data rate 16 bit coeff. accur.
Digital Signal Processing:		Narrow- and wide-band
	Bus environment: Host processor: Lag profile proc.: Input data format: Output data format: Processing rate:	VME Sparc and 68040 TMS 'C40x4 at 50 MHz 16+16 bit complex 32+32 bit complex 30 MOPS/channel
Total System Figure of Merit:		Peak Power x Aperture per System Temp.: 3 MW m²/K

The complex configuration of the ESR system, consisting of a multitude of individual parts, has been specified after careful considerations of all anticipated requirements for scientific experiments. These specifications have been reviewed several times and are laid down in several documents, as there is the original report by the PCR Working Group of the Council, published in August 1991. The system review took place in September 1992, and the results are published in the proceedings of the **ESR Design Review Meeting DRM-01**. Summaries of the development are also published in EISCAT Annual Reports since 1990 and the ESR brochures.

Technical documents prepared by EISCAT executives and staff are:
Baseline Description Document
Version 2.1, 20.2.93 and 9.3.93.
System Description Document
Version 1.0, 24.2.93, 20.2.94.
Proceedings of the ARM and ESR Mid-Term Review Meeting, 4-7 March 1994
ESR Development Schedule, 17.1.1995.
System Integration Document, 25.4.1995.

Minutes of the 15 management meetings (MM) and the 30 installation team meetings (ITM) and numerous internal memos, reports, company communications and manuals are filed at HQ and the ESR site.

Following the meticulous system integration preparations, the receiver-controller-exciter-DSP tests successfully took place in November 1995 at the Kiruna site, where signals from Tromsø were received, converted to the ESR equipment and lag- and power profiles computed. The graphs show these test results.

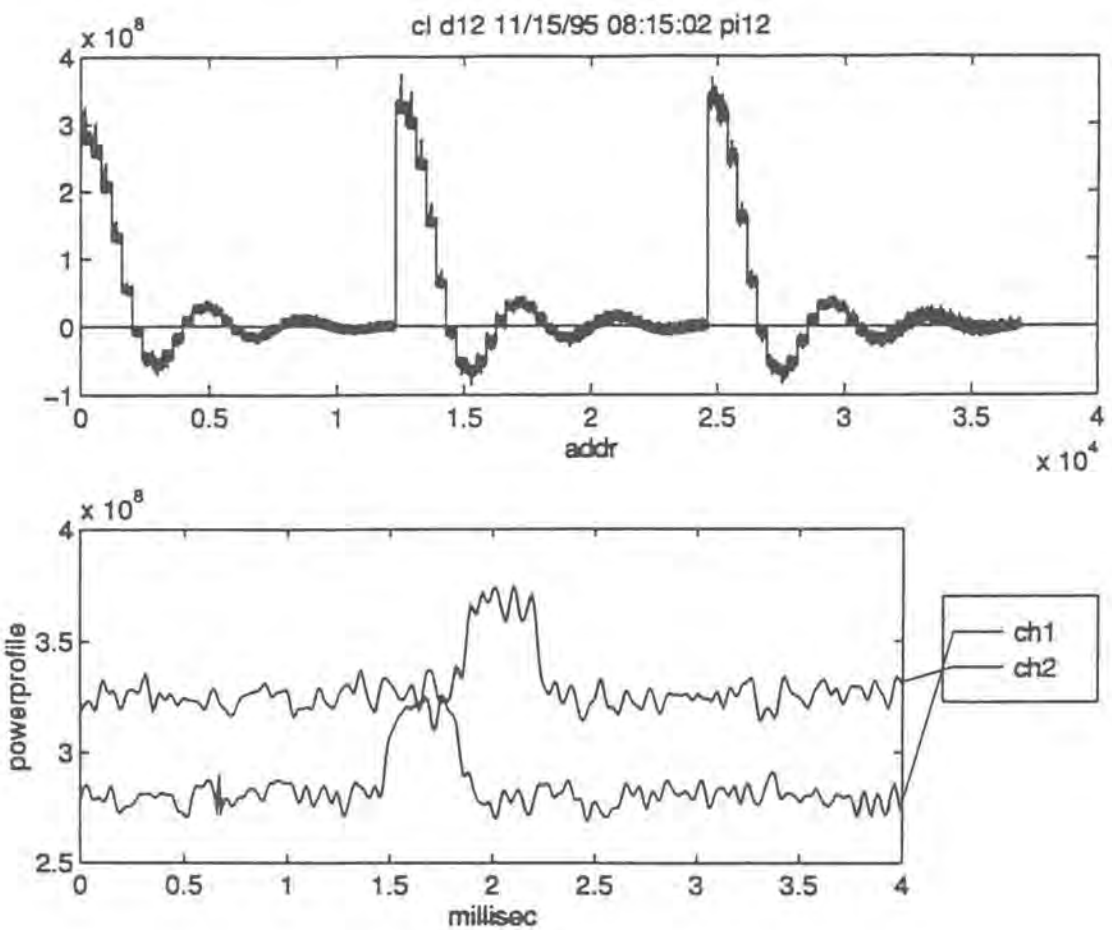

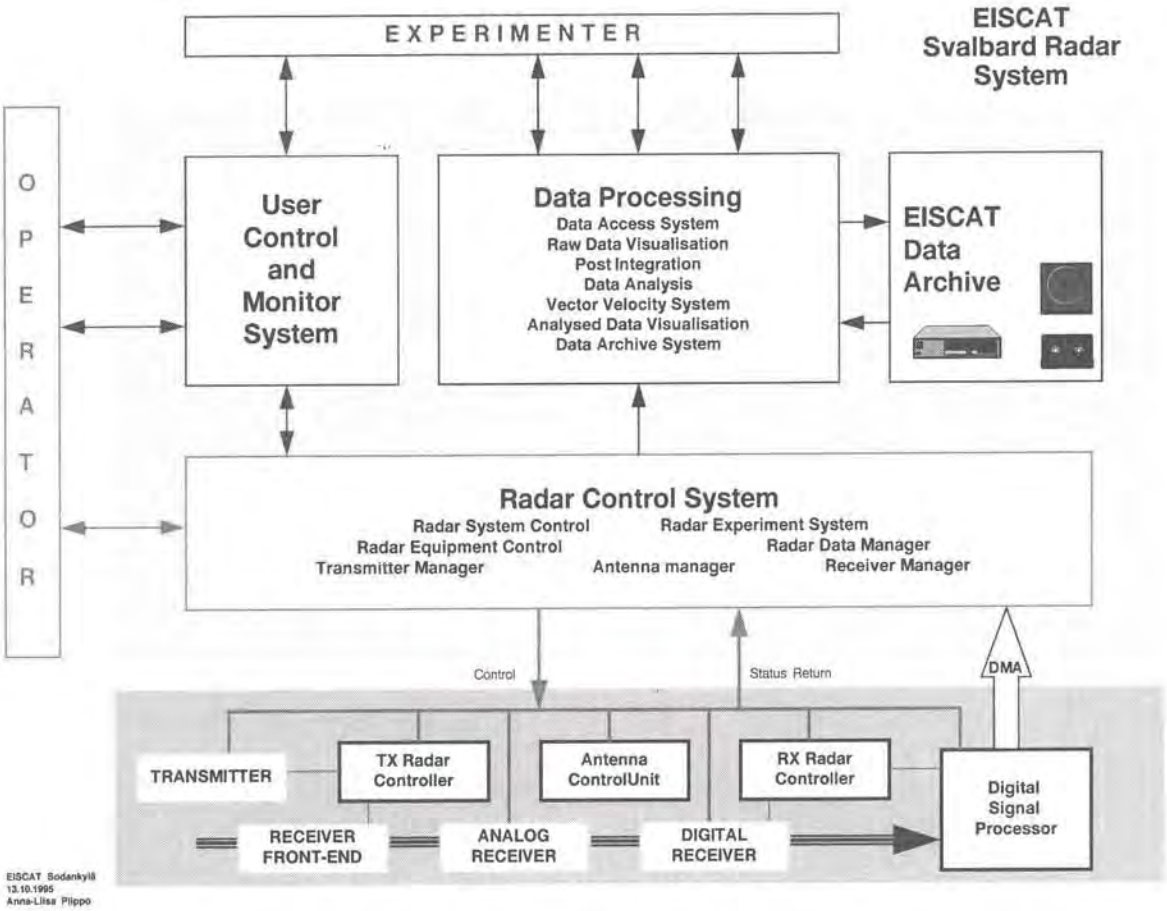

The ESR software is designed in two levels, the system and engineering level (hardware-oriented level 1) and the experimenter-operator level (user-oriented level 2). The block diagram shows approximately the main elements of the software. The level 1 is primarily done by EISCAT staff, whereas the level 2 is essentially through in-kind contributions by Associates' projects or direct contract-controlled design by Associates. To specify and supervise the latter developments, the SAC had formed a specialists' group, the ESR Software Project Group (ESPG). This group had three major meetings. The second meeting was in Abingdon, United Kingdom, in May 1994, and the participants are shown in the photo.

The budget for the EISCAT Svalbard Radar construction was provided in portions to the EISCAT administration. The provision of funds matched quite properly the expenses accruing during the project development. These were estimated from the outset and there was no shortfall of funds at any time. The total ESR budget income 1991-1995 was 115.3 million SEK (MSEK), whereof 97.2 MSEK were spent by the end of 1995. A major outstanding payment of 8.2 MSEK was delayed into early 1996, since the final antenna acceptance and take-over had to be postponed.

The positive balance in 1996 is earmarked for the transmitter upgrade. During the years 1991-1995 a significant fraction of the normal EISCAT staff, paid through the annual KST budget (25.5 MSEK in 1995), worked for the ESR project (a total of the order of 50 man years). This has to be added to the total project costs. However, the estimate needs to be taken with care, since the normal staff had also to work for the KST operation and the dual assignments cannot strictly be separated. The graphs below show summaries of the budget figures.

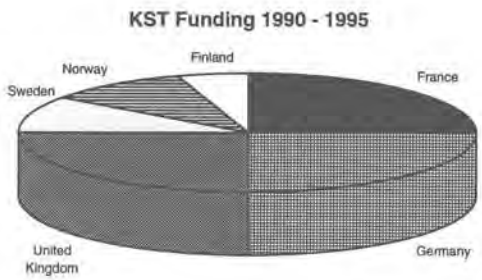

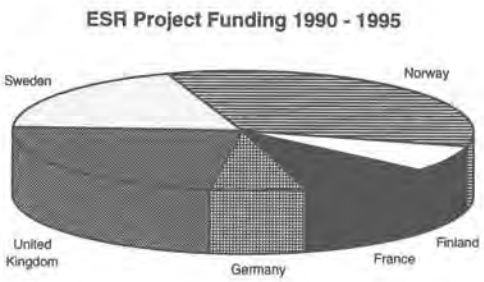

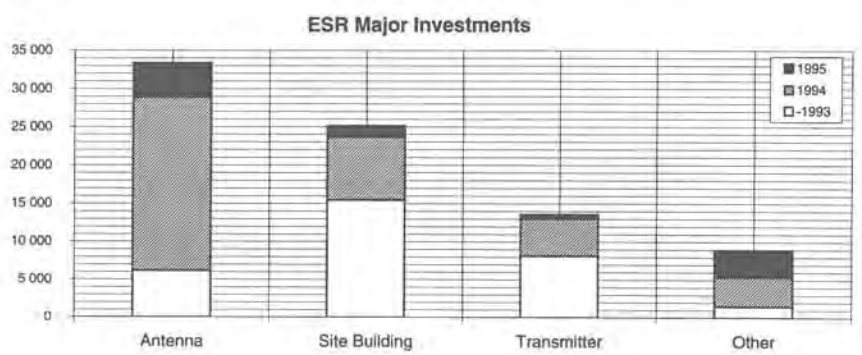

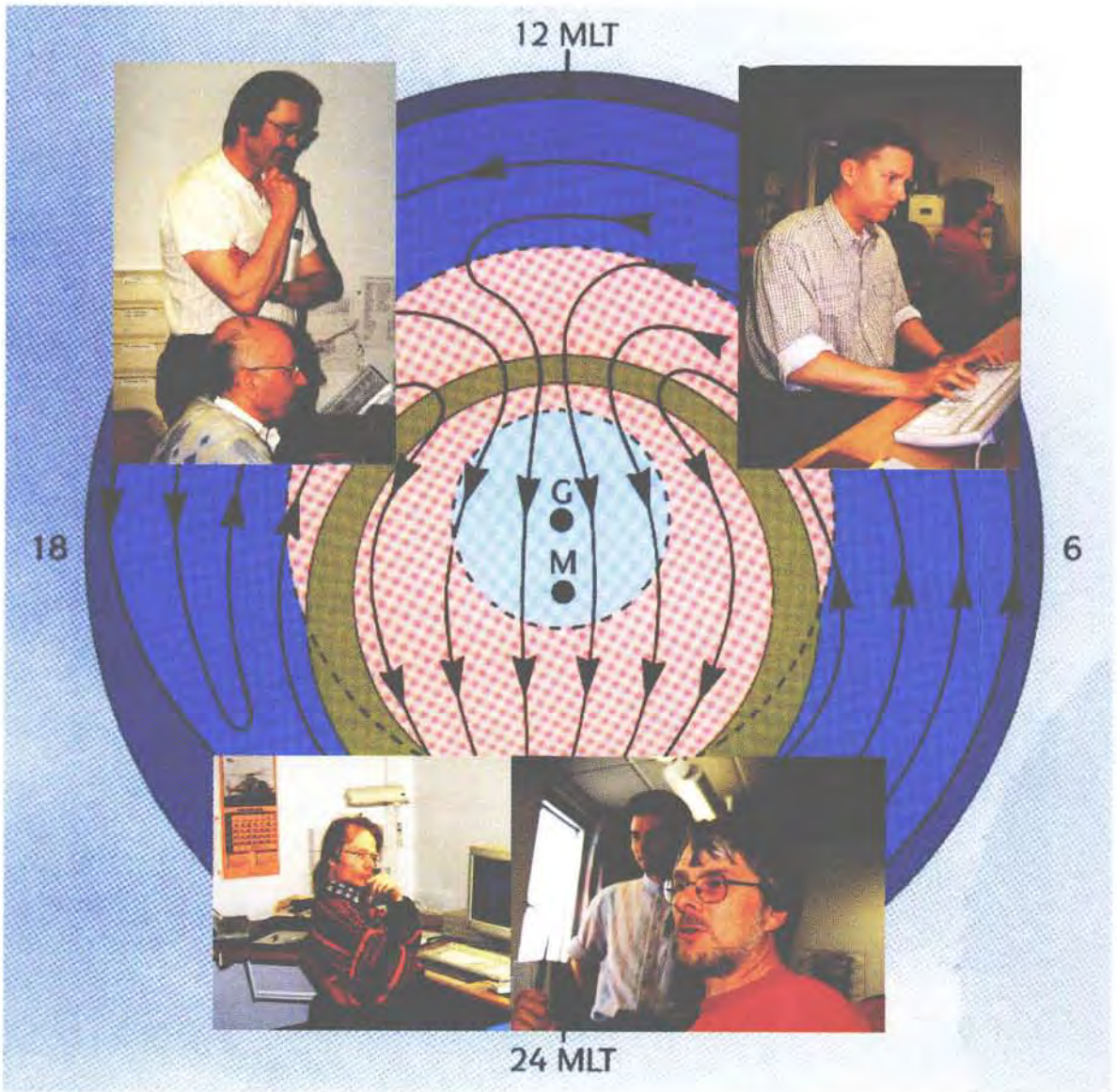

The EISCAT Associates had decided in 1992 to develop and operate a radar facility on Svalbard - the EISCAT Svalbard Radar. The main goal was to study many scientifically exciting ionospheric and atmospheric phenomena in the magnetospheric cusp region and in particular the high latitude plasma convection, as shown in the underlying graph above.

This project is regarded as the most relevant evolutionary step into the future of EISCAT, and the Associates provided additional funds for this purpose.

The design and construction of the EISCAT Svalbard Radar was performed as a special project by EISCAT executive and staff, some of them are shown on the photos taken at the EISCAT Svalbard Radar site during system tests in 1996.

I express my sincere acknowledgement and thanks to all, who were and are involved in this project and who contributed with their unselfish and highly dedicated efforts to reach the milestone of first operation within the projected time scale.

Jürgen Röttger

EISCAT on the World Wide Web

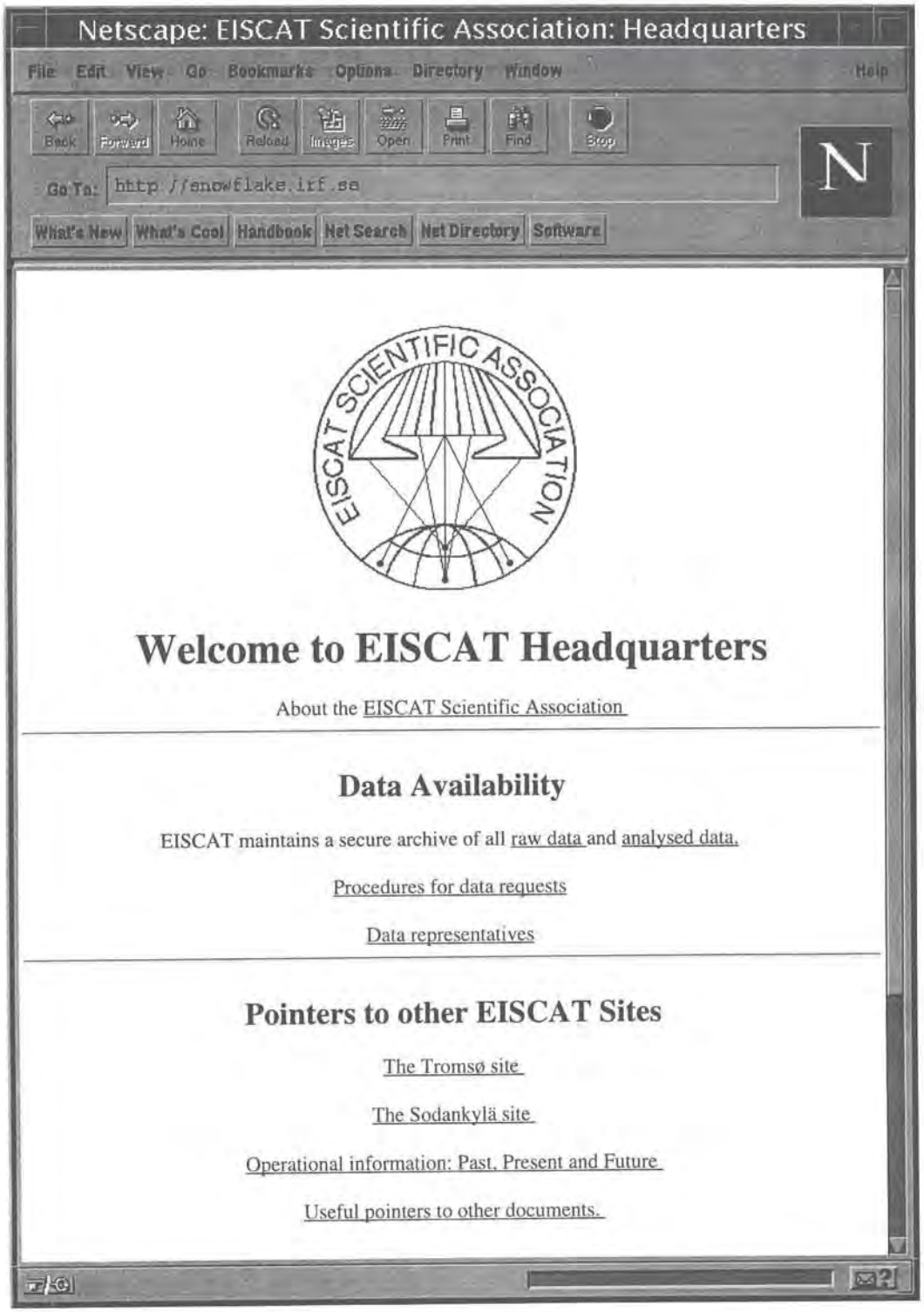

Much of the information concerning the EISCAT facilities, operations, data availability, etc. can be accessed via the World Wide Web. The above figure shows the home page of EISCAT Headquarters in Kiruna (http://snowflake.irf.se). The Tromsø site (http://seldon.eiscat.no) and the Sodankylä site (http://sgo.fi) can also be visited. (Some areas of the servers have access restrictions).

Common Programme Operations During 1994 and 1995

UHF Common Programmes during 1994

94-02-07 22UT 02-09 23UT CP-3-G WD
94-03-15 16UT 03-16 23UT CP-1-K WD
94-04-12 16UT 04-13 22UT CP-1-K WD
94-06-08 16UT 06-09 22UT CP-1-K WD
94-12-06 08UT 12-08 23UT CP-3-G WD
94-12-19 13UT 12-22 23UT CP-2-E

VHF Common Programmes during 1994

94-01-11 07UT 01-14 16UT CP-4-B WD
94-02-07 22UT 09-09 23UT CP-7-E WD
94-03-15 16UT 03-16 23UT CP-6-B WD
94-04-12 16UT 04-13 22UT CP-7-F WD
94-05-03 13UT 05-04 22UT CP-7-F WD
94-05-25 14UT 05-26 22UT CP-6-B
94-07-05 19UT 07-06 22UT CP-4-B WD
94-07-11 17UT 07-12 17UT CP-6-B
94-08-11 17UT 08-13 11UT CP-6-B WD
94-09-06 19UT 09-07 22UT CP-7-F WD
94-10-04 14UT 10-05 24UT CP-7-F WD

UHF Common Programmes during 1995

95-02-01 08UT 02-04 23UT CP-3-G WD
95-02-28 14UT 03-02 17UT CP-1-K WD
95-03-28 15UT 03-29 20UT CP-1-K WD
95-05-22 14UT 05-23 16UT CP-2-E
95-06-20 12UT 06-21 18UT CP-1-K WD
95-07-13 08UT 07-14 14UT CP-1-K
95-09-27 12UT 09-28 16UT CP-1-K WD
95-11-21 11UT 11-22 16UT CP-3-G WD
95-12-18 08UT 12-21 10UT CP-2-E
95-12-21 10UT 12-22 16UT CP-1-K

VHF Common Programmes during 1995

95-02-01 09UT 02-04 08UT CP-7-F WD
95-02-28 14UT 03-02 22UT CP-4-B WD
95-03-28 15UT 03-29 20UT CP-7-F WD
95-05-02 13UT 05-05 05UT CP-6-B WD
95-05-22 12UT 05-23 16UT CP-6-B
95-06-20 12UT 06-21 18UT CP-7-F WD
95-07-13 08UT 07-14 14UT CP-6-B
95-10-24 09UT 10-25 08UT CP-6-B WD
95-10-26 19UT 10-27 16UT CP-6-B WD
95-12-18 09UT 12-22 06UT CP-4-B

Overview of EISCAT Common Programme experiments during 1994 and 1995. WD indicates a World Day operation, the results from which are also sent to the CEDAR data base at NCAR in Boulder, USA.

Operating Modes Employed in 1994/5

Common Programme One, CP-1, uses a fixed transmitting antenna, pointing along the geomagnetic field direction. The three-dimensional velocity and anisotropy in other parameters are measured by means of the receiving stations at Kiruna and Sodankylä (see map, inside front cover). CP-1 is capable of providing results with very good time resolution and is suitable for the study of substorm phenomena, particularly auroral processes where conditions might change rapidly. The basic time resolution is 5 sec. Continuous electric field measurements are derived from the tristatic F-region data. On longer time scales, CP-1 measurements support studies of diurnal changes, such as atmospheric tides, as well as seasonal and solar-cycle variations. The present scheme uses alternating codes and long pulses for ACF measurements, as well as short pulses for power profiles.

Common Programme Two, CP-2, is designed to make measurements from a small, rapid transmitter antenna scan. One aim is to identify wave-like phenomena with length and time scales comparable with, or larger than, the scan (a few tens of km and about ten minutes). The present version consists of a four-position scan which is completed in six minutes. The first three positions form a triangle with vertical, south and south-east positions, while the fourth is aligned with the geomagnetic field. The remote site antennas provide three-dimensional velocity measurements in the F-region. The pulse scheme is identical with that of CP-1.

Common Programme Three, CP-3, covers a 10° latitudinal range in the F-region with a 17-position scan up to 74°N in a 30 minute cycle. The observations are

made in a plane defined by the magnetic meridian through Tromsø, with the remote site antennas making continuous measurements at 275 km altitude. A power profile and long pulse ACFs are measured. The principle aim of CP-3 is the mapping of ionospheric and electrodynamic parameters over a broad latitude range.

Common Programmes One, Two and Three are run on the UHF radar. Three further programmes are designed for use with the VHF system. The UHF and VHF radars were often operated simultaneously during the CP experiments in 1994 and 1995. Such observations offer comprehensive data sets for atmospheric, ionospheric and magnetospheric studies.

Common Programme Four, CP-4, covers geographic latitudes up to almost 80°N (77°N invariant latitude) using a low elevation, split-beam configuration. CP-4 is particularly suitable for studies of high latitude plasma convection and polar cap phenomena.

Common Programme Six, CP-6, is designed for low altitude studies, providing spectral measurements at mesospheric heights. Velocity and electron density are derived from the measurements and the spectra contain information on the aeronomy of the mesosphere. Vertical antenna pointing is normally used.

Common Programme Seven, CP-7, probes high altitudes and is particularly aimed at polar wind studies. The present version uses both of the VHF klystrons and is designed to cover altitudes up to 2500 km vertically above Ramfjordmoen.

(Opposite) An example of common programme results from an operation of CP-1 on 20-21 June, 1995. The plot covers 24 hours, starting at 12 UT on 20 June. The four panels show altitude profiles (along the geomagnetic field direction) between 150 and 600 km of:
(top panel) electron density on a logarithmic scale from $10^{10.1}$ to $10^{11.5}$ m^{-3}
(second panel) electron temperature on a linear scale from 200 to 3000 K
(third panel) ion temperature on a linear scale from 600 to 2000 K
(lower panel) line-of-sight ion velocity on a linear scale from -70 to +70 ms^{-1}, where positive values are away from the radar.
The ionosphere was in sunlight throughout this summer solstice operation, though the diurnal changes in electron density and temperature are still clearly seen, together with more rapid geophysical variations. Impulsive increases in ion temperature are a signature of electric field enhancements (not shown). The ion velocities reveal the presence of persistent wave activity.
These results are from the long pulse modulation in CP-1. These are complemented by those from an alternating code pulse scheme providing improved height resolution for E-region and lower F-region studies, as well as two independent power profile schemes measuring electron density over two different height ranges with different height resolutions.

EISCAT Scientific Association

EISCAT CP1/2 LP 1995 6 20 1200 - 21 1200

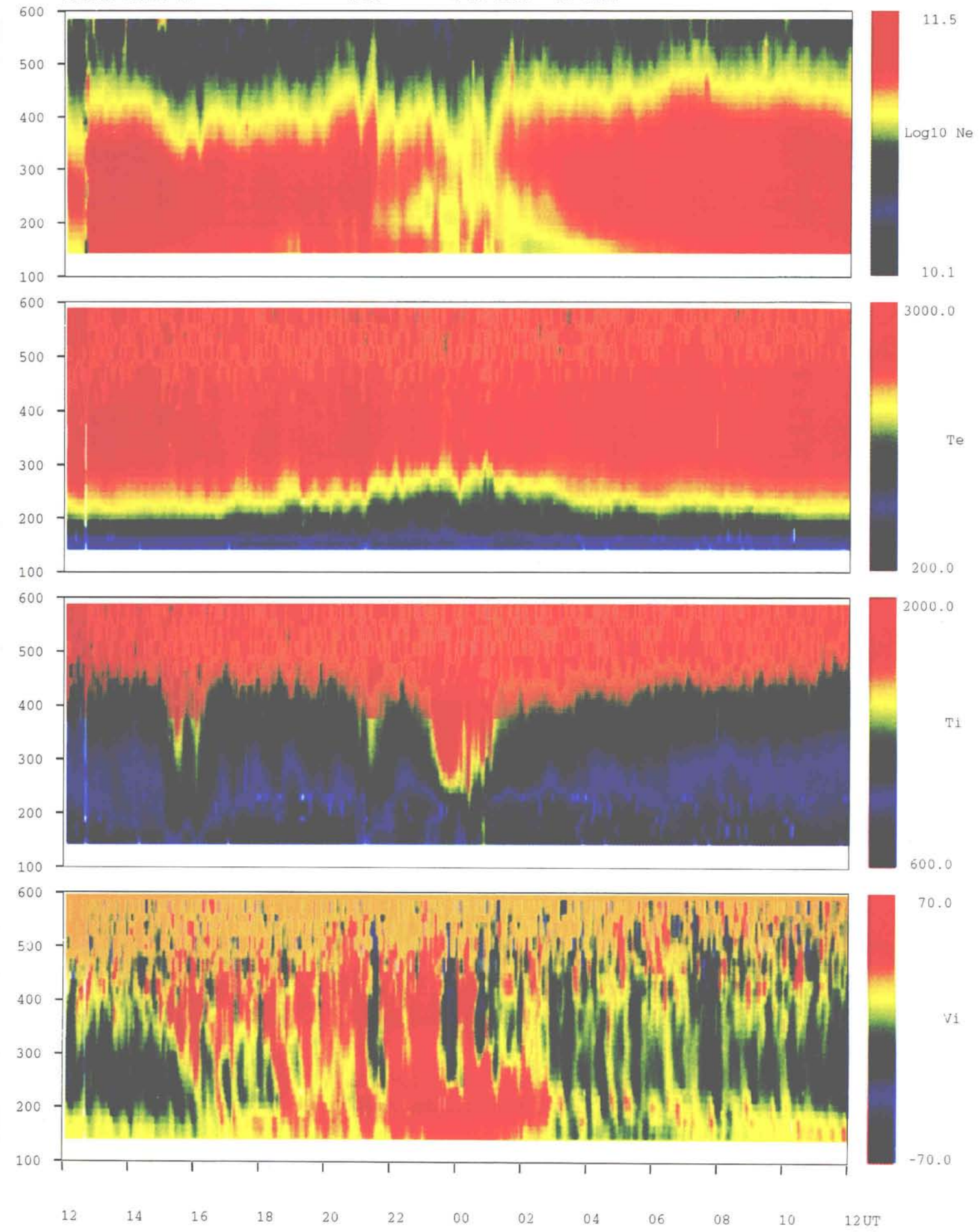

EISCAT Operations 1994-1995

COMMON PROGRAMMES 1994

1994	Jan	Feb	Mar	Apr	May	Jun	Jul	Aug	Sep	Oct	Nov	Dec	Tot	%
CP1			31			30							61	10
CP2												74	74	12
CP3		49										62	111	18
CP4	82						29						111	18
CP6			15		32		24	41					112	18
CP7		24		30	33				27	35			149	24
TOTAL	82	73	46	30	65	30	53	41	27	35	0	136	618	100%
%	13	12	7	5	11	5	9	7	4	6	0	22	100 %	

SPECIAL PROGRAMMES 1994

1994	Jan	Feb	Mar	Apr	May	Jun	Jul	Aug	Sep	Oct	Nov	Dec	Tot	%
EI	2	8				1		1	10	12	3	1	38	10
FI								7		20			27	12
FR	9	16	15			33			50				123	18
GE					19	15		35				21	90	18
NO	14	16					24					2	56	18
SW	19				5		1	14					39	24
UK	80			1	26	6	4	23	3	2	18	78	241	0
TOTAL	124	40	15	1	50	55	29	80	63	34	21	102	614	100%
%	20	7	2	0	8	9	5	13	10	6	3	17	100 %	

COMMON PROGRAMMES 1995

1995	Jan	Feb	Mar	Apr	May	Jun	Jul	Aug	Sep	Oct	Nov	Dec	Tot	%
CP1		6	50			30	15		14			20	135	10
CP2					26							29	55	12
CP3		62									30		92	18
CP4		11	43									52	106	18
CP6					67		30			44			141	18
CP7		33	15			45			28		15		136	24
TOTAL	0	112	108	0	93	75	45	0	42	44	45	101	665	100%
%	0	17	16	0	14	11	7	0	6	7	7	15	100 %	

SPECIAL PROGRAMMES 1995

1995	Jan	Feb	Mar	Apr	May	Jun	Jul	Aug	Sep	Oct	Nov	Dec	Tot	%
3rdP											20		20	2
EI		1			2	3	15	13	2		2		38	4
FI	5										38		43	5
FR	67		75									20	162	5
GE	36	26				30	30		20	5	28		175	18
NO	5		28	18				13			20		84	20
SW	5	10	23	10	14						11	14	87	10
UK	50	68			46	55	5	3	5		43		275	10
TOTAL	168	105	126	28	62	88	50	29	27	5	162	34	884	100%
%	19	12	14	3	7	10	6	3	3	1	18	4	100 %	

These tables show the accounted operating hours for 1994 and 1995 (except where stated as a percentage). The Special Programme time includes 92 hours and 190 hours of Heating operation for 1994 and 1995, respectively.

SCIENTIFIC RESEARCH AND DEVELOPMENTS

The range of topics studied with the EISCAT system, and their associated applications, become increasingly varied and less easy to categorise as the use of the facility continues to expand. This applies particularly in the present case where we are reviewing the highlights of two years' work, rather than the usual one year. In this section we have collected together brief reports and descriptions of studies substantially under way, or published, during 1994-95. This material was mainly contributed by the people directly involved in the various research projects. Following earlier practice, work in progress or in press is referenced by the names of the workers associated with each item, while those published during 1994 or 1995 also include the year. Published papers can be found in the reference list at the end of this Report.

This section on scientific research and developments is organised roughly according to distance from the Earth, commencing with solar wind studies and concluding with the mesosphere. Other categories include ionospheric modification with the EISCAT Heating facility and fundamental aspects of analysis techniques applied to incoherent scatter radar data. It is important to bear in mind, and often obvious from the descriptions of the various topics, that the Earth's atmosphere, ionosphere and magnetosphere, and the solar wind, constitute a coupled system with different degrees of interplay between the components. The section headings should therefore be looked on as a convenient way of organising the material while recognising that some studies comprise several themes and have relevance to a number of areas.

The Solar Wind

EISCAT observations of interplanetary scintillation (IPS) have been used to measure the velocity of the solar wind at distances between 15 and 130 solar radii ($R_\odot$) from the Sun. The first EISCAT observations of IPS were made in 1981 and since 1990 a regular series of measurements have been made. The observations made in the summers of 1994 and 1995 were particularly significant as they were designed to complement the measurements made by the Ulysses spacecraft as it passed over the poles of the Sun.

When in use as an IPS system, EISCAT employs a special detector in the receiver to provide 100 power samples per second. The frequency band of 8 MHz is centred on 931.5 MHz, allowing measurements of weakly-scattered scintillation to be made as close to the Sun as 15 $R_\odot$. A radio source of small angular diameter (for example a quasar) is observed by two of the EISCAT antennae at a time when the parallel lines of sight from the antennae to the source pass through the solar atmosphere in the same radial plane. Under these circumstances, the fluctuations seen in signal strength at the two antennae generally show high correlation, and the time-lag for maximum cross-correlation of the scintillations can be used to estimate the velocity of the solar wind. When the line of sight to the source is in a region of weak scattering (generally true outside 15-25 $R_\odot$) the observed scintillation pattern is simply the weighted average of contributions from the whole line of sight. The baselines between the EISCAT sites are very long, up to 390 km, allowing accurate estimates of the solar wind velocity which makes it

possible to detect the presence of two distinct velocities in the line of sight. An example of an observation of two velocities in the solar wind is shown as Fig. 1a. A revised model for fitting the data was adopted which considered the solar wind to consist of two components, each with small intrinsic rms variation. The results confirmed that this model represented the two-peak correlation functions very well (Fig. 1b).

In the light of this result, the entire data set was re-analysed assuming the presence of a fast and a slow stream in the solar wind. In almost all cases the accuracy of the fit was improved over the single-stream model. When the results were summarised the solar wind velocity was found to have a clear two-component distribution, with fast streams with apparent velocities of ~600-650 kms^{-1} (~750-800 kms^{-1} true velocity) dominating at high latitudes and slow streams dominating at low latitudes. When only clearly dominant streams (contributing more than 70% of the scintillation) are considered these peaks are even more marked: these results have led to a view of the solar wind as consisting of fast (800 kms^{-1}) and slow (400 kms^{-1}) streams, with any intermediate velocities arising from the interaction of fast and slow streams.

EISCAT observations can be directly related to coronal features by mapping the IPS line of sight back on to a white-light map produced by a coronagraph. The well-established connection between fast streams of solar wind and regions of open magnetic flux (coronal holes) is confirmed by the observations, while regions in which fast and slow streams are interacting appear to give rise to velocities intermediate between the normal fast and slow speeds. These results represent a major advance in IPS observations of the solar wind. The observations of fast stream / slow stream interactions suggest that EISCAT is capable of detailed studies of co-rotating interaction regions much closer to the Sun than has hitherto been possible.

EISCAT has also been used to study the variation of solar wind velocity with distance from the Sun. Fig. 2a summarises measurements made between 1993 and 1995 at all heliographic latitudes. The solid lines are the mean apparent velocities of the fast and slow streams: there is no evidence in these data of any variation of fast or slow stream velocity with radial distance, suggesting that the acceleration region of the solar wind lies inside 15 $R_\odot$ for fast streams and inside 25 $R_\odot$ for slow streams. The fast stream results have been extended in a series of co-ordinated observations involving EISCAT and the VLA. These results are shown in Fig. 2b and indicate that the acceleration of the fast solar wind at high heliographic latitudes lies inside 10 $R_\odot$, while velocity estimates inferred from white-light measurements indicate that the acceleration region may be inside 5 $R_\odot$. This result is most unexpected and places severe constraints on any model seeking to explain the acceleration of the solar wind. This demonstration that the fast solar wind reaches its final (Ulysses) velocity so close to the Sun is perhaps the most important result yet produced by EISCAT in its role as an IPS system.

The results of EISCAT observations of IPS during 1994 and 1995 confirm EISCAT as the finest ground-based instrument available for study of the solar wind. Having provided a data set that is complementary to the observations made by Ulysses, EISCAT is now well placed to do the same with SOHO and WIND during the period of increasing solar activity (Breen, Coles, Esser, Grall, Klinglesmith, Løvhaug, J. Markkanen, Misawa, Moran, Tegid and Williams).

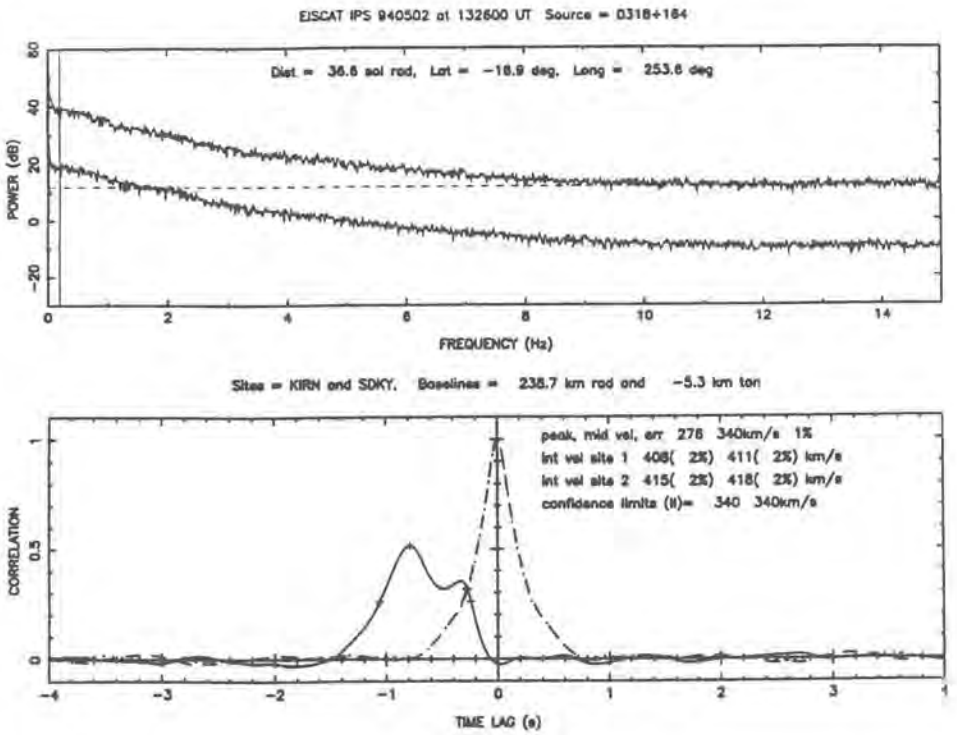

Fig. 1(a). The IPS spectra for the radio source 0318+164 observed from Kiruna and Sodankylä on 2 May 1994 and the corresponding correlation functions. The cross-correlation function shows two clear peaks, suggesting that there are two streams of solar wind present in the IPS line of sight.

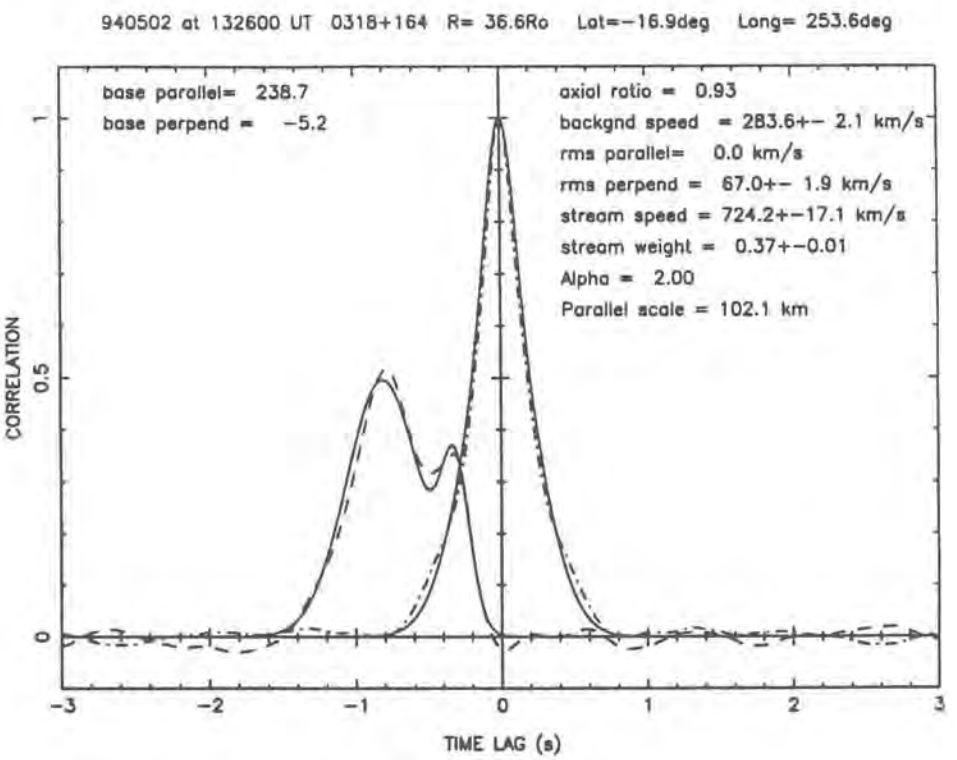

Fig. 1(b) Correlation functions for 0318+164 on 2 May 1994 fitted using the two-velocity model. Observed correlation functions are shown as dashed lines, model fits as solid lines.

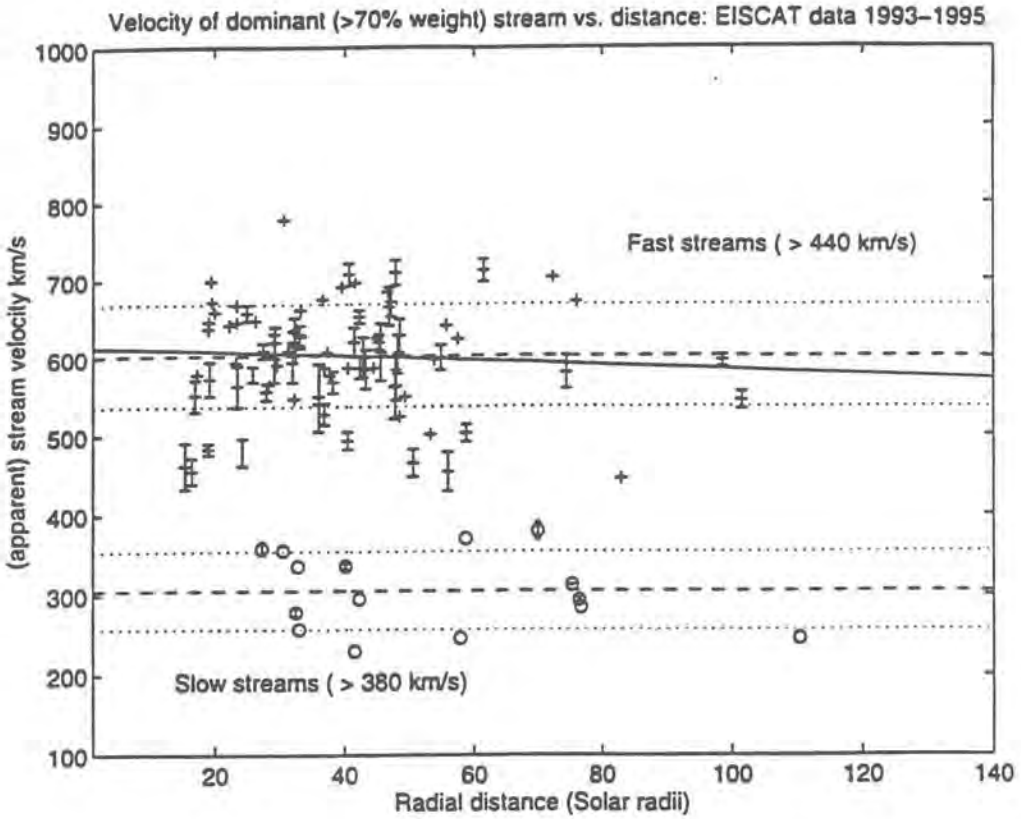

Fig. 2(a). Variation with radial distance of dominant stream velocity. Data from 1993-1995.

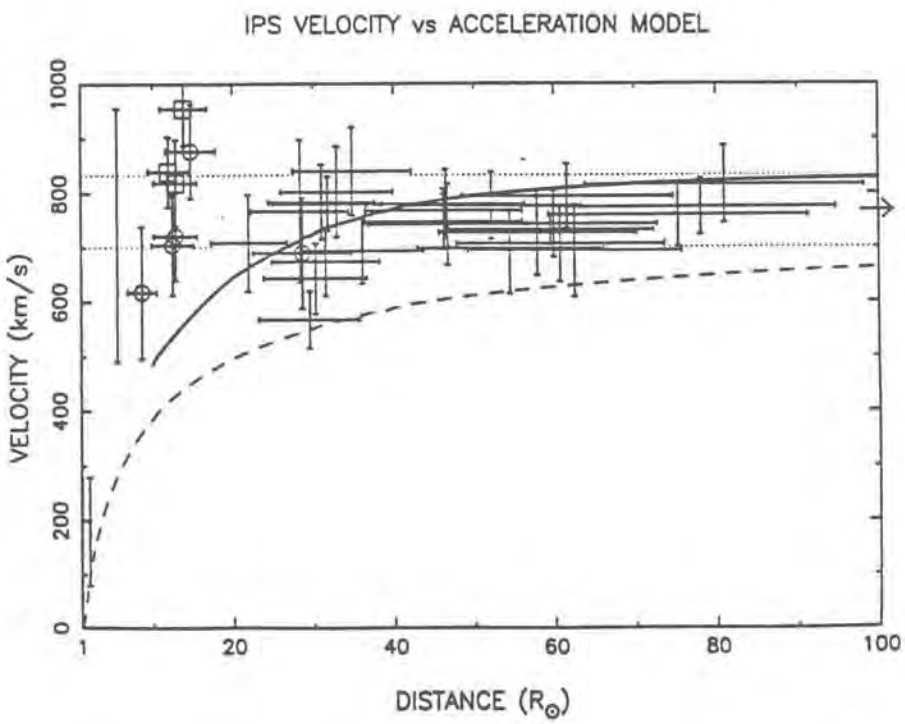

Fig. 2(b) Variation of velocity of high-latitude fast streams determined from EISCAT and VLA measurements.

Ionospheric Modification

Fig. 3 shows EISCAT VHF-observations from an EISCAT/Heating campaign in May 1994. At the top of the graph are presented 10 spectral gates of heater induced up-shifted plasma line (VHF-UPL) and below these are 10 gates of the corresponding ion line (VHF-ION). The gate distance is only 300 m, so the whole series of gates covers 3 km in altitude. In the lower plasma line gates we see very pronounced line spectra; in two cases they only consist of a strong first decay line. In the higher gates broad unstructured spectra are observed. So far, this result is similar to an observation that was already presented in the EISCAT Annual Report 1993, except that in these new data a gap appears between these two kinds of spectra, so there are actually two separate altitude regions of excitation. There are, however, some more experimental differences. First, in the 1994 observations there were additional power profiles with high altitude resolution that are shown in the lower part of Fig. 3. In the plasma line power two peaks appear about 2 km apart, which correspond well with the two regions of excitation in the plasma line spectra. In the ion spectra hardly any excitation is seen in the lower gates (different from the results of 1993), while the higher gates corresponding to the broad spectra in the plasma line gates show strong unstructured ion spectra. The respective power profile shows only one peak between 246 km and 247 km altitude corresponding to the second peak in the plasma line power profile. In the 1994 campaign there was also a chirped channel whose results are shown at the bottom of Fig. 3 (CHIRP). As the chirp technique (see separate section) converts altitude differences into frequency differences the chirp spectra are double humped, and the frequency difference between the two peaks corresponds to 2 km, which is in agreement with the other observations. For the future it would be interesting to investigate the relationship between plasma line and ion line intensities theoretically. This may lead to further insight into the nature of the involved processes (Kohl and Rietveld).

In the EISCAT Annual Report 1993 it was reported that third harmonics of the ion acoustic frequency sometimes appeared in the ion line spectra. An interaction between the first cascade in the decay spectrum and the HF pump was considered as a possible explanation. Indeed, a calculation using an extended Zakharov model has confirmed this suggestion. The calculation was performed for a wave number $k = 9.4\ m^{-1}$ (VHF radar), for a heater frequency of $f_h = 4.5$ MHz and for three slightly different plasma frequencies f_p that are given at the right hand side of Fig. 4, which presents the results of the calculation. From top to bottom, spectra for the oscillating two stream instability, the first decay line, and the first cascade line are shown in the left hand part of Fig. 4. They appear at different plasma frequencies, because a constant wavenumber was assumed. The right hand side of Fig. 4 shows the corresponding ion spectra, where the calculated third harmonics appear at a plasma frequency of 4876.6 kHz (Kohl and Rietveld).

Large-scale changes in the electron density which occur during artificial modification of the ionosphere are expected to lead to the focusing and defocusing of radio waves propagating through the affected region. The effect of a Gaussian-shaped increase in electron density calculated for the ray paths of a radio signal propagating obliquely through the heated region is depicted in Fig. 5. In this figure it is clear that the ray density, a quantity which is closely related to the signal strength, has been reduced by RF heating at locations in the vicinity of the receiver site. Measurements of the unheated elec

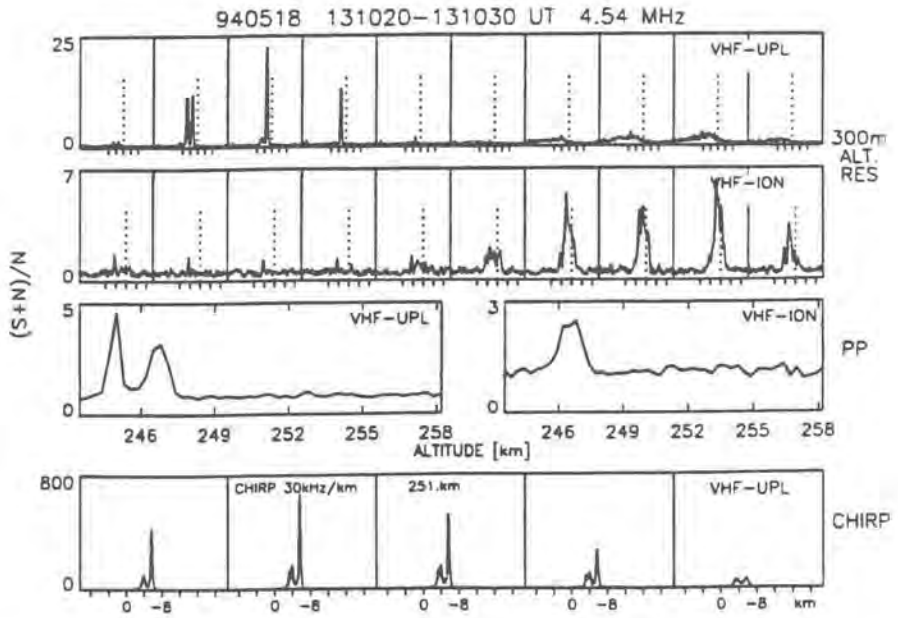

Fig. 3. From top to bottom: 10 gates of upshifted plasma line spectra with 300 m gate distance (VHF-UPL), where the dotted line corresponds to the heater frequency and the frequency marks are 10 kHz apart; the corresponding 10 gates of ion line spectra (VHF-ION); plasma line and ion line power profiles (PP); a chirped channel (CHIRP) also for upshifted plasma line spectra. Five gates with 4.8 km distance were measured. The frequency scale was replaced by a relative altitude scale, where '0' is 251 km actual altitude.

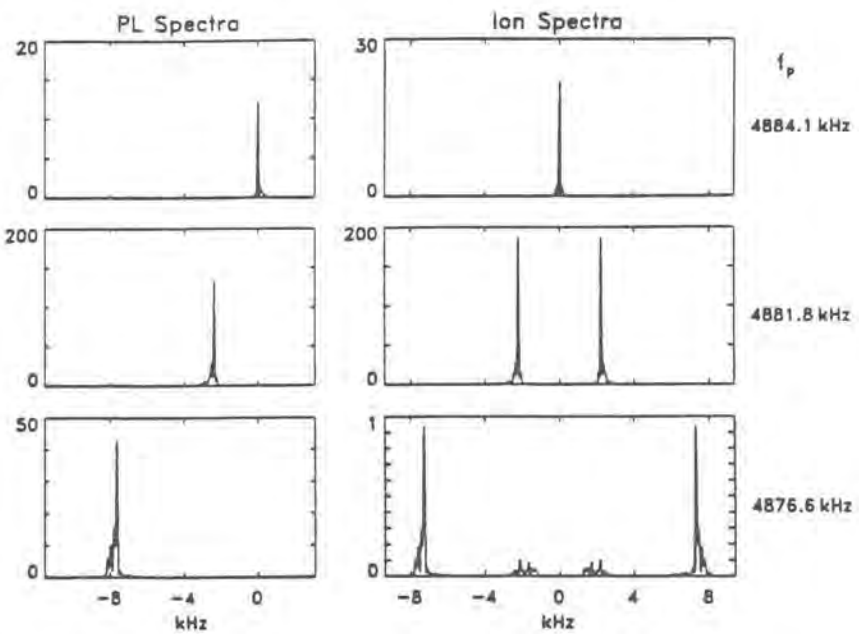

Fig. 4. Calculated plasma line spectra (left) and ion spectra (right) for three slightly different plasma frequencies noted at the right edge of the figure. A heater frequency f_h= 4.9 MHz and a wavenumber k= 9.4 m^{-1} (VHF-radar) were assumed. From top to bottom the spectra represent the oscillating two-stream instability, the first decay line and the first cascade line together with the corresponding ion spectra. The third harmonic of the ion acoustic frequency appears in the lower right panel of the Figure.

tron density profile made by the EISCAT UHF radar have been employed in these calculations. Observations consistent with such defocusing have been made for waves reflected in both the E-and F-regions (Stocker, Robinson, Jones, Stubbe).

Robinson et al. (1995) have presented the first direct observations of artificial modification of the auroral electrojet. A series of experiments have now been conducted during which the E-region has been artificially heated under a variety of electrojet conditions. Fig. 6 illustrates some preliminary results from these experiments, which indicate that the electron temperature changes caused by RF heating are reduced for increasing electrojet currents. During an EISCAT heating campaign in February 1995 the effects of RF heating on naturally occurring Farley-Buneman irregularities, which are responsible for electron heating in the electrojet, were investigated. The experiments indicated that, under certain conditions, the effect of the heater was to reduce the electrojet temperature in agreement with earlier theoretical predictions (Robinson, 1994). Fig. 6 illustrates this heater-induced cooling effect. The upper panel depicts the E x B drift speed. In the lower panel, the 'off' curve represents an average electron temperature during heater off whilst the 'on' curve was obtained during heater on. Normal heating is apparent after 1830 UT when the electrojet was absent. However, during two periods of intense electrojet flow, just before 1600 UT and just after 17:30 UT the anomalous cooling effect is apparent.

The first heating campaign utilising the CUTLASS system was undertaken in May/June 1995, soon after the Finnish component of CUTLASS became operational. F-region heating was carried out in conjunction with a multitude of diagnostics which included the CUTLASS HF radar, the RAPIER mobile VHF radar, Leicester HF radio diagnostics, stimulated electromagnetic emission receivers and the EISCAT UHF radar. Fig. 7 illustrates data obtained from simultaneous observations of electron temperature (EISCAT, upper panel), anomalous absorption (HF radio diagnostic amplitude, middle panel) and field aligned irregularity amplitudes (CUTLASS backscatter intensity). These results confirm the view that small scale field-aligned irregularities are responsible for anomalous absorption and anomalous pump heating (Robinson et al., 1995).

In recent heating experiments performed at Tromsø, the anomalous absorption, the spectrum of the reflected heater wave and the electron temperature enhancement have been measured. A number of effects occur when the heater transmits at frequencies close to harmonics of the electron gyro-frequency. These effects include a reduction in the level of anomalous absorption, electron temperature enhancement and diagnostic signal strength, and changes in the intensity and frequency distribution of features in the spectrum of the reflected heater wave (Honary et al., 1995). Although significant progress has been made in understanding these results, and recent theoretical work has demonstrated that anomalous absorption, electron temperature enhancement, and down-shifted maximum (which are all related to the presence of small scale striations) are considerably reduced close to the electron gyroharmonics, there are other observations as yet not understood. The unexpected minimum in the level of signal strength for the period of no heating immediately after the pump has operated at the third gyro-harmonic is among those which cannot be explained by existing theories. One possible mechanism is the generation of fast electrons which in turn could produce ionised patches responsible for scattering radio waves and therefore

causing the observed reduction in the received diagnostic signal strength. To investigate the possibility of generation of highly energetic electrons (in the keV range), when heating close to the third electron gyro-harmonic, EISCAT observations of heater-induced down-shifted and upshifted plasma-line spectra, and power profiles of ion-line and plasma-line, were made in June 1995. It was found that the so-called ion-line overshoot usually present in the EISCAT ion-line spectrum during the first few seconds after heater switch-on persisted at varying strengths while the heater was transmitting at frequencies close to the third electron gyro-harmonic. In addition, the strength of both heater-induced ion-line and plasma-line were at least a factor of two greater when the heater was operating close to the third gyro-harmonic. Although no direct evidence of the presence of energetic electrons was observed in the June 1995 campaign, the theory regarding the production of fast electrons at frequencies close to the electron gyro-harmonics cannot be ruled out since the EISCAT experiment that was carried out was not the optimum design for looking at enhanced plasma lines due to energetic electrons.

Heater-induced scintillation has been observed for the first time by an imaging riometer (IRIS, located at Kilpisjärvi). The coverage area of this system includes a wide range of altitudes above Tromsø, providing a useful diagnostic for ionospheric modification experiments. Simultaneous observations of heater-induced scintillation (using data from IRIS beams that intersect the heated volume in the F-region above Tromsø) and heater-induced absorption (using data from IRIS beams which intersect the heated E-region above Tromsø) have been made. For this experiment, which was carried out in June 1995, an O-mode pump wave was transmitted along the local geomagnetic field line into the F-region above Tromsø, while the heater induced scintillation of radio noise from Cassiopeia-A was observed in the IRIS beams directed towards the heated volume. It was found that heater-induced irregularities with 1-2 km scale sizes were generated. The growth and relaxation times for these field-aligned irregularities are approximately 1 and 2 minutes respectively (Honary).

Since 1993, the EISCAT Heating Facility at Tromsø has been used to make diagnostics of the ionosphere by the API-technique, a resonance scattering method based on generation of Artificial Periodic Irregularities. In the lower D-region, the API signals are primarily due to the changes in the electron attachment rate during heating. Thus the API technique should be useful for investigations of the negative ion chemistry.

In a typical API experiment, heating is on for 4 seconds and off for 16 seconds. A detailed ion chemistry scheme was used to interpret the API experiment data measured at Ramfjordmoen on 15 September, 1994. A D-region ion chemistry model with 55 ion components was used. The Sodankylä Ion Chemistry (SIC) model was developed as an alternative approach to those D-region ion chemistry models which combine the more doubtful chemical reactions to effective parameters whose values are set against experimental data. The model covers the altitude range from 45 to 120 km. The altitude coverage of the API data, relevant to this comparison, was from 45 to 70 km.

As a first approximation, it is assumed that the electron temperature is doubled in the time-scale of milliseconds when heating is switched on. Since the chemical response times are known to be much slower, the time behaviour can be simply calculated by studying what happens to

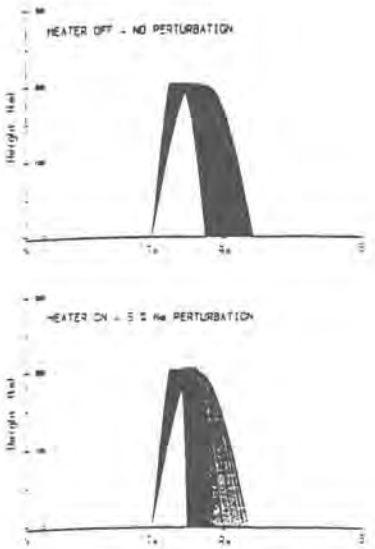

Fig. 5. Effect of a gaussian-shaped increase in electron density on the ray paths of a signal propagating obliquely through a heated region. The ray density is reduced by RF heating at locations close to the receiver (Rx) site.

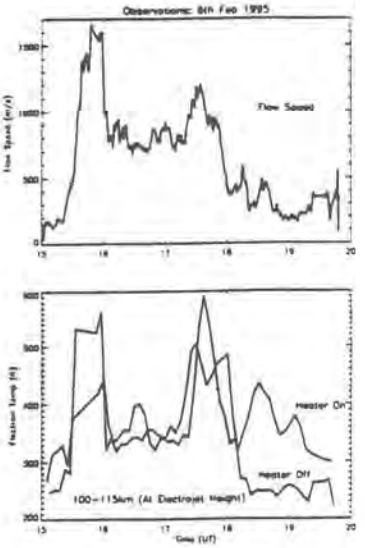

Fig. 6. EISCAT measurements of the F-region plasma flow speed (top panel) and the electron temperature in the E-region (100 - 115 km) during intervals when the heater was off or on.

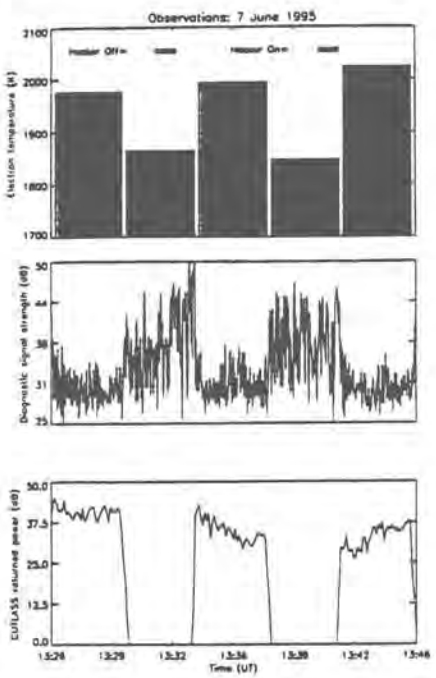

Fig.7. Electron temperature measured during an interval of heater induced irregularities observed by CUTLASS. The electron temperatures are in the top panel, the HF diagnostic signal strength in the middle panel and the CUTLASS returned power from the range beam cell above Tromsø is in the bottom panel.

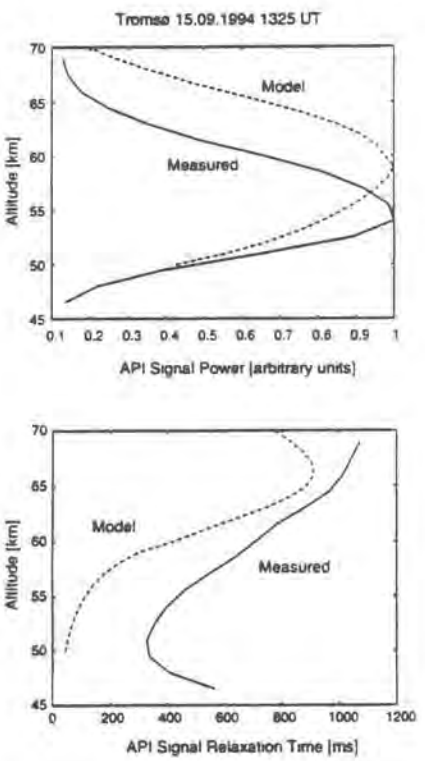

Fig. 8. Comparison between the measured and model values of signal relaxation times (upper panel) and relative signal power (lower panel) for the API experiment at Tromsø on 15 September, 1994, 1325 UT.

the equilibrium ion concentrations when the electron temperature is doubled for 4 seconds and then halved back to the normal value for 16 seconds.

As a result of the model calculations the time behaviour of each ion concentration during the API cycle is obtained. The positive ions are unaffected by the API heating cycle. The concentration of negative ions responds rapidly to the heating, so that during 4 seconds a decrease of 12% in electron density is observed in the example case at the altitude of 70 km. When heating is switched off the electron concentration relaxes to the equilibrium value, with a characteristic time which can then be compared with the measured API signal relaxation times. The most important ions responsible for the rapid electron concentration changes appear to be O_2^-, CO_3^- and CO_4^-.

Fig. 8 shows the comparison between measured and model values of signal relaxation times and relative signal power. Model calculations were done in the altitude range between 50 and 70 km. The form of the model profiles of API signal power is in good agreement with the measurements, except that the altitude of maximum signal is a few km higher in the model. The relaxation times show a corresponding behaviour. At the higher altitudes the smallest deviation between the model and measurements is only of the order of 10%. At the lower altitudes the model fails to reproduce the measured relaxation times, Note that in this comparison no adjustments were made to the model parameters. Values from MSIS-90 were used for the neutral atmosphere. Thus the API measurement has potential to verify unknown parameters in the ion chemistry (E. Turunen, Matveinen, Rietveld, Goncharov).

The Chirp Technique

The incoherent scatter chirp technique was simultaneously operated on the EISCAT VHF and UHF radar systems for the first time in April 1995 and was successfully used to observe simultaneous day-time natural and HF-enhanced plasma lines on both radars. The radar experiments contained several data channels in addition to the chirp, including multi-pulse spectra with 1 kHz frequency and 300 m range resolution, standard and 300 m resolution power profiles, long pulse ion line ACF measurements, and UHF remote site measurements.

An interesting example that vividly illustrates the power of these techniques and the puzzling physical processes involved in HF-ionosphere interaction experiments is shown in Fig. 9. The top channels show spectra during a 2-sec HF-off cycle while the bottom panels show spectra during the previous cycle with HF-on. The left panels show spectra from unchirped channels while the spectra on the right panels are from chirped channels. The bandwidth of each channel is 0.5 MHz. The HF frequency was 4.913 MHz. Note that the VHF radar (a) measured only the up-shifted side-band and the UHF radar (b) measured only the down-shifted sideband. The data in both figures were taken simultaneously. However, the UHF antenna was pointed along the geomagnetic field direction while the VHF antenna was vertical. Thus the data are not collocated. Both figures show HF-enhanced plasma line spectra during HF-on and both show a weak natural plasma line during HF-off in the chirped channels as well. The intensities of these signals were below the detectability threshold of the unchirped channels, demonstrating the power of the chirp technique.

The VHF data show that there were four layers present during the HF-on period.

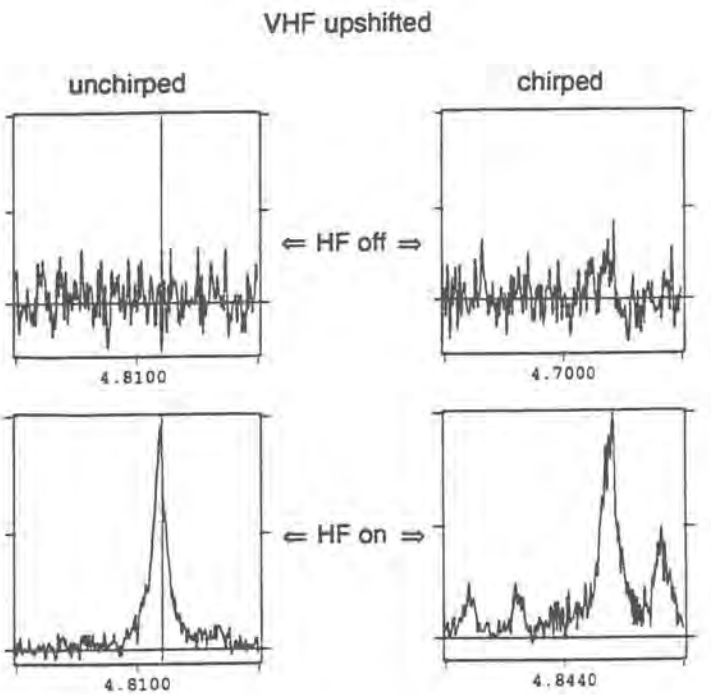

Fig. 9(a). Upshifted plasma line spectra measured with the VHF radar. The vertical axis is self-normalised spectral power in arbitrary units. The horizontal axis is frequency covering a bandwidth of 1 MHz. The top panels were measured during a heater off cycle of 2 s and the bottom panels during the previous cycle with heater on. The transmitter pulse was not chirped for the left panels while it was for the right.

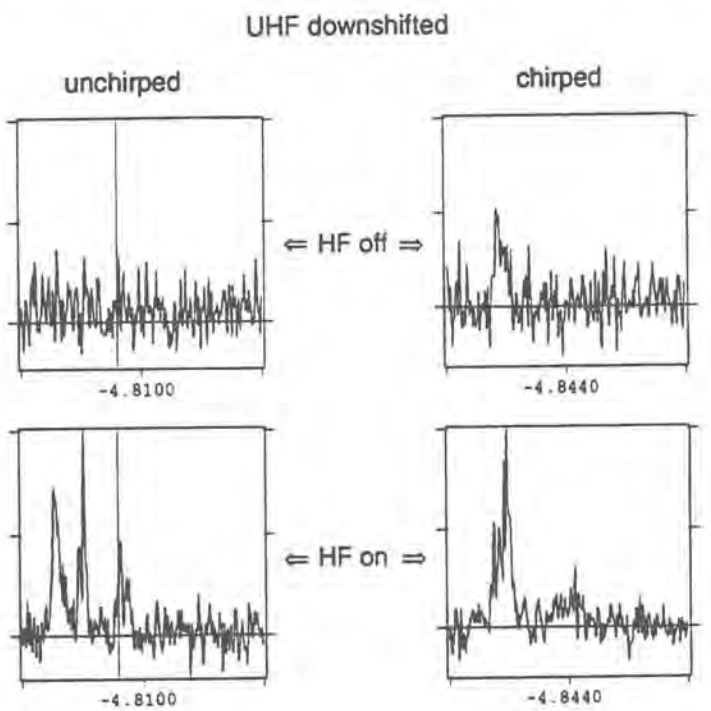

Fig. 9(b). Down-shifted plasma line spectra measured with the UHF radar. See (a) for additional explanation. The measurements shown in (a) and (b) were taken simultaneously.

This can be understood as follows. Only one line appears in the unchirped channel. This is because the altitude resolution of the chirped and unchirped gates (nominally 39.6 km) is larger than the separation between the layers, causing spectral lines which are distinct in height but identical in frequency to be summed at one frequency. On the other hand, four lines appear in the chirped channel. This is because of the varying carrier modulation frequency imposed by the chirp, which produces a frequency shift proportional to the relative height of any excitation observed within each gate. In effect, the chirped channel functions as an altitude analyser. From other measurements we know that the two lower-frequency (left-most) lines are aliased from the high-frequency side of the spectrum. Taking into account the chirp rate employed (30 kHz/km) and the frequency shift of the lines, the three new layers must lie below the usual HF-enhanced region with a spacing of about 7 km between adjacent layers.

Curiously enough, the simultaneous, although in this case not co-located, UHF measurements show precisely the opposite behaviour during HF-on, namely multiple spectral lines in the unchirped spectrum which map into one line in the chirped spectrum. The unchirped channel reveals the normal HF-enhanced plasma line (HFPL) lying at the HF pump frequency (indicated by the solid vertical line) and two out-shifted lines approximately -150 and -300 kHz from the normal enhanced line. In contrast there are only two lines in the chirped channel. From chirped and unchirped data containing only the HFPL, we know that the weaker line, located at about -4.8 MHz on the chirped plot, is the HFPL. The strong line is thus the chirped manifestation of the two out-shifted lines. This implies that the out-shifted lines lie on a frequency/height profile determined by the chirp rate, with the consequence that they map on top of each other to produce a single chirped line. The frequency/height profile is in fact the natural Langmuir frequency profile, as is shown by the natural plasma line which appears at the same frequency in the chirp channel during the HF-off period. The out-shifted lines are thus enhanced natural plasma lines, similar or perhaps identical to the free mode lines seen during Arecibo HF interaction experiments. Theory suggests that Arecibo free mode lines are excited by processes induced by the HF pump near the reflection height. The existence of such a process at EISCAT is shown by the HFPL, shifted in the chirped channel by about +300 kHz from the frequency of the natural Langmuir line. From the 30 kHz/km chirp rate we know that this corresponds to a point of origin for the HFPL of about 10 km higher than that where the UHF radar detects the natural plasma line, which is roughly the reflection height.

The physical processes leading to the complex structures observed during these measurements are not well-understood at present. One of the primary goals is to take advantage of simultaneous VHF and UHF data taken using a variety of techniques, including chirp, to provide constraints sufficient to assist in the formulation of a clear theoretical picture of high power HF-ionosphere interactions. (La Hoz, Isham, Leyser, Rietveld and Hagfors).

Data Analysis and Techniques

The self-noise, which is generated by the uncorrelated scatter of the transmitted signal from all simultaneously illuminated altitudes, makes an important contribution to the accuracy of incoherent scatter measurements, when the snr is high. Although the self-noise is often taken into account in calculating the

variances of the observations, the fact that it gives rise to a significant correlation between observations is normally neglected. Numerical estimates show that covariances of measurements are important for long pulse and alternating code measurements. If they are not included in the error estimation, a factor of two underestimation may result for errors from long pulse measurements, and a factor of 1.5 error for alternating codes. The covariances are important for typical long pulse experiments even for a low snr because the experiments are oversampled.

As the mutual covariances and self-noise are important for alternating codes but not for multipulses, they both must be included when the relative accuracy of multipulse and alternating code experiments is studied. When the multipulse version (H) and the alternating code version (K) of EISCAT CP-1 experiments are compared, the latter is better when the snr is less than 10%, that is, in most practical cases. The accuracy of the alternating codes is especially good in the velocity determination. The conclusion is that the alternating codes combine a superior performance at low snr with a good one at high snr (Huuskonen and Lehtinen).

A normal alternating code experiment gives equal lag and range resolutions. In the EISCAT CP1K experiment, for instance, both resolutions are 21 μs, which is adequate in the E-region, where the plasma scale height is small and the plasma autocorrelation function long. When approaching the upper E-region and lower F-region the plasma scale height gets larger and the autocorrelation function shorter, and equal lag and range resolutions are not the optimum combination any more. Adding range gates together is a solution to the problem, but the correlations between adjacent gates, which often exist in alternating codes experiments because of high snr, reduce the speed gain by range integration.

Adding two or three gates together results in a speed gain of 1.5 or 2 only, instead of a factor of 2 or 3 valid for a low snr. Similar restrictions hold if analysis results from adjacent range gates are averaged. A better solution is to use an alternating code, where the basic baud is longer than the sampling interval. Some of the first alternating code experiments with the EISCAT UHF radar used this method, but the complicated data processing and analysis have limited its application. Fractionally sampled alternating codes are advantageous in many respects. If double oversampling is used (baud length is 30 μs and sampling interval 15 μs), and 30 μs resolution is used in the data analysis, the experiment is 1.5-2 times faster than a standard alternating code experiment using a 15 μs baud. At a very low snr the speed increase is 2.5 fold. The use of the fractional principle will now be easy with the advent of fast signal processors and general analysis programs, and the standard alternating code experiments for the ESR will use the fractional alternating code principle (Huuskonen, Lehtinen, Pirttilä).

The GUISDAP system for design and analysis of IS measurements has been developed to be used as the main tool for ESR experiment design and analysis. This work involves the restructuring and rewriting of the programs in the C language. The development of an object-oriented solution to the rather complex task of describing an arbitrary incoherent scatter experiment in a general and accurate enough way to facilitate fully automatic analysis of any kinds of measurements in one fixed program package forms the core of this work.

The first applications of the new GUISDAP package have been in the full

profile analysis of IS data. By fitting whole plasma parameter profiles over the ionosphere, instead of point values of the parameters supposed to be approximately constant over small range intervals, full profile analysis is free of underlying assumptions about the slow variation of the plasma parameters as a function of range. Full profile analysis was defined as a mathematical inversion problem formalism and it was compared to the traditional gated analysis as an inverse problem.

The bias introduced to traditional analysis results using realistic model ionospheres was studied. By applying the full profile method to data generated from the model ionospheres, it was demonstrated that full profile analysis is free from this kind of bias. Fig. 10 shows an example of analysis of real data by full profile and gated analysis. The parameter grid spacing is 6 km below the 150 km altitude, 12 km up to the 200 km altitude, and either 36 km (full circles, solid line) or 24 km (crosses, dashed line) above the 200 km altitude. The model parameter profiles are given by the thin solid line and the gated analysis results of the long pulse data by the open circles (Lehtinen, Huuskonen, Pirttilä).

In modern incoherent scatter measurements very complicated coding schemes are used to achieve the necessary statistical accuracy in the measurements. The ambiguity functions specify how the measurement weights the plasma autocorrelation function in the two-dimensional space of range and lag. Alternatively one can work in the space of range and frequency, and it is necessary to derive the ambiguity (instrument, weighting) functions also in terms of these variables. The theory of ambiguity functions and the use of lag profiles as tools of describing arbitrary kinds of incoherent scatter measurements have been summarised, including a discussion of how the formalism is used in the GUISDAP (Grand Unified Incoherent Scatter Design and Analysis Package) software, Fig. 11 (Lehtinen and Huuskonen).

An extremely powerful method for finding strong alternating codes has been discovered. A search up to a length of 4194304 bits has been carried out, which means that codes for any practical purpose are now available. The method was discovered by studying the regularities hidden in the known codes of 8D32 bits, and it has an interesting property that the search can be converted into a domino game with special symbols depending on the code length (M. Markkanen and Nygrén).

A theoretical study has been made of the errors introduced by random noise in velocity measurements made by a full-fit analysis. The study first considered two narrow frequency bands equally spaced on either side of the transmitted frequency. The results from these were then integrated over the ion-acoustic spectrum for values of T_e/T_i lying between 1.0 and 3.0. Small corrections were added to take into account the convolution of the ion-acoustic spectrum with the spectrum of the transmitted signal, and any further convolution introduced in the correlator. The effect of subtracting the mean noise power from a number of background gates was also calculated.

The observed level of noise error was determined from CP-4-A data by comparing analysed results from the six closely-spaced but independent channels, where the same pulse code was transmitted in the same direction simultaneously. The variance in the values of plasma velocity is a measure of the square of the random noise error, and by binning the data according to the predicted error level the mean variance could be calculated.

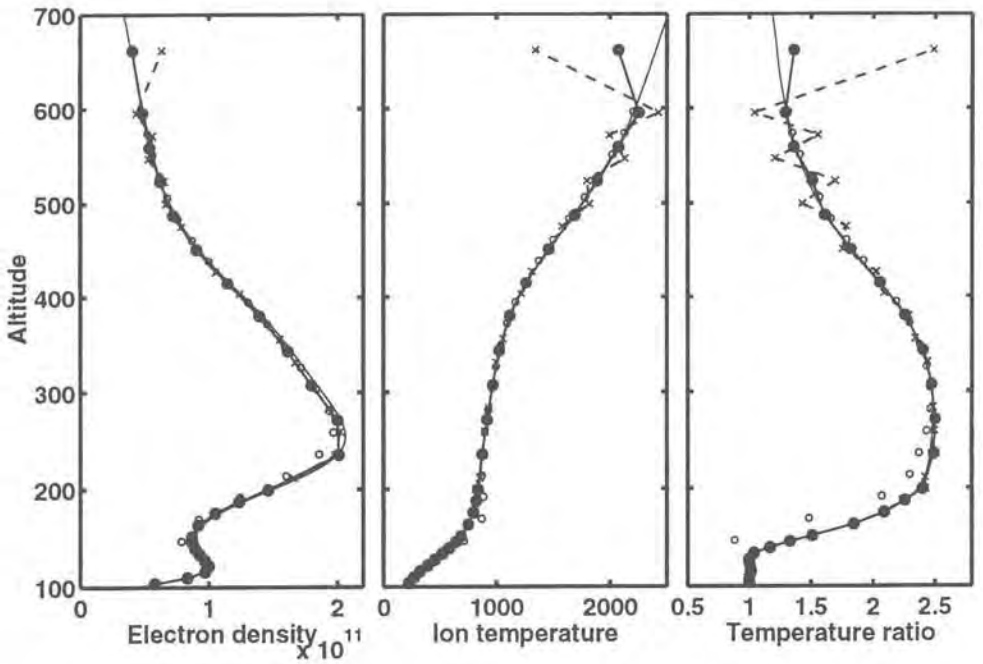

Fig. 10. Full profile analysis results (full circles) of EISCAT UHF data measured on February 16, 1993, at 1110--1140 UT. The parameter grid spacing is 6 km below the 150 km altitude, 12 km up to the 200 km altitude, and 30 km above the 200 km altitude. The gated analysis results of the long pulse data by the open circles.

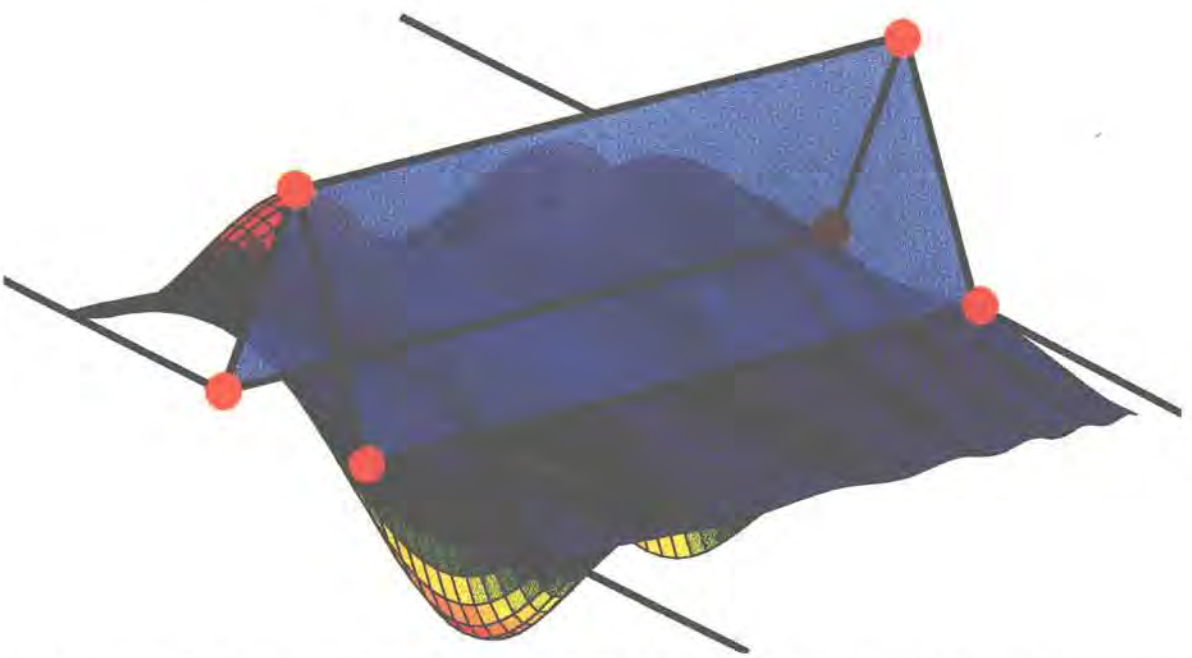

Fig. 11. The internal operations in GUISDAP: a two-dimensional frequency(x) vs range(y) ambiguity function is shown together with a base spline for linear interpolation for coefficient calculations. Several thousands of instrument functions like this are calculated and related to models of height-dependent ionospheres. Most of the cpu time in the initialisation for full profile analysis is used in the calculation of such functions, which are then stored and applied subsequently in the non-linear fits of plasma parameter profiles to measured data.

When the observed rms error in plasma velocity was plotted against the error predicted theoretically, the results give a slope of 0.991 with a correlation coefficient as high as 99.3% (Fig. 12).

A general formula, which takes into account all sources of error except the convolution of the spectrum by the transmitted signal and in the correlator, has been determined. In the case of CP-4-A, convolution increases the error level by 8%, and a similar increase will apply in all long-pulse experiments - but the exact value needs to be calculated depending on pulse length and radar wavelength (Williams, Etemadi, McCrea, Todd).

It has long been recognised that in the presence of sharp spatial or temporal changes in F-region plasma velocity, beam-swinging by a single antenna is incapable of measuring the full vector of the velocity. Not only is the technique incapable of monitoring any high-frequency, small-scale variations in velocity, but when these occur they even result in the generation of entirely spurious components in the calculated vector.

This has been demonstrated by simulating the steady passage of a quiet auroral arc over the site of a single antenna which is measuring components of plasma velocity over a scanning cycle. EISCAT tristatic measurements have established that such an arc is characterised by a very narrow region of low electric field coinciding with the arc and a parallel band of greatly enhanced electric field. The simulation shows that single-antenna beam-swinging measurements seriously underestimate the strength of the enhanced electric field, fail to observe the narrow region of very low electric field, and generate a second band of enhanced electric field which is totally spurious (Figs 13a, 13b).

However, reliable results can be obtained from a single site if simultaneous measurements are made in three non-planar directions. If the spatial variation of plasma velocity associated with the feature follows a fixed pattern as it drifts through the three beams, cross-correlation of scalar measurements, such as electron concentration or ion temperature, (or alternatively dynasonde measurements) can be used to determine the drift velocity of the feature, and appropriate time-shifts can be applied to the three components of plasma velocity before they are combined to give the full vector. When this is done the three-antenna measurements faithfully represent the main features (Figs 13c, 13d).

A similar result occurs when the boundary marking a sharp reversal in plasma velocity passes over the radar. This analysis justifies the construction of a multi-antenna capability at Longyearbyen. Such a multi-antenna facility will provide the further advantage of improved sensitivity for topside, field-aligned measurements and will, in general, offer great flexibility in the operation of the ESR. The full benefits will require three antennas but the advantages of two antennas are so great that the addition of a second antenna is the highest priority (Williams, 1995).

Reconnection and Flux Transfer

Studies of dayside auroral and flow transients have continued using the EISCAT UHF and VHF radars, the IMAGE magnetometer chain and optical instruments on Svalbard. These studies are revealing a distinction between two classes of phenomena, namely poleward-moving auroral events, with associated flow bursts, and travelling convection vortices (TCVs). The combined observations also reveal poleward-moving auroral forms which break away from the poleward edge of the background cusp/cleft aurora.

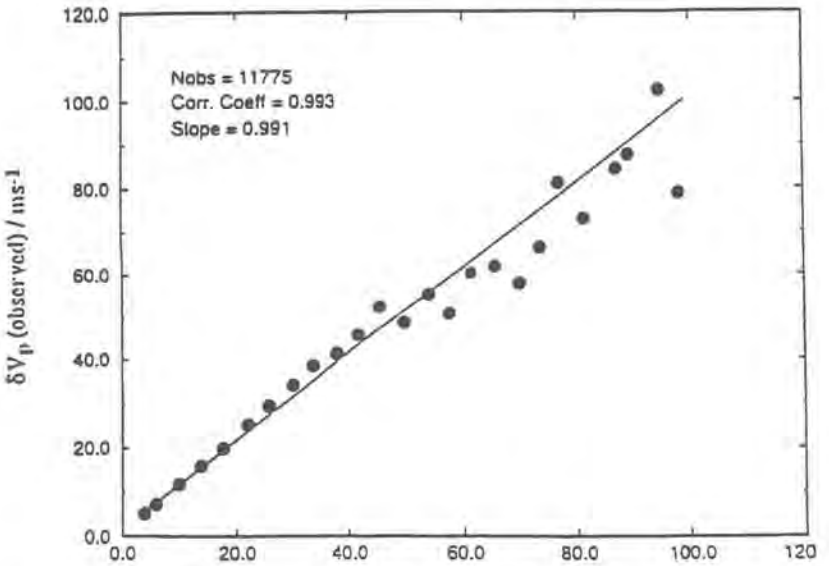

Fig. 12. Relationship between the predicted and observed values of the rms error in measuring plasma velocity (data analysed by the full-fit method).

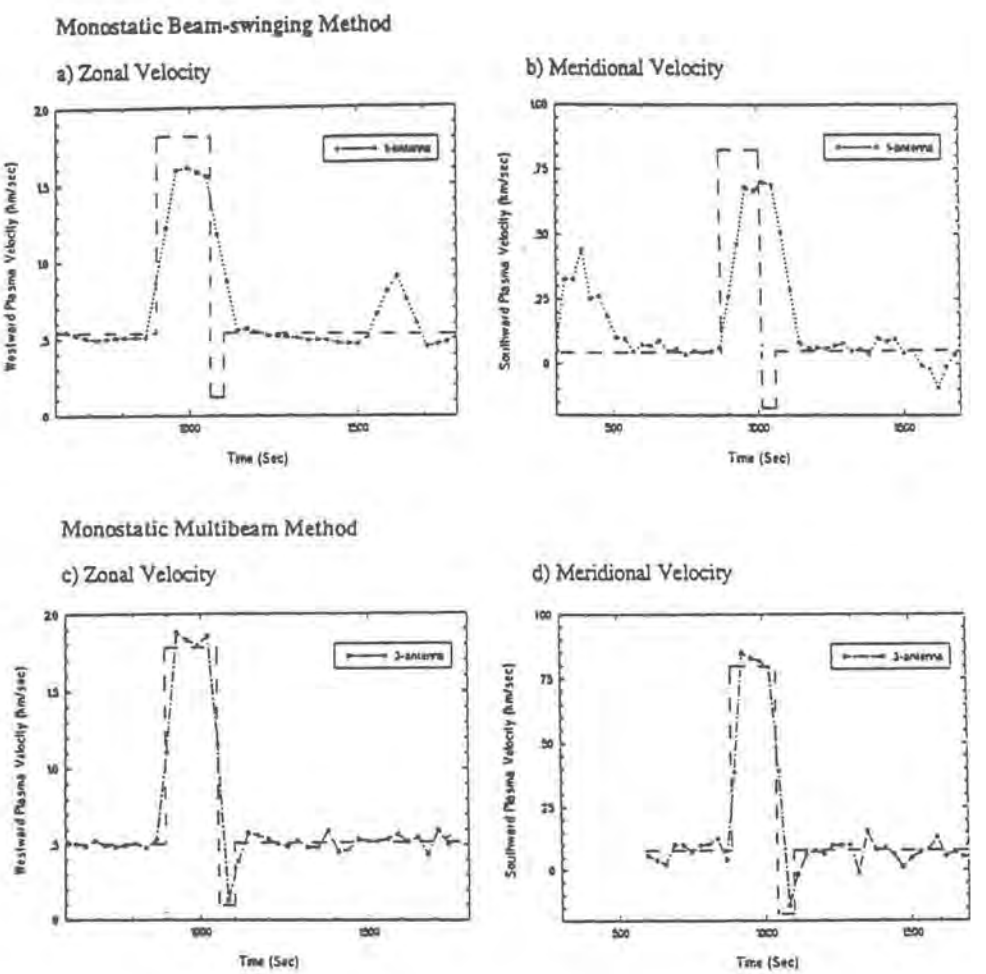

Fig. 13. A comparison of the simulated results obtained by a monostatic single-antenna beam-swinging method and a monostatic three-antenna multibeam method when observing an auroral arc drifting over the radar.

Modelling has shown that this background aurora can consist of a sequence of these events with each one abutted equatorward of its predecessor and all events drifting poleward. Such events, which also move eastward under magnetic tension, show the new feature forming at the equatorward edge of the band of 630 nm emission shortly before the old event fades at its poleward edge. Because of this overlap in the event lifetimes, the 630 nm band is continuously present. The EISCAT data show that within the events the flow is greatly enhanced. The combined data show that these events are consistent with the theory that they are produced by transient reconnection bursts, and inconsistent with a rival theory that they are caused by changes in the dawn-dusk component of the magnetosheath field for steady reconnection. The data show that the reconnection rate is at least 13 times greater in the pulses than it was between them (Davis, Lockwood, Palmer).

EISCAT data have provided a vital complement to inferred variations of the magnetopause reconnection rate from low-altitude cusp ion observations, studied in collaboration with Phillips Laboratory. These data have been used to show that the cusp ion step is indeed the result of temporal, rather than spatial, variations in the reconnection rate, by providing the associated plasma flow at and around the step and also by revealing the poleward-moving events predicted by the temporal theory. In addition, comparison of the cusp ion data with the interval between the events seen by the radars tells us the field-aligned distance from the ionosphere to the reconnection site. Using this, and the line-of-sight convection velocity seen by the meridionally-pointing UHF radar, the reconnection rate can be computed as a function of time. The results from a close conjunction of the DMSP-F10 satellite with the field-of-view of the EISCAT radars, operating in the CONV mode, are shown in Fig. 14. Two clear pulses of reconnection are revealed, separated by an interval of no detectable reconnection. The accuracy of this technique has been assessed using numerical simulation and found to be consistent with the uncertainties shown in the figure, which are derived from the instrument characteristics. The best estimate of the reconnection X-line position is $16\,R_E$ from the ionosphere, which places it at low magnetic latitudes on the dayside (Lockwood et al., 1995).

Large Scale Electrodynamics and Convection

In a continuation of several studies of the proper motion of auroral arcs (Haerendel et al., 1993) earlier measurements from 1988 and 1992 have been analysed, and new optical observations in the magnetic zenith of Tromsø have been used together with CP-3 data to investigate the large- and small-scale electrodynamics of auroral arcs.

The studies emphasized the comparison of normal motions of auroral arcs near magnetic zenith of Kiruna with the plasma velocities measured by EISCAT. Relative motions between arcs and the background plasma of the order of $200\ ms^{-1}$ were found. The existence of plasma flows through auroral arcs and changes of the tangential velocity of plasma traversing the arcs could be determined (Fig. 15). Generally, the results confirm the origin of auroral arcs from the breakdown of magnetic flux freezing in thin current layers at high altitudes, and from the resulting appearance of strong parallel electric fields. The plasma flow is interpreted in terms of the inflow or outflow of energy to or from the current system which drives the primary electron precipitation in the upward directed field

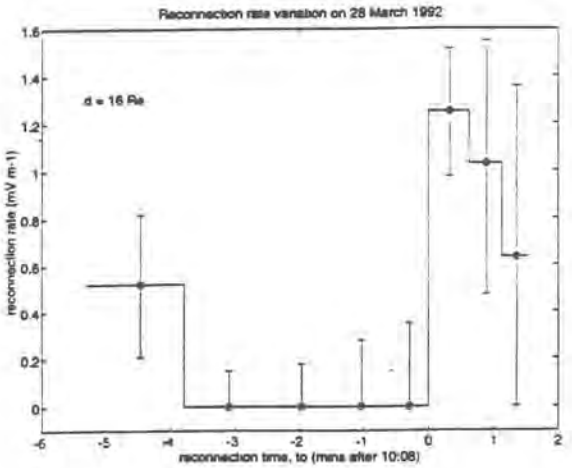

Fig. 14. Reconnection rate variation derived from combined EISCAT and DMSP-F10 observations of the cusp on 28 March 1992. The reconnection is shown to occur in two separated pulses at an X-line which is of order 16 R_E from the ionosphere.

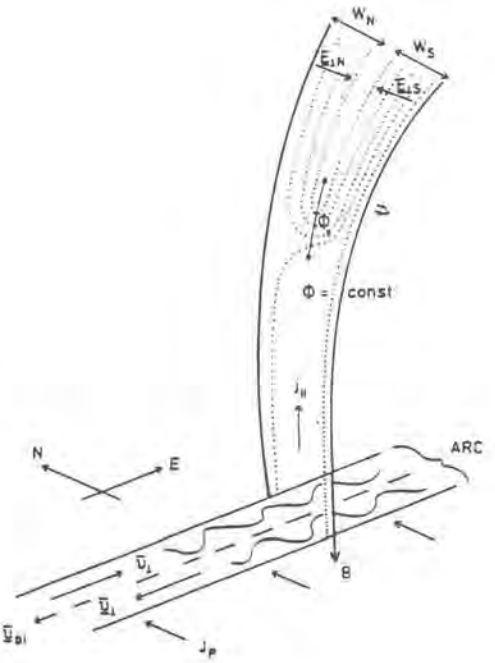

Fig. 16. Framework for the interpretation of the motions of auroral small-scale structures and of their counterflow signature. The apparent velocities $v_\perp$ of the luminous features are traced back to E-W drifts of density irregularities inside and above the auroral acceleration region. Electric fields and potentials deduced from the observed value of $v_\perp$ and their widths are only of the order of the true quantities at the level of the acceleration region.

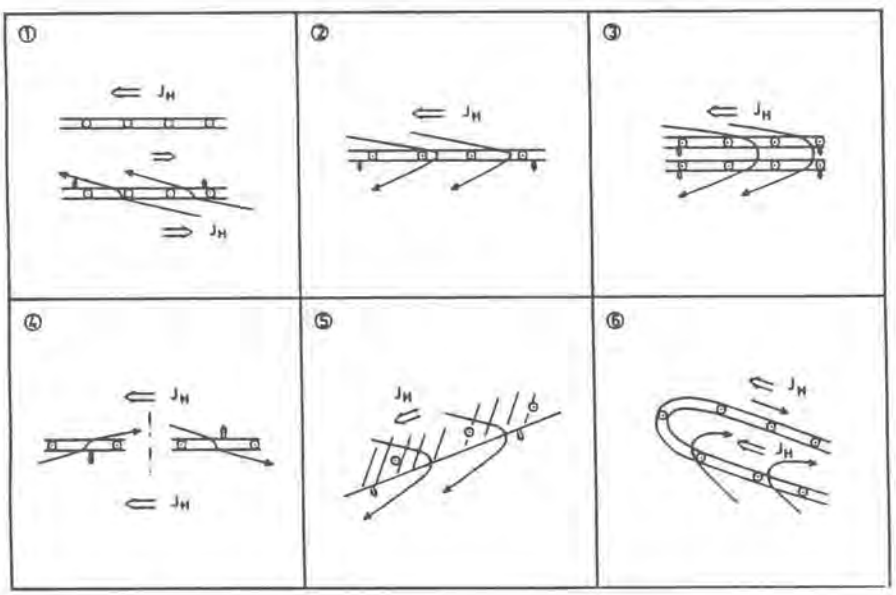

Fig. 15. Schematic summary of the observed plasma flow relative to the auroral arcs (curved arrowed lines), the velocity of the arc in the arc normal direction relative to the observer (short double arrows), and the Hall current.

aligned current sheet of the auroral arc (Frey et al.).

Other studies concentrated on the comparison of apparent motions of auroral arcs and small-scale structures with plasma motions in the adjacent F-region. A large difference between the velocity of folds and curls, moving along the arcs with average velocities of 10 to 20 kms^{-1}, and of the tangential plasma flow at 300 km altitude with velocities of 0.3 to 0.8 kms^{-1} could be determined. Additionally, for all luminous bands exhibiting fast motions of small-scale structures, the direction of this motion was westward on the equatorward edge and on most occasions, a fainter eastward directed counterflow could be observed on the poleward edge. This is interpreted as a manifestation of physical motions of small-scale structures in the local plasma environment of the auroral acceleration region. The attendant electric fields are shorted out by parallel potential drops and the counterflow is the visible expression of the existence of a U-shaped potential (Fig. 16). The asymmetry in brightness, definition, and speed of the counterflowing folds and curls is attributed to their location at the leading or trailing edge of the arc propagating relative to the plasma frame and the current circuit (Haerendel et al.)

A travelling convection vortices (TCV) event has been studied extensively during a coordinated ground-based observational campaign comprising EISCAT radar, IMAGE magnetometer and optical measurements on Svalbard. EISCAT was operated with the UHF beam directed towards magnetic north and the VHF beam towards geographic north. During the passage of a TCV, identified in the magnetic field recordings, bursts of plasma flows with alternating directions southward, northward, southward were observed. A westward speed of the structures of 2.5 kms^{-1} was deduced from the magnetic field measurements. Fig. 17 shows line-of-sight (los) velocities obtained by the UHF and VHF radars, and the overlaid white arrows represent equivalent plasma convections deduced from nearby magnetic field observations. The north/south component of the convection arrows are in good qualitative agreement with the los-velocities, therefore the east/west component can be used to complement the EISCAT measurements.

From Fig. 17 two convection cells with opposite senses of rotation result. Since the event is moving through the radar beams from east to west, and if we assume that the temporal changes are small during the passage, we may interpret the observed variations as a scan through the current system. The time scale across the bottom has deliberately been chosen that for a velocity of 2.5 kms^{-1} the spatial scales in the north/south and east/west directions are the same. Fig. 17 thus shows for the first time an undistorted picture of the shape of the vortices and furthermore it allows the distance between the vortex centres to be estimated as 820 km. Convection vortices in the ionosphere are manifestations of field-aligned current (FAC) filaments. According to the sense of rotation we expect a downward directed FAC in the western cell and an upward one in the eastern cell. Comparisons with optical observations reveal that discrete auroras sometimes show up in association with the upward FAC, but only at certain spots. There is no band of auroras tracking the path of TCVs. We may conclude that the FACs originating from the low latitude boundary layer are only rarely connected to regions containing a plasma population that can excite auroral emissions (Luhr, Lockwood, Sandholt, Hansen).

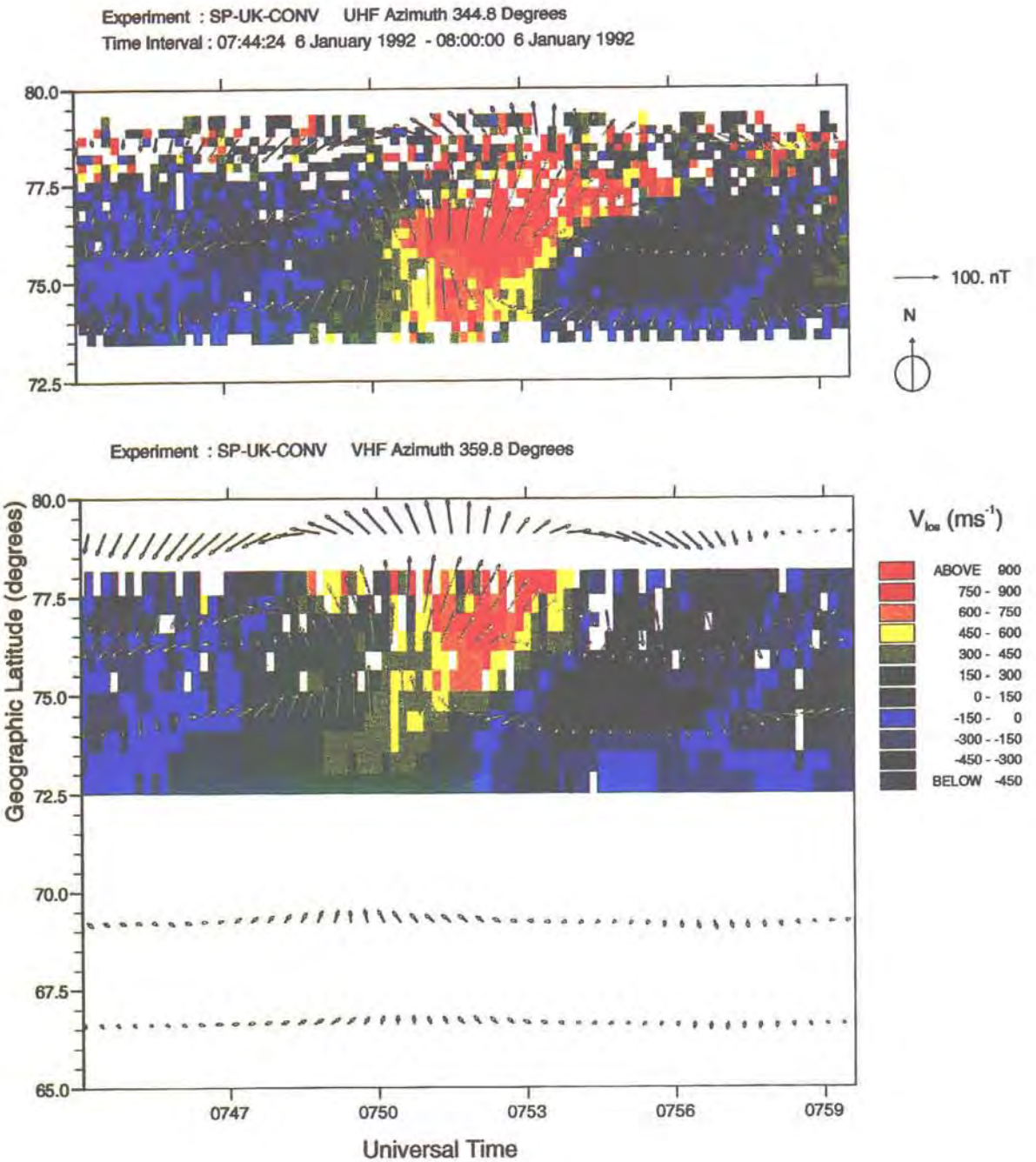

Fig. 17. Line-of-sight velocities observed during the passage of a travelling convection vortices event. Positive values denote velocities towards magnetic north in the upper panel and toward geographic north in the lower panel. The white arrows represent equivalent plasma convections deduced from magnetic field recordings of nearby stations. The two sets of measurements have been corrected for propagation delays taking into account the longitudinal separation of the various sites. Two convection vortices with opposite senses of rotation can be identified.

Statistical analyses of the main parameters of ionospheric electrodynamics from the EISCAT data base provide a large-scale description of the auroral processes in the stable conditions that prevail before the development of any time-dependent event. These can be used in a variety of investigations, for example the relevance and limits of theories.

Fluid theories generally explain the origin of region-2 field-aligned currents by the closure of the ring current, itself driven by the azimuthal pressure gradients generated in the inner magnetosphere during the sunward convection. The linearised equations of the adiabatic convection predict a phase quadrature in local time between the distributions of the convection potential and of region-2 field-aligned currents. On the other hand, statistics performed from the EISCAT data base for periods of moderate activity reveal a rotation toward the phase opposition. These experimental results are attributed to the effects of non-adiabatic processes, in particular of magnetospheric ion losses mainly by precipitation into the ionosphere, which are neglected in the linear adiabatic formulation.

The large-scale convection of the auroral ionospheric plasma strongly depends on the coupling processes with the magnetosphere, such as the precipitating fluxes of magnetospheric particles into the ionosphere and the flow of field-aligned currents between both regions, which develop during the sunward transport of the magnetospheric plasma injected from the geomagnetic tail. The resulting modification of the electrodynamical properties of the ionospheric plasma induces a variation of the electric field distribution at ionospheric altitudes. It is then transmitted along magnetic field lines to the magnetosphere, where in turn it affects the plasma transport and the magnetosphere/ionosphere coupling processes. Finally, the description of the ionospheric plasma convection requires taking into account the whole loop of these feedback effects between the ionosphere and the magnetosphere. For this purpose, a self-consistent and time-dependent numerical model has been constructed, making use of the finite element technique. In a first approach, the code was run to simulate the evolution of the convection from an initial state in the absence any magnetospheric and coupling processes, up to reach the steady state with a continuous injection of magnetospheric plasma from the tail, its sunward transport, and the associated development of couplings. The numerical results in the steady state were found to be comparable to available statistical observations of electric fields and currents from EISCAT and of precipitation fluxes from the satellite DMSP. An example is given in Fig. 18 with the polar distribution of observed and simulated field-aligned currents in conditions of stable and moderate magnetic activity. This numerical tool allowed an evaluation of the individual effects of field-aligned currents and precipitation on the large-scale convection observed at auroral latitude, and on its penetration toward lower latitudes (Peymirat and Fontaine, 1994).

Topside Ionosphere

Previous studies have shown that at altitudes above about 600 km, inelastic collisions for electrons become negligible compared to coulomb collisions As a consequence, the field-aligned transport of the energy is conservative above 600 km. This property has been used to propose a method of inferring the topside heat flow from the topside measurement of the electron temperature profile, as well as the F-region heat flow from the classical Fourier law. Using two case studies of summer and winter observations, it was shown that the F2 -region

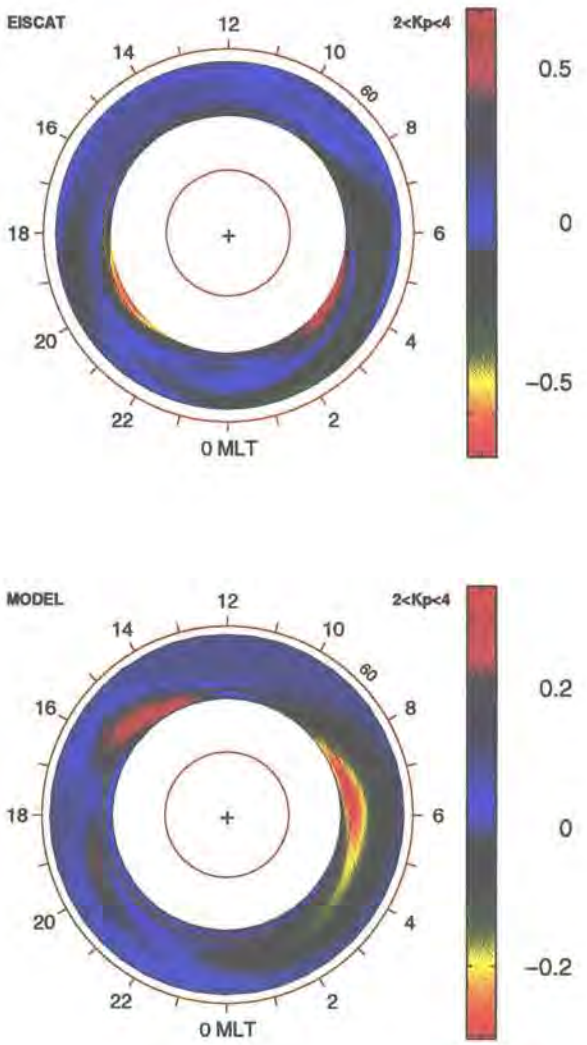

Fig. 18. Polar representation of field-aligned currents by EISCAT (top) and computed by the numerical model in similar conditions (bottom panel). The intensities are comparable. On the night side, EISCAT observes a small part of the region-1 currents, which are not included in the simulations. The poleward shift of the simulated region-2 currents is attributed to the use of a dipolar magnetic field model which maps the magnetospheric processes at more poleward latitudes than the reality. Positive values are currents flowing into the ionosphere.

heat flow is mainly controlled by the EUV solar heating, with larger downward heat flows in summer than in winter. Also, the passage of the terminators (in the winter case) cause significant increases of the downward heat flow, due to the energy transfer from the still sunlit high altitude regions down to the lower altitudes already in the dark. The topside heat flow showed weaker diurnal variations than at F2 heights, for the winter period, and a quite constant heat flow in the summer case; this confirms that the topside heat flow is not significantly controlled by the solar EUV flux but rather results from magnetosphere-ionosphere coupling (Blelly and Alcaydé, 1994).

Intermittent variations were also studied by Blelly et Alcaydé (1994), who showed that events of large O^+ ion outflows and of large electron temperatures were associated with large increases of both the estimated F2 and topside downward heat flow. Such increases could be due to upward currents and it was shown that the enhancements of the electron temperatures up to 7000 K, and the O^+ outflows up to 800 ms^{-1}, were associated with estimated upward currents of about 14 mAm^{-2}. It was subsequently shown, on the basis of numerical modelling using a fluid approach, that such currents are able to heat the electron gas up to the observed temperatures, and that the pressure gradients set up by this heating can lead to an acceleration of the O^+ ions of the same magnitude as the observed velocities (Blelly, Robineau, Alcaydé).

Observations from the UK Special Program UFIS have contributed to an investigation into plasma outflows from the topside ionosphere. The UFIS (Up-Flowing Ions) experiment employs the UHF and VHF radars operating together in the vertical pointing direction. A run of

approximately six hours commenced at 21:00 UT on 17 January 1990. Three occurrences of outward ion flow were observed, with vertical velocities of up to 300 ms^{-1} at 800 km altitude detected. At 22:00 UT, an outflow was observed (Fig. 19a) simultaneous with an interval of ion frictional heating (panel b). The vertical ion temperature was enhanced by some 2000 K at 500 km altitude. The frictional heating of the ions resulted from an enhanced zonal plasma drift (panel c), corresponding to a meridional electric field of up to 60 mVm^{-1}. Directly following the ion outflow, enhanced E-region and F-region electron densities were observed (panel d), resulting from particle precipitation, which was simultaneous with an increase in the F-region electron temperature. The observations were indicative of the passage of an auroral arc through the radar field-of-view; the enhanced electric field was situated on one edge of the arc. Plasma pressure gradients at 22:00 UT were not consistent with outward plasma flow above an altitude of 250 km; rather, the outflow is thought to have been associated with the current system of the auroral arc.

Ionospheric Modelling

The thermal aspects of ion outflows, namely the thermal polar wind, and also the bursts of O^+ ion outflows as observed by EISCAT have been modelled. A first model was built with a two ion (O^+ and H^+) and electron ionosphere, essentially for topside studies. It was shown that the set of 8-moment equations is well adapted for that kind of study when anisotropy effects (or departures from a Maxwellian distribution function) are not considered. It was important however to test the validity of the numerical equation solver: for that purpose two numerical schemes were used and compared, leading to the conclusion that they give almost identical results (Robineau et al., 1995) and thus that the results are not solver-dependent. Also the validity of the 8-moment truncation was tested with an estimate of the error introduced when neglecting higher order moment terms in the transport equation. It was shown that this 8-moment approximation is adequate, with the exception of H^+ at very high altitudes (above 2000 km) for which the approximation starts to fail when this ion reaches a supersonic regime (Robineau, Blelly, Fontanari, Lilensten, Lummerzheim).

These models were subsequently used to test the effects of field-aligned currents flowing out of the ionosphere; also for a full comparison with EISCAT observations during which Joule heating of the ions was also present during the O^+ ion outflow, the effect of an ExB electric field was introduced during the event simulation. The combination of these two mechanisms, namely an upward current of about 14 mAm^{-2} and a transverse electric field of 50 mVm^{-1} were able to quantitatively reproduce all the observed effects, e.g. the increase of the electron temperature up to 7000 K, the acceleration of the O^+ ions up to velocities of 700 ms^{-1} (field-aligned), the corresponding observed decrease of the electron concentration by a factor of two, and the frictional heating of the ions. The main conclusion of this study was that field-aligned currents, which can be carried by precipitating electrons, are likely the cause of the ion outflows as observed by EISCAT, when they occur simultaneously with events of electron temperature enhancements.

To extend the previous two-ion model down to the E-region, where important processes of production and heating occur, it was necessary to work in two directions: firstly by introducing a more complete chemistry scheme with now six ions and the neutral NO solved, and secondly by coupling this model with a

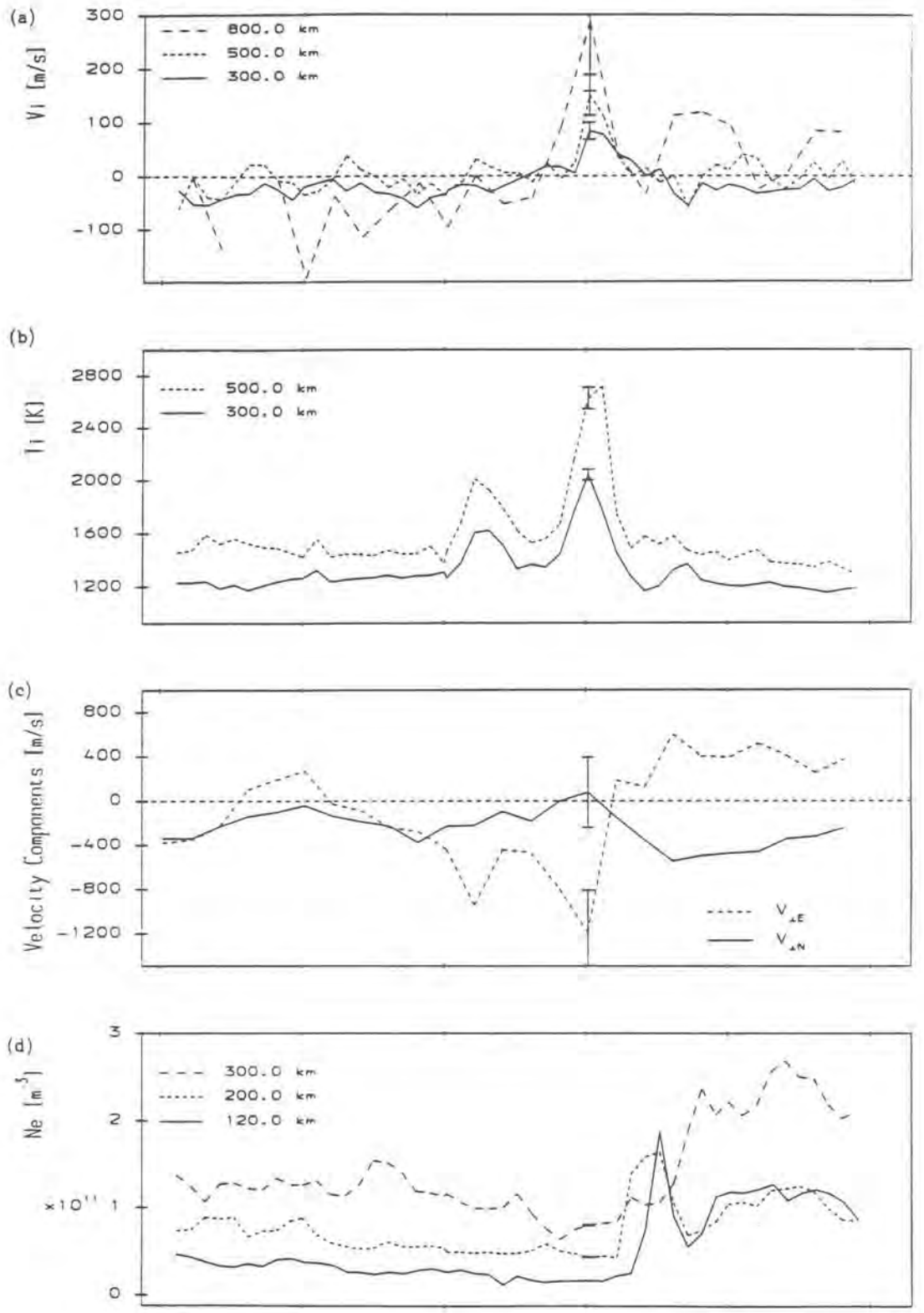

Fig. 19. EISCAT observations from 17 January 1990; (a) Line-of-sight (vertical) ion velocities measured by the UHF (300 and 500 km) and VHF (800km) radars; (b) Line-of-sight ion temperature at 300 and 500 km altitude measured by the UHF radar; (c) Zonal and meridional components of plasma drift velocity, calculated from tristatic observations at 315 km; (d) Electron density at 200 and 300 km (from long-pulse) and at 120 km altitude (from power profile).

kinetic transport model for the suprathermal electrons produced by EUV as well as by precipitating electrons.

This kinetic code was then coupled with the six-ion fluid code and the resulting code was named TRANSCAR (Blelly, Diloy et al.). The fluid part solves 22 reactions of production and losses for the ions and thermal electrons; some of them are known to be strongly dependent on the ion temperature, and consequently to the presence of convection electric fields. The kinetic part solves the field-aligned transport of suprathermal electrons, from several tens of keV down to a few eV, taking into account sources of electrons (i.e. primary precipitating electron or photoelectrons and their secondary products) as well losses by collisions with neutrals and thermal electrons.

The diurnal variation of the molecular to atomic ion transition region has been studied as well as for events of frictional heating. The solar zenith angle influence on this transition region was shown to correspond to EISCAT observations of the ion composition, and the introduction of frictional heating showed that the ionosphere reacts quite instantaneously to the ExB disturbance. These numerical results exhibit features which are qualitatively (and proved later to be also quantitatively) consistent with observed structures at EISCAT latitudes. Thus this model was proposed to be used as a standard one for ESR preparation: GIVEME, a MATLAB-based tool for visualisation and extraction of ionospheric profiles, was built), provided to and used by several groups within the EISCAT community (Alcaydé et al., 1994).

This numerical model is dependent upon the MSIS neutral atmosphere model, and relies also on collision frequencies and reaction rates. However when one compares the model outputs to observations, one has to adjust slightly some of the model values and even the coefficients. With such adjustments, the model is then able to reproduce fairly well the observed electron and ion temperatures and densities (and the ion velocities as well), and can pass through most of the data points within their error bars, as shown in Fig. 20 for quiet daytime and Fig. 21 for night-time and energetic precipitation conditions. This needs of adjusting some external parameters follow and extend previously proposed but more rudimentary methods of inferring neutral atmosphere parameters such as, for example, the exospheric temperature, the atomic oxygen density, or the meridional wind.

The plasmasphere and ionosphere part of the UCL/Sheffield/SEL model has been used by the group at the University of Sheffield to model an ion frictional heating event observed by EISCAT. A closed sub-auroral tube of plasma is considered in the model, which has been developed to include temperature anisotropy in the NO^+ as well as in the O^+ ion populations. During the event, the O^+ temperature distribution became more anisotropic than the NO^+. This meant that in the F-region the temperature of the NO^+ ions parallel to the magnetic field was substantially greater than the temperature of the O^+ ions parallel to the magnetic field (Fig. 22). The model predicted that the ion composition in the F-region would become more molecular during the event. At an altitude of 300 km the composition changed from 100% O^+ ions to 70% NO^+ ions (Jenkins, Moffett, Davies, Lester).

To account for a change in ion composition which is not considered in standard EISCAT analysis, the EISCAT data were re-analysed using the ion composition predicted by the model. To compare with the measured ion temperature, an average ion temperature was calculated from the model O^+ and NO^+ distributions. An

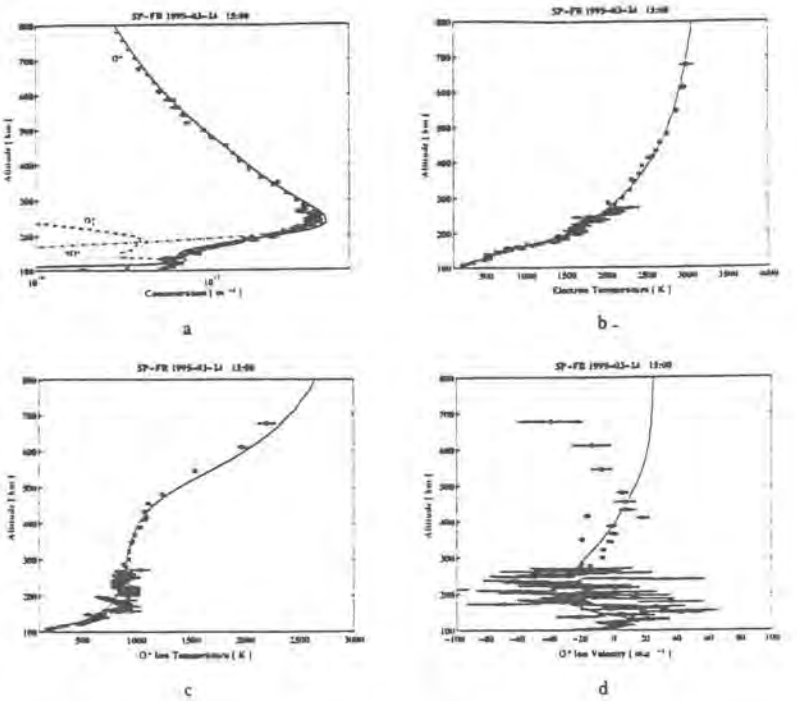

Fig. 20. Comparison of TRANSCAR model results with UHF (field-aligned, crosses) and VHF (vertical, circles) experiments during the March 24, 1995; quiet daytime conditions (15:00 UT). The model is represented by a full line which goes through the EISCAT data points with their error bars: (a) Electron concentration; (b) Electron temperature; (c) O^+ ion temperature and (d) O^+ ion velocity.

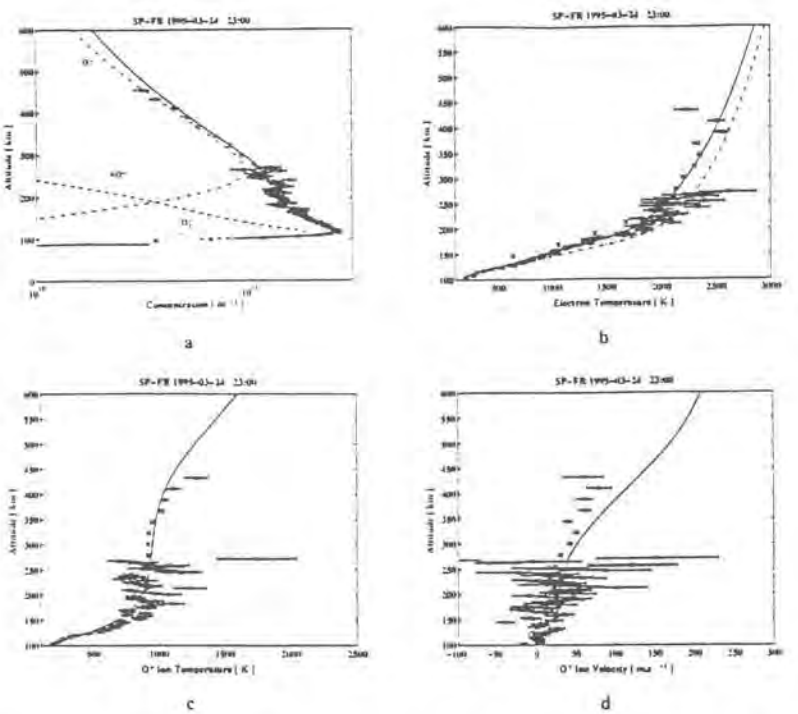

Fig. 21. Same as Fig. 20, but for night-time conditions (March 24, 1995; 23:00 UT) and during energetic electron precipitation events. Only UHF data are shown. The two curves in the electron temperature panel (b) correspond to different values of the vibrational collision frequencies on N_2: standard (dash-dotted) and enhanced by a factor of 2 (full line).

additional heat source was introduced to enhance the model electron temperatures. There was then reasonable agreement between the modelled and measured parameters.

A zonal ExB ion drift signature, modelling that observed over EISCAT during the above heating event, was imposed on the Sheffield University Plasmasphere and Ionosphere Model (SUPIM). The model yields densities, temperatures and field-aligned velocities for the six major ion species. The plasma parameters modelled at F-region altitudes were compared with those measured by the EISCAT radar and although they tended to exhibit the same general trends, the model results predicted substantially larger field-parallel ion temperature enhancements than were observed. However, the inclusion of a time-dependent calculated neutral wind, caused by ion drag, reduced the modelled field-parallel temperature to the values measured by EISCAT without severely affecting the other parameters. During extended periods of high speed ion flow, particularly on the dayside, an enhanced neutral wind thus becomes highly significant in determining the frictional heating of the ion population.

F-region Irregularities

A major advance in the probing of the high-latitude ionosphere above the EISCAT and ESR radars has been the inception of the CUTLASS HF radar facility. Both the Finland and Iceland sites began producing reliable and interesting data in 1995. A comparison has been performed between the irregularity drift velocity measured by the CUTLASS Finland HF coherent radar and simultaneous EISCAT UHF observations of F-region ion velocity. Observations have been compared from an extended run of the UHF common programme CP-1-K, and a short run of a special programme similar to CP-1. The tristatic altitude of the EISCAT experiments corresponds to range gate 18 of beam 5 in the CUTLASS field of view. The component of the F-region ion vector velocity along the CUTLASS beam measured by EISCAT in both experiment modes has been compared to the plasma irregularity drift speed measured by the CUTLASS radar in beam 5, range gate 18. Fig. 23 illustrates a scatter plot of the CUTLASS irregularity drift velocity against the component of the F-region ion velocity observed by EISCAT along the CUTLASS beam direction. Filled dots represent points from the CP-1-K/CUTLASS comparison, crosses represent points from the SP/CUTLASS comparison. Positive velocities indicate flow away from the radar. The velocities measured by the two systems demonstrate a reasonable correspondence over the limited velocity regime encountered during the simultaneous occurrence of coherent and incoherent scatter.

Ion Composition in the Lower F-region

An ion composition model in the lower F-region for the daytime period of summer seasons has been obtained by correcting the current EISCAT model with the ratio between measured and modelled ion temperatures using Waldteufel's mapping relation. The model profile of ion temperature has been estimated with a fit of a $\tan^{-1}$ function to the observations under assumptions stating that the ion temperature should exhibit the same height profile as the neutral temperature. In order to warrant this assumption, data periods were selected during which the effect of frictional heating was negligibly small, i.e. that the F-region d.c. electric field remained below 4 mVm^{-1} in magnitude.

The composition model obtained has a clear local-time dependence. The transition altitude between molecular and

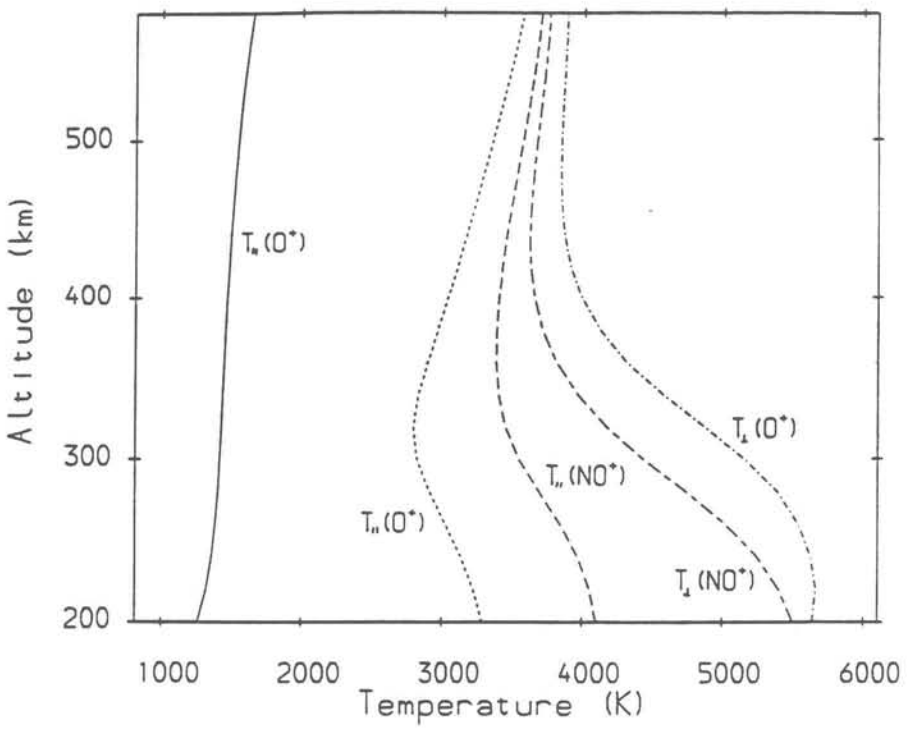

Fig. 22. Model ion temperatures as a function of altitude at 50 minutes elapsed time during the heating event of 5 September 1989. The continuous line represents the altitude variation of the field-parallel O^+ temperature before the start of the event.

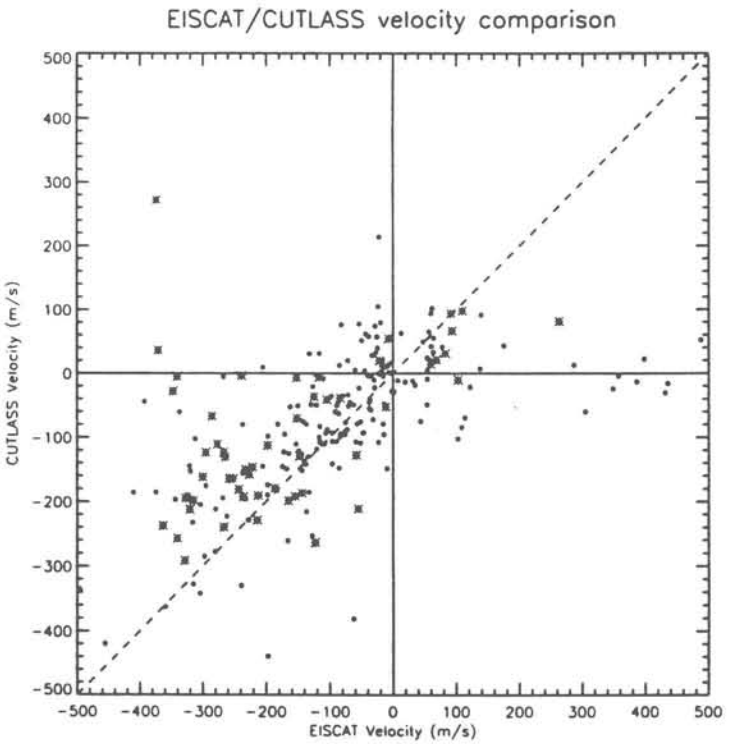

Fig. 23. Scatter plot of EISCAT ion velocity and CUTLASS irregularity drift velocity measurements.

oxygen ions varies diurnally with a minimum altitude of about 187 km around 13 LT. This minimum altitude and the phase of the diurnal variation are in good agreement with the results of Lathuillere and Pibaret (1992) who obtained the ion composition by using a more rigorous method, i.e., the full five-parameter fitting of the measured ACFs.

The data in the present analysis are from EISCAT CP1 experiments using a multipulse or an alternating code scheme. This experimental mode provides an altitude resolution of about 3 km, and therefore has a great advantage for studying the details of the ion composition profile in its transition region. Fig. 24 shows a comparison between the altitude variations of the new ion composition profile p_{new} and the Lathuillere and Pibaret (L-P) model. This reveals that in the altitude range 170-200 km the p_{new} values agree well with those of the L-P model, whereas for regions below 170 km and above 200 km the pnew tends to have smaller values than the L-P model (Shibata, Inoue, Schlegel).

A database of EISCAT results, consisting of seven selected high resolution experiments, all with mainly alternating codes, has been formed for a study to investigate the ionospheric composition in the lower F-region above Tromsø. The ion composition has been derived using profile fitting of the ionospheric temperatures, giving reasonably good results for many different levels of activity. The technique was compared with direct fitting of the composition and gave similar results when the direct method worked. Empirical formulas for the ionospheric content of O^+ from 120 to 300 km were derived, one based on the solar zenith angle and another, giving better agreement, based on the lower F-region electron density. The latter, shown in Fig 25, had a correlation coefficient of 0.83 and is expressed as:

$$h(50\%\ O^+) = 346\text{-}29\log(N_e(210\ km))\ km$$

The width of the region showed no correlation and the 1/e levels were 30 km both up- and downwards.

Large-Scale F-Region Structure and Tomography

EISCAT can only make monostatic measurements along a single beam direction whereas the dynasonde facility at Ramfjordmoen can receive echoes from a wide angle, and measure the angle of arrival. This enables the dynasonde to make simultaneous measurements over a large horizontal area. Such measurements are especially effective when a precipitation feature in the ionosphere is associated with quasi-elliptical isoionic contours, so that reflection occurs for signals arriving from a wide range of incident angles. A comparison of EISCAT data with dynasonde measurements made every 3 minutes has been used to illustrate this advantage of joint observations. The dynasonde observed a feature in the F-region drifting steadily southwards, confirmed by EISCAT measurements made in a 3-minute north-south scanning cycle, Figs. 26, 27 (Sedgemore, Williams, Jones, Wright).

As a side product of the GUISDAP project (see section on data analysis and techniques), a new tomographic inversion method and software package has been developed, which has been applied in satellite radio tomography and auroral tomography. The method has been tested using both data simulation and inversion of real observations. A chain of four receivers was used to measure the phase difference of 400 MHz and 150 MHz radio waves transmitted by a navigational satellite at 1000 km altitude. In Fig. 28

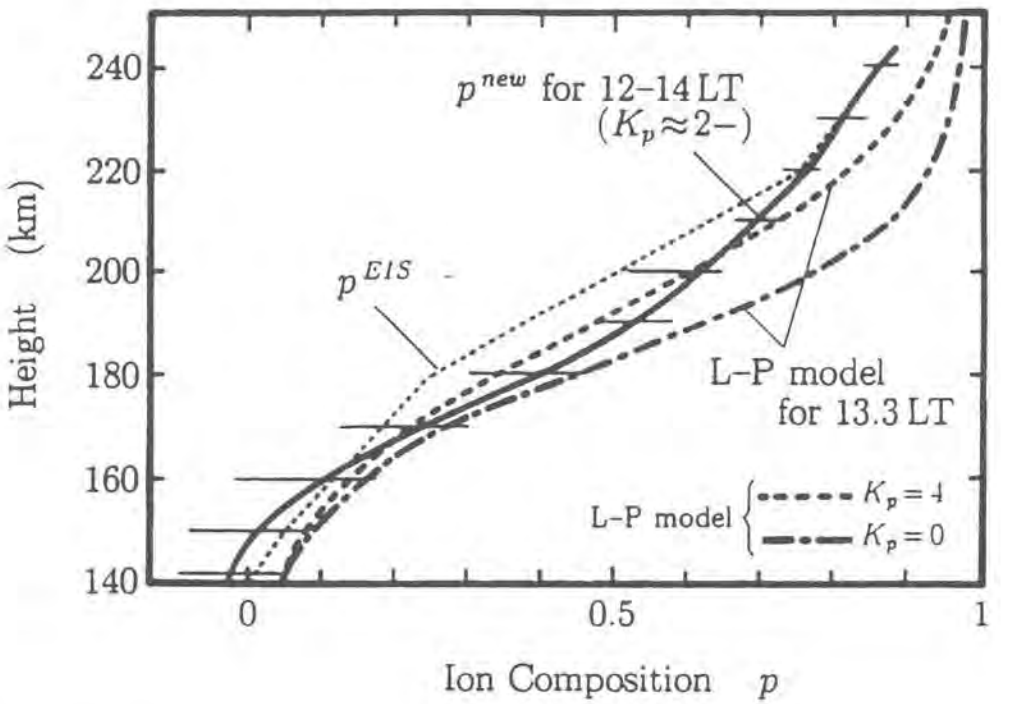

Fig. 24. New ion composition model for 12-14 LT as compared to the summer model for 12 UT (approx. 13.3 LT) of Lathuillere and Pibaret (1992). The horizontal bars attached to the pnew curve denote the deviation range among the 8 sample profiles available in the interval 12-14 LT. The thin dotted line represents the standard model.

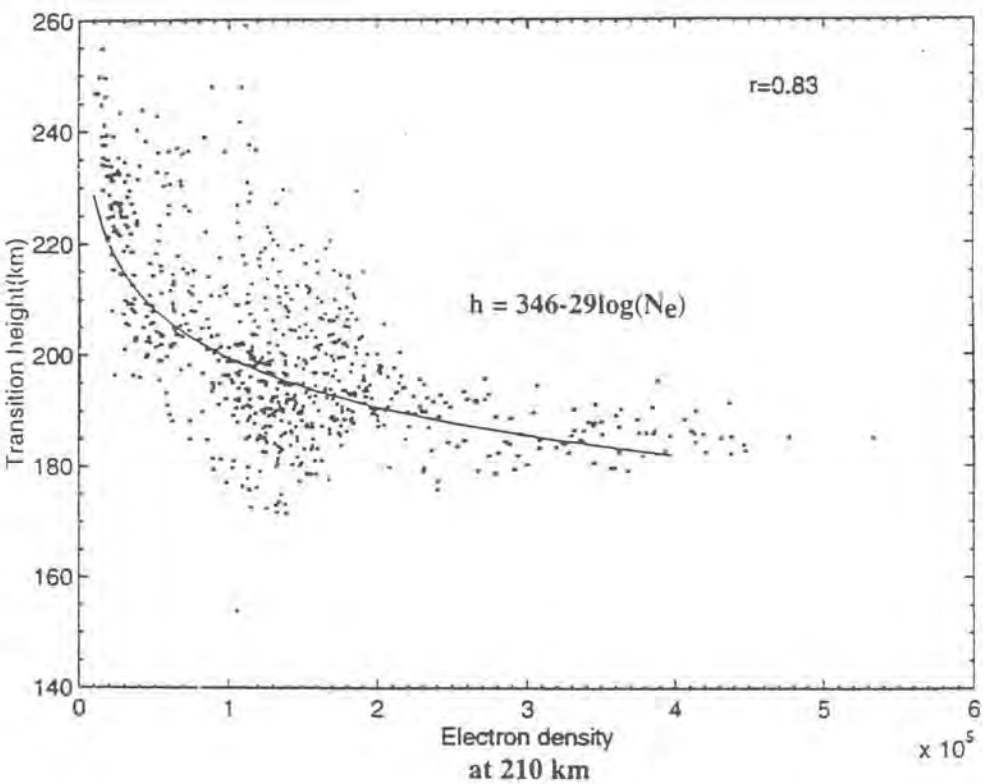

Fig 25. The altitude with an ion content of 50% O^+ as a function of electron density at 210 km together with the best fit. The error bars (omitted) are higher for lower densities.

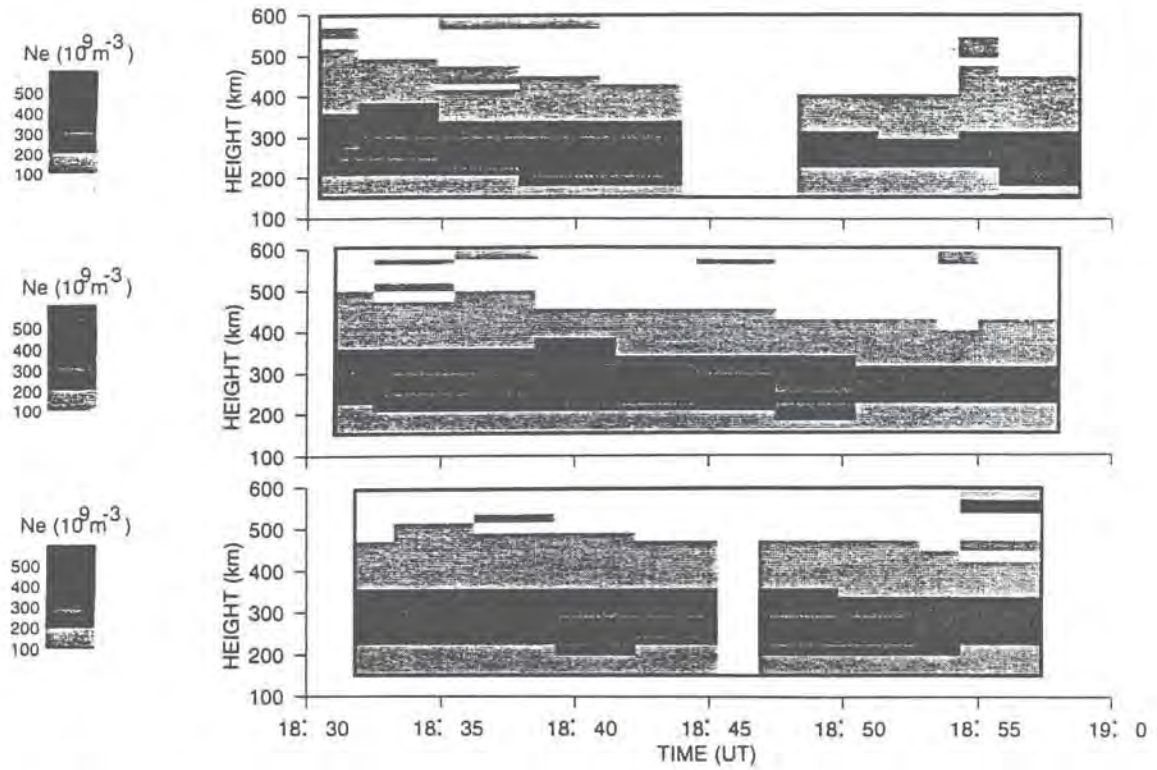

Fig. 26. EISCAT long pulse electron density contours on 23 May 1994. The panels, from top to bottom, correspond to beam elevations 96° (north), 90° and 84° (south). An F-region feature is seen first in the top panel at 18:36 UT. It then moved southwards through the other two positions, finally disappearing at around 18:50 UT.

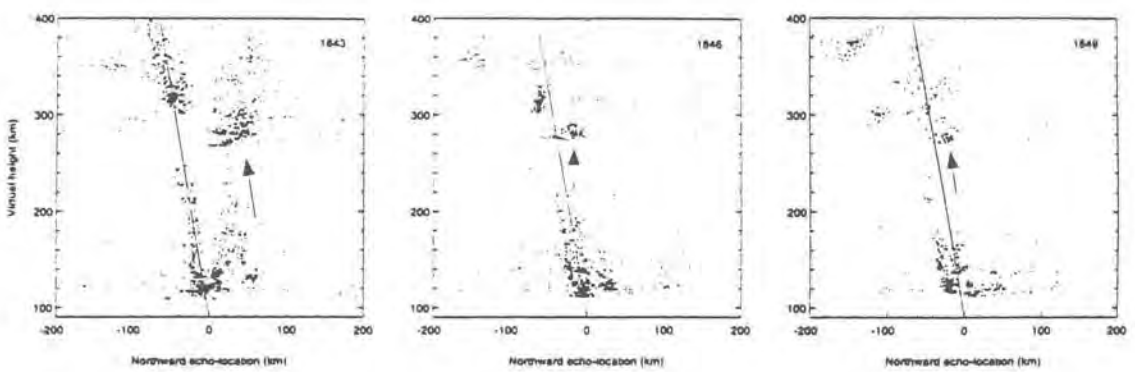

Fig. 27. Time series of Dynasonde skymaps showing the North-South movement of an F-region electron density enhancement (arrowed) from 18:43 to 18:53 UT. The feature is at a real height of around 240 km.

the results given by the tomographic method are compared with those from the radar.

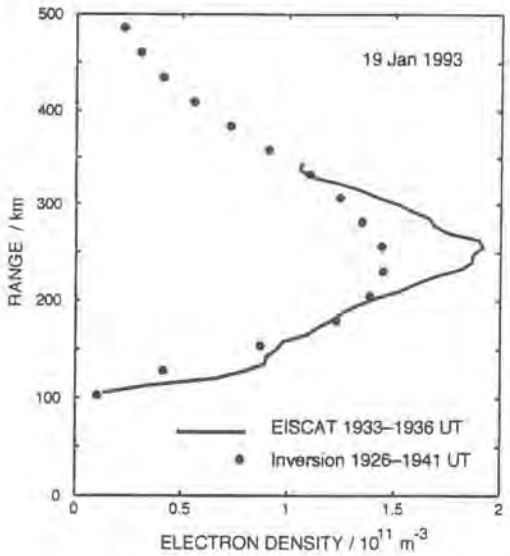

Fig. 28. Comparison of N_e profiles deduced from satellite radio-tomography and measured by the EISCAT radar.

The EISCAT radar has played a key role in establishing this new ionospheric imaging technique by providing independent verification of the tomographic reconstructions of electron density (Kersley and Pryse, 1994). Early comparisons between tomography and CP-3 measurements indicated the potential of the method for imaging structures on scales of hundreds of kilometres. Special programmes have since enabled the comparison of images of structures with horizontal scales of less than ~100 km. Lack of horizontal ray paths in ionospheric tomography necessitates initialisation of the reconstruction with a background profile. Earlier work reflected the inadequacy of the International Reference Ionosphere (IRI-90) model at auroral latitudes. However, recent promising developments have been made by using more realistic vertical profiles for the initial estimate. In particular, ionosonde information has been used to give the bottomside profile and peak layer height and normalised profiles from a vast database of incoherent scatter electron density profiles have provided improved topside shapes (Heaton et al., 1995). Comparisons of tomographic images have been made with EISCAT special programmes designed to investigate the structure of auroral field-aligned features on horizontal scales of a few tens of kilometres. The correspondence of such structures in the tomographic images and the EISCAT verification has been extremely good under quiet geomagnetic conditions (Mitchell et al., 1994, 1995) illustrating the power of tomography to image the field-aligned structures at high latitudes where the vertical ionisation profile is of secondary importance. A detailed comparison of the ionisation measured by the two techniques is presented in Fig. 29, which shows the electron density as a function of latitude at a constant height of 310 km. Excellent agreement can be seen between the two independent sets of observations. Fig. 30 shows that the main trough, centred at about 67°N, is observed by both techniques. The tomographic image shows the minimum density to be less than 0.15×10^{10} m^{-3}, though the corresponding value is not shown on the EISCAT plot due to the low signal-to-noise ratio. The field-aligned blob at the poleward edge agrees well in both images.

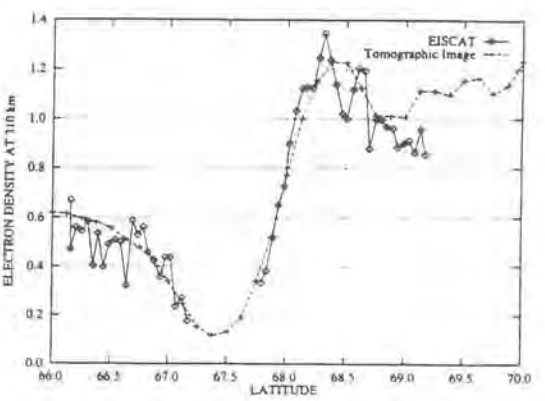

Fig. 29. Profile of electron density (10^{11} m^{-3}) with latitude, through the tomographic image and the EISCAT data shown in Fig. 30, at 310 km.

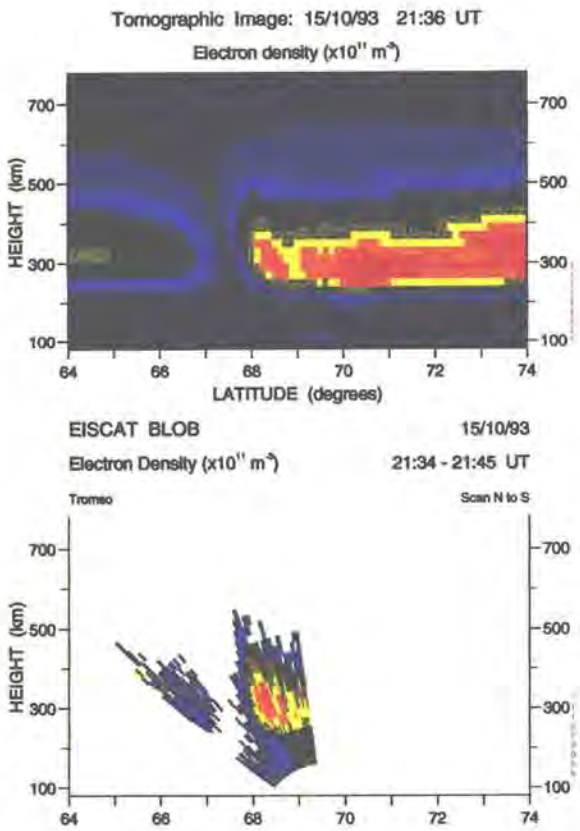

Fig. 30. Tomographic image of the main trough on 15 October 1993, and simultaneous EISCAT observations.

Results show several different types of mechanisms causing the irregularities occurring over a time interval of a few hours. The field alignment of the structures has been confirmed. A long-lived poleward trough wall, in which the density increased some five fold over about 0.25° latitude, has been used to estimate the alignment of the geomagnetic field. The measured inclination of 78.0±0.6° is in agreement with the value of 77.8° given by the IGRF90 model. Studies of irregularities and ionisation patches in the polar-cap ionosphere have also been undertaken in preparation for observations with the ESR radar (Kersley et al., 1994; Pryse, Kersley, Walker).

Non-Maxwellian and Non-thermal Plasmas

During magnetically disturbed periods, the ion velocity distribution function departs from a Maxwellian, and therefore the classical analysis of incoherent scatter spectra does not provide accurate estimates of the ionospheric parameters. Two models of non-Maxwellian distributions function have been extensively compared: the polynomial expansion approximation which is a solution of the Boltzmann equation, and a numerical distribution based on a Monte Carlo method. Both approaches lead to identical results for electric fields up to 100 mVm^{-1} and for the two ions species O^+ and NO^+. These comparisons have resulted in new collision cross-section models depending on the electric field strength (Gaimard, St-Maurice, Hubert, Lathuillere). New characteristics of the O^+ ion distribution in a background of atomic neutrals subjected to intense external cross electro-magnetic forces were found. The one dimensional distribution function along the magnetic field displays a core-halo shape which can be accurately fitted by a two Maxwellian model at different temperatures. The Maxwellian shape for an angle of 21° is confirmed at the accuracy level of Monte Carlo simulations (Hubert and Leblanc). The information that can be extracted from simulated non-Maxwellian incoherent radar spectra has been analysed. It was shown that in a case of a pure ionosphere, a non-constraining model such as the 1-D Raman one allows the derivation of all parameters, including the ion temperature anisotropy, from two different aspect angle measurements. Moreover in that case, the ion velocity distribution function can be shaped simultaneously. In the case of a composite ionosphere of O^+ and NO^+ ions, an independent measurement of the electron temperature allows the deduction of the ion composition from spectra

obtained at the specific angle of 21°. A routine which depends on the ion distribution models is then required for deriving the two ion temperatures and anisotropies. If the electron temperature is not given, no information can be extracted without a model dependent routine: the better the ion distribution models are, the more accurately derived the plasma parameters will be. The 1-D Raman fitting routine can be used to keep a check on the coherency of the results obtained (Hubert, Leblanc, Moncuquet, Gaimard, Lathuillere).

The analytical ion velocity distribution function was chosen for developing a new analysis of incoherent scatter spectra, that is valid during periods of electric fields up to 100 mVm^{-1}. This new analysis works with a mixture of ions (O^+ and NO^+) in a neutral atmosphere of O, N_2 and O_2 and allows the deduction of the ion composition during highly disturbed periods. Tests on simulations and sensitivity studies to the models used were performed. Ion composition was obtained from EISCAT spectra that displayed non-Maxwellian characteristics, showing that the ion population is mainly molecular at 280 km altitude for an electric field of about 100 mVm^{-1} (Lathuillere et al. 1995, Gaimard). Finally, using special experiments measuring at 170 km altitude, the error in the line of sight ion temperature made when the standard EISCAT analysis is used has been quantified (Fig. 31). This error estimation is valid for molecular ions and electric fields up to 100 mVm^{-1} and for all aspect angles (Gaimard).

Many factors contribute to strong departures from the thermal, Maxwellian, equilibrium configuration in auroral types of situations. The large electric fields can, by themselves or in combination with other factors such as gradients or intense precipitation events, generate plasma instabilities at times. The radar spectra in those cases are much more difficult to interpret than in the thermal case, while the power received from the plasma echoes can be several orders of magnitude more powerful than those received from thermal plasma. Finally, the irregularities will sometimes modify the properties of the plasma and lead, for example, to the observation of an anomalous increase in the electron temperature.

One of the situations or events resulting in distortions of incoherent scatter spectra is the presence for brief periods of ionospheric structures or turbulence at smaller scales than the typical radar space and time resolution. This case violates the classical assumption of space and time uniformity within the scattering volume, which is used in the standard analysis. Presently, efforts are being developed to simulate distorted spectra, and to propose an analysis procedure for enlarged and flattened spectra occasionally detected by EISCAT. The envisaged interpretation rests on rapid and intense velocity fluctuations within the scattering volume or the time integration, such as velocity shears or more complex velocity structures (Fontaine and Forme, 1995).

The case of enhanced ion acoustic echoes is another situation which prevents the application of the standard analysis procedure, due to the strongly asymmetry and enhanced power of the received signal. However, the plasma characteristics derived in the surrounding regions give some insight into the physics related to these echoes. This is illustrated in Fig. 32, which displays 45 minutes of VHF observations in the F-region. Within the regions of enhanced acoustic echoes, the strong distortions of the spectra cause the failure of the standard analysis, and the corresponding plasma parameters are not fitted (dark zones in the figure). But close to it, very clear signatures are identified, and can be separated into two classes. The

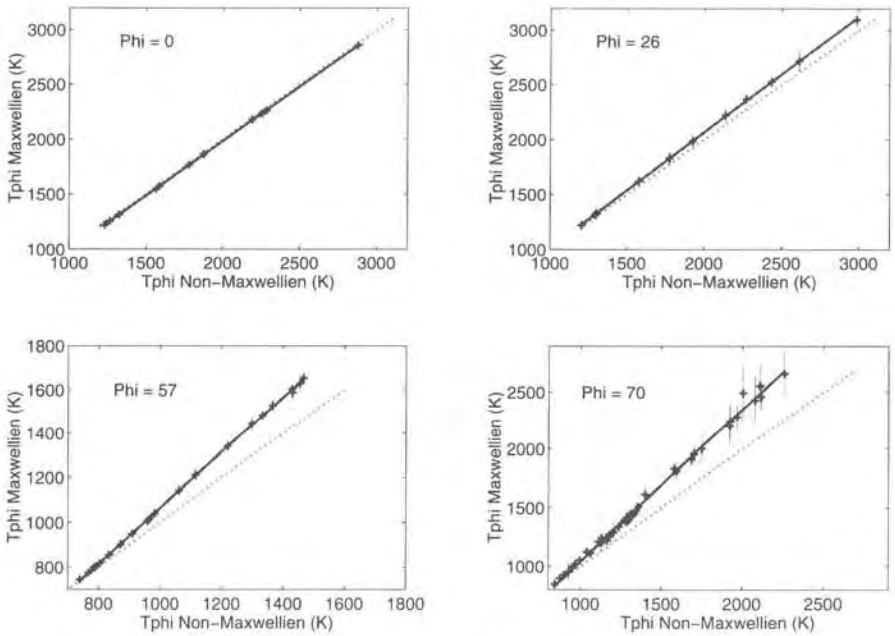

Fig. 31. Line of sight temperature of NO^+ ions obtained by the standard EISCAT analysis as a function of the line of sight temperature obtained with non-Maxwellian analysis. Each panel corresponds to a different aspect angle (phi) and allows quantification of the NO^+ line of sight temperature overestimation, when the standard EISCAT analysis is used.

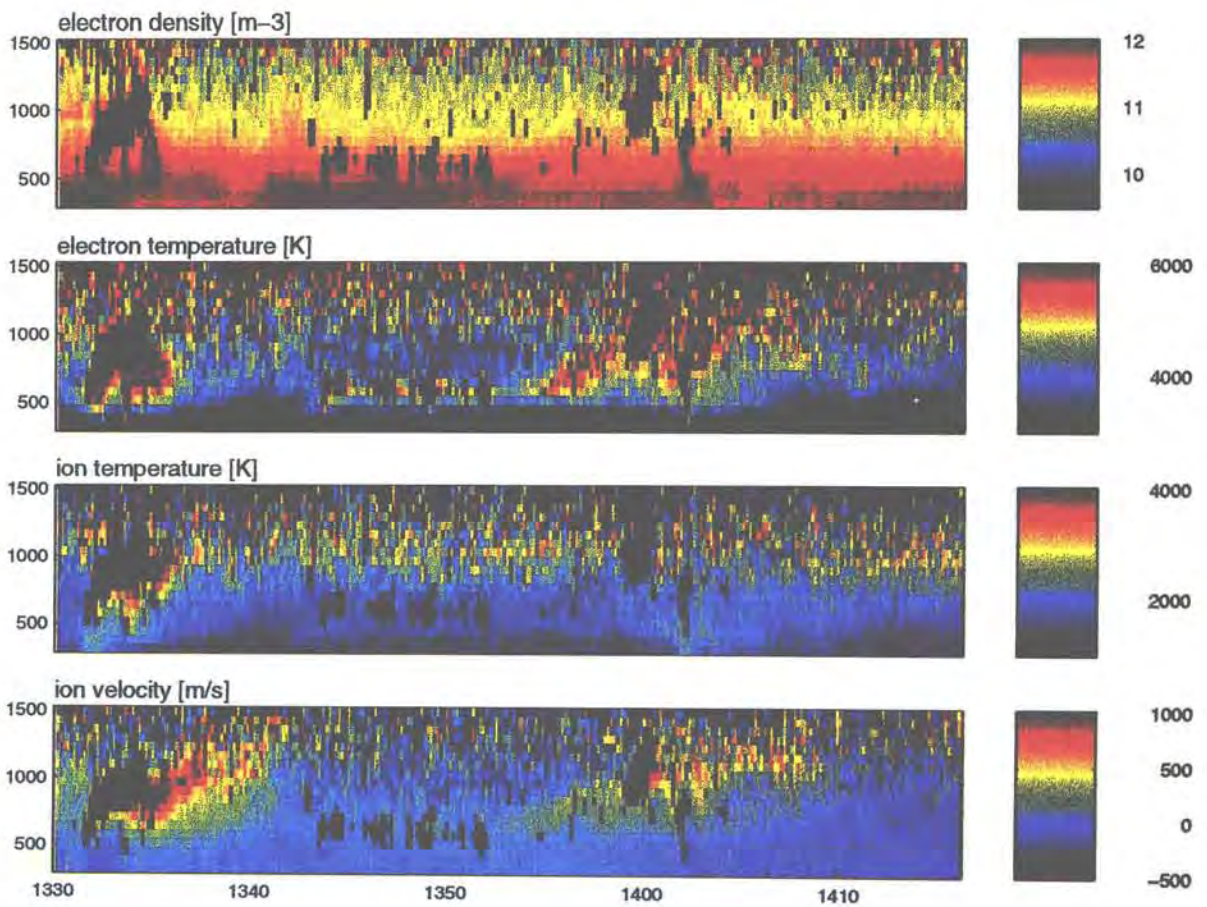

Fig. 32. High-altitude VHF observations of the plasma parameters near regions of enhanced acoustic echoes (dark zones).

first one, near wide turbulent regions (height extent of several hundred km), involves high electron temperatures and large ion outflows, while these effects disappear near regions of lesser height extent at somewhat lower altitudes. Simultaneous observations by the UHF radar also reveal the presence of soft electron precipitation (below 1 keV) correlated to the acoustic echoes. Systematically observed in conjunction with echoes, the soft electron precipitation are suggested to be the source of free energy able to trigger acoustic instabilities, more likely than occasional ion outflows (Forme et al., 1995).

A number of independent and diverse ionospheric electric field, current, particle, and plasma wave observations can be interpreted in terms of intense parallel current density bursts that would require parallel electric fields of the order of up to a few mVm^{-1} to exist at ionospheric altitudes. The conditions under which the ionosphere could possibly sustain very large parallel fields and current densities have been explored theoretically. Since this is a first attempt at this question, we look for the simplest possible requirements, that is, we study the possibility for the presence of a quasi-static electric field on time scales greater than the electron collision time and the Alfven transit time. One important conclusion is that for the generation of parallel fields intense enough to generate ion-acoustic waves along the geomagnetic field as well as the generation of shears of the order of meters per second per meter, 100 m horizontal gradient scales are required. Another result is that for larger horizontal gradient scales, a substantial fraction of the returning currents carried by the thermal electrons will flow along the same magnetic field lines that the precipitating electrons come from. This leads to a substantial reduction in the net parallel current densities when compared to the currents borne by each type of carrier (St-Maurice, Kofman, James).

E-region Studies

The COSCAT system has been employed in the study of the characteristics of 16-cm wavelength, E-region, auroral plasma irregularities in comparison with plasma irregularities at other wavelengths (Eglitis et al., 1995) and with the properties of the plasma flow measured by EISCAT. A series of new experiments has involved the transmission of a phase modulated signal to investigate the spatial distribution of the plasma irregularities in the scattering volume. The experiment was one of the first to employ the matched filters at the EISCAT remote receivers. A continuous wave, 13-bit Barker code was transmitted from Oulu. Plasma irregularities excited in the radar field of view scatter the signal, which was detected by the EISCAT receivers in Sodankylä and Kiruna. The observations are strongly dependent on the spatial length of the Barker code relative to the range extent of the scattering region. In Fig. 33, results from observations at baud lengths of 40, 70 and 100 ms from campaigns run in 1994 and 1995 are presented. Each panel depicts a time series of 5 s averages of the 13-bit response function of the Barker code, sampled at Sodankylä for different baud lengths. At 100 ms baud length (bottom panel) the spatial extent of the code is greater than the slant range extent within which the irregularities are excited. The variations in received power are then determined by the distribution of scattering centres with range. At significantly shorter code lengths (e.g. top panel, 40 ms) multiple code lengths fill the scattering region and the power received continuously exceeds the noise level. If the code length matches the slant range extent, the received signal power is constant across the 13-bit response function of the Barker code (middle panel, 70 ms).

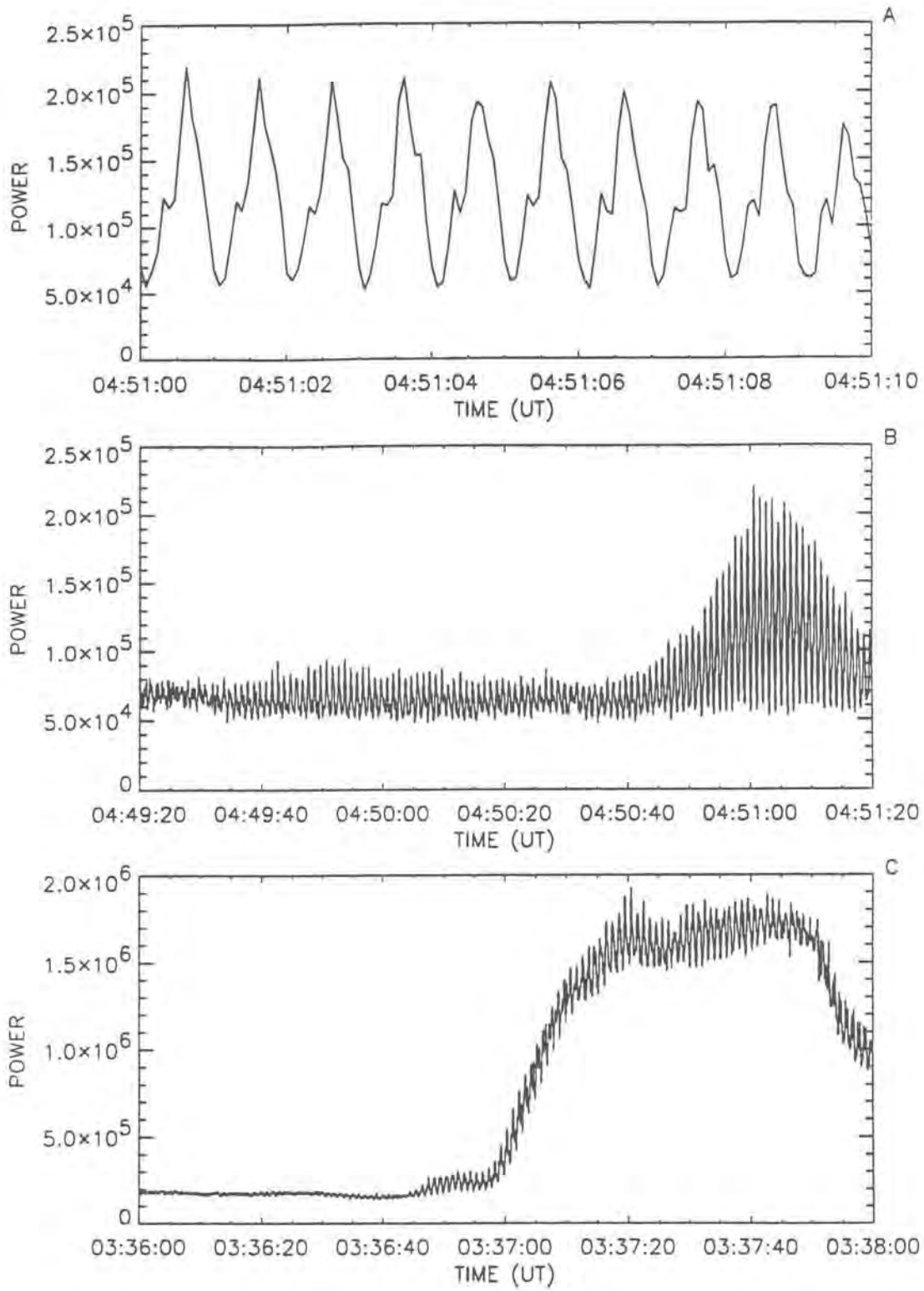

Fig. 33. Pseudo-time-series data from a passive Barker coded experiment run at Sodankylä. The plots were constructed by averaging the response to the Barker code into a 13-point function, and plotting these functions consecutively. Each group of 13 points is thus from a single integration period (1 s). Panel A illustrates an interval of strong scatter where the 13 point periodicity of the response function is clear. Panel B and C are longer intervals that illustrate the differences between observations at baud lengths of 100 and 40 ms respectively. (A and B, 24 May, 1994; C, 29 May, 1995.)

The results indicate that it is possible to measure the irregularity power profile with long baud length (e.g. 100 ms) Barker codes. When examining the geometry of the experiment, it was found that the measurements at 70 ms implied the EISCAT receiver beams were entirely full of scattering irregularities throughout their intersection with the E-region (approximately 150 km in slant range). The possibility now exists to run these Barker coded modes in conjunction with the passive and active experiments carried out in previous campaigns. This will allow the spatial structure of the scattering region to be compared to the spectral characteristics of the backscatter, and enable observations to be made of the way in which the scattering region changes in response to changes in the magnitude and direction of the electric field (Eglitis, McCrea, Robinson, Jones, Schlegel, Nygrén).

The high-latitude ionosphere is subject to electric fields perpendicular to the magnetic field. In the F-region, these electric fields drive ion flow relative to the neutral atmosphere, which results in frictional heating of the ion population. Furthermore, in the ionospheric E-region, such electric fields can generate instabilities which heat the E-region electrons through electron turbulent heating. More than 770 hours of EISCAT UHF common programme observations taken between March 1992 and March 1995 have been employed to derive statistically the electric field dependence of both ion frictional heating and electron turbulent heating. The upper panel of Fig. 34 depicts a scatter plot of F-region field-parallel ion temperature at 301 km altitude with perpendicular electric field magnitude, both of which are derived from long pulse measurements. The median and quartiles of the ion temperature binned with respect to electric field, with a bin width of 5 mVm^{-1}, are also shown. The field-parallel component of the ion temperature exhibits a systematic increase with increasing electric field, as expected theoretically. The lower panel of Fig. 34 illustrates a scatter plot of E-region electron temperature at 111 km altitude with perpendicular electric field; the electron temperature is derived from the alternating code pulse scheme. Again, the median and quartiles are illustrated. The E-region electron temperature tends to increase with increasing perpendicular electric field over a threshold of some 20 mVm^{-1}. Below this threshold electric field, strong Farley-Buneman instabilities are not generated. These results suggest that, in spite of differences in the mechanisms involved, E-region wave heating is as systematic as F-region ion heating in the auroral ionosphere (Davies and Robinson).

Meteor studies are a new application of the sensitive incoherent scatter radars. This method is expected to be able to give new information about the meteoric interaction and deposition processes in the atmosphere. The campaigns during the Geminid meteor showers in December 1990 and 1991 and the Perseid shower in 1993 have already given new results. Meteor echoes have been classified as head or trail echoes, and their altitude distributions and some statistics have been presented. Some incoherent trail echoes has been studied in detail and head echo characteristics thoroughly analysed. For example, the meteor velocity can be determined from the head echo forms.

It is possible to observe a meteor traversing the radar beam with a special wrap-around technique in the radar program mode. Fig. 35 shows a meteor observed simultaneously with both the UHF (a) and VHF (b) radars. Each panel or time slice shows a 6 ms power profile. The UHF echo is only visible in four time slices, but the VHF echo can be traced over eight

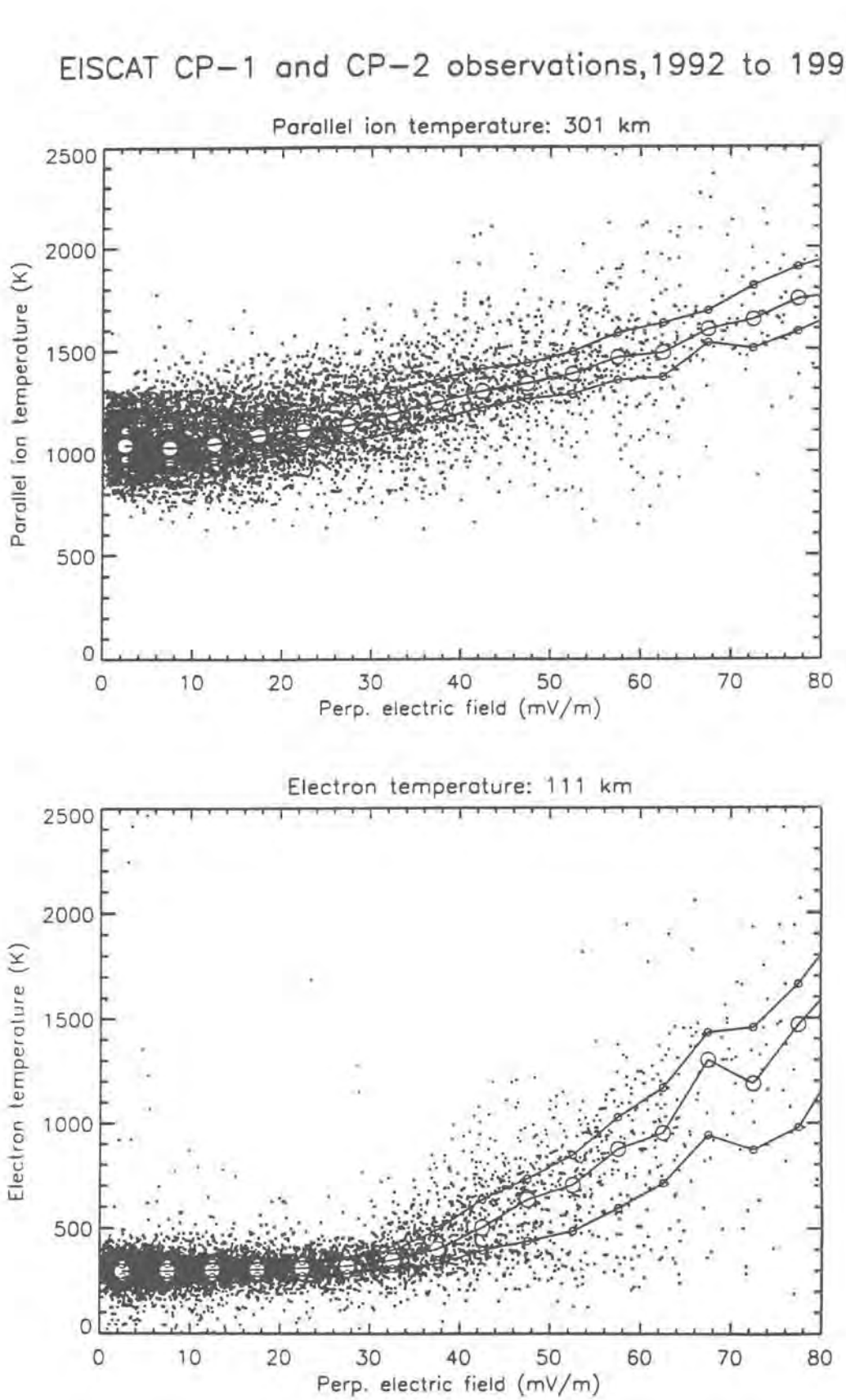

Fig. 34. The measured parallel ion temperature as a function of the perpendicular electric field measured by EISCAT CP-1 and CP-2 experiments from 1990 - 1995. Simultaneous measurements of the electron temperature at 111 km as a function of the perpendicular electric field are given in the bottom panel.

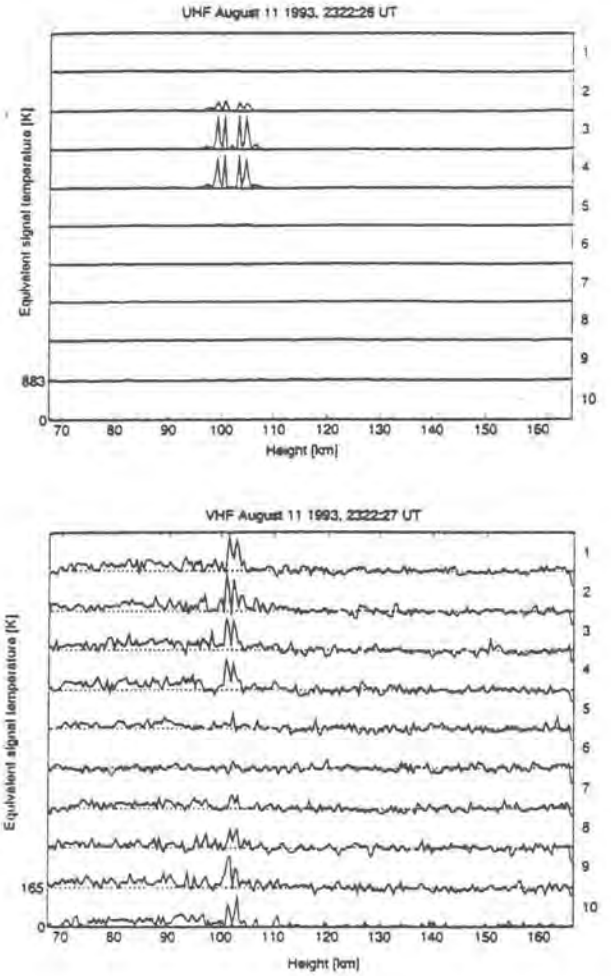

Fig. 35. A time-resolved dual radar meteor event from the Perseid operation on August 11, 1993, UHF data (a) and VHF data (b). The velocity fits yield 17.4 and 17.5 kms^{-1} respectively, showing that this is probably a sporadic meteor rather than a shower.

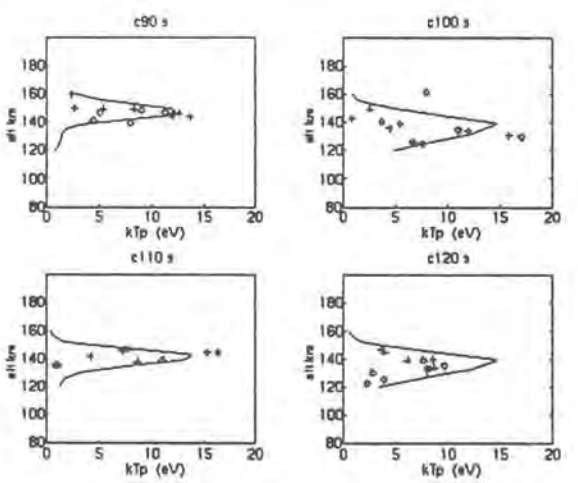

Fig. 36. Measurements of plasma line intensity (o down-shifted lines, + up-shifted lines) during auroral precipitation, compared with predicted plasma-line intensities (solid line) from the modelled suprathermal electron flux.

or nine slices, showing the effect of the difference in the two antenna beam widths. The UHF echo is split into four major peaks, while the VHF echo is two-peaked and much less structured. When they are analysed for velocity, taking the radar frequencies into account, the velocities come out as 17.4 kms^{-1} and 17.5 kms^{-1} respectively, indicating that the echoes are indeed from the same meteor and that neither echo is frequency-aliased (Pellinen-Wannberg).

Strongly enhanced E-region plasma lines observed during auroral activity have been analysed to see whether there is any evidence for a contribution from plasma turbulence to their intensity or whether they can be explained by suprathermal electron fluxes. The results indicate that the enhancements, even up to 200 times the thermal level, can be well explained by suprathermal fluxes. Strong enhancements for plasma-line offsets between 5.5 and 6.5 MHz (for the UHF radar) result from a sharp minimum in suprathermal fluxes between 1 and 3 eV energies which in turn is a result of the excitation of vibrational levels in N_2 (Fig. 36) (Kirkwood, Nilsson, Lilensten, Galand)

Intervals of periodic enhancements of E-region electron density have been observed by EISCAT. The periods are typically between 40 and 60 minutes. Statistical characteristics have been derived from 6 years of EISCAT data. This phenomenon is observed during relatively quiet times but after geomagnetic disturbances, and may last up to 6 hours. It can occur at all times of the day with a maximum probability in the MLT morning sector. The latitudinal extent derived from CP-3 measurements is a few degrees, presumably longitudinally-extended but this is not known. It is concluded that these events are due to periodically modulated fluxes of electron precipitation. The time constants of the inner, closed magnetosphere are much shorter, thus it is assumed that the long periods of this phenomenon are controlled by processes in the distant magnetospheric tail. For two events, Sondre Stromfjord electron density data were available and in both cases similar periodicities, but with longer periods, were found. At these times EISCAT is on closed magnetic field lines whereas Sondre Stromfjord is connected to the magnetospheric lobes with open field lines. In principle, this coincidence supports the idea that tail dynamics generates these oscillations, which couple to the inner magnetosphere and finally lead to the modulated precipitation (Rinnert).

Ionospheric Conductivity

Simultaneous high time resolution observations of the height-integrated Hall and Pedersen conductivities (σ_H and σ_P), the ionospheric electric field and the ground magnetic field during a magnetospheric substorm have been reported. The EISCAT UHF radar provided continuous 10 s time resolution measurements of the electron density and the ion vector velocity, from which σ_H and σ_P and the ionospheric electric field were calculated. During the substorm growth phase, σ_H and σ_P were less than 10 S and the ratio, $R = \sigma_H / \sigma_P$, was less than 1 (Fig. 37). Although both σ_H and σ_P increased at the onset of the expansion phase, R remained close to 1. This ratio provides information on the mean energy of the precipitating particles responsible for the enhanced conductances. A ratio of 1 implies a mean energy of the particles of 2 keV. Both σ_H and σ_P increased towards the end of the expansion phase, with peak values of 71 S and 34 S respectively. The ratio R also increased to values exceeding 2, equivalent to mean energies of more than 6 keV. The largest value of R was 3.25 during the substorm recovery phase, which is equivalent to mean energies of more than 10 keV. The maximum Hall

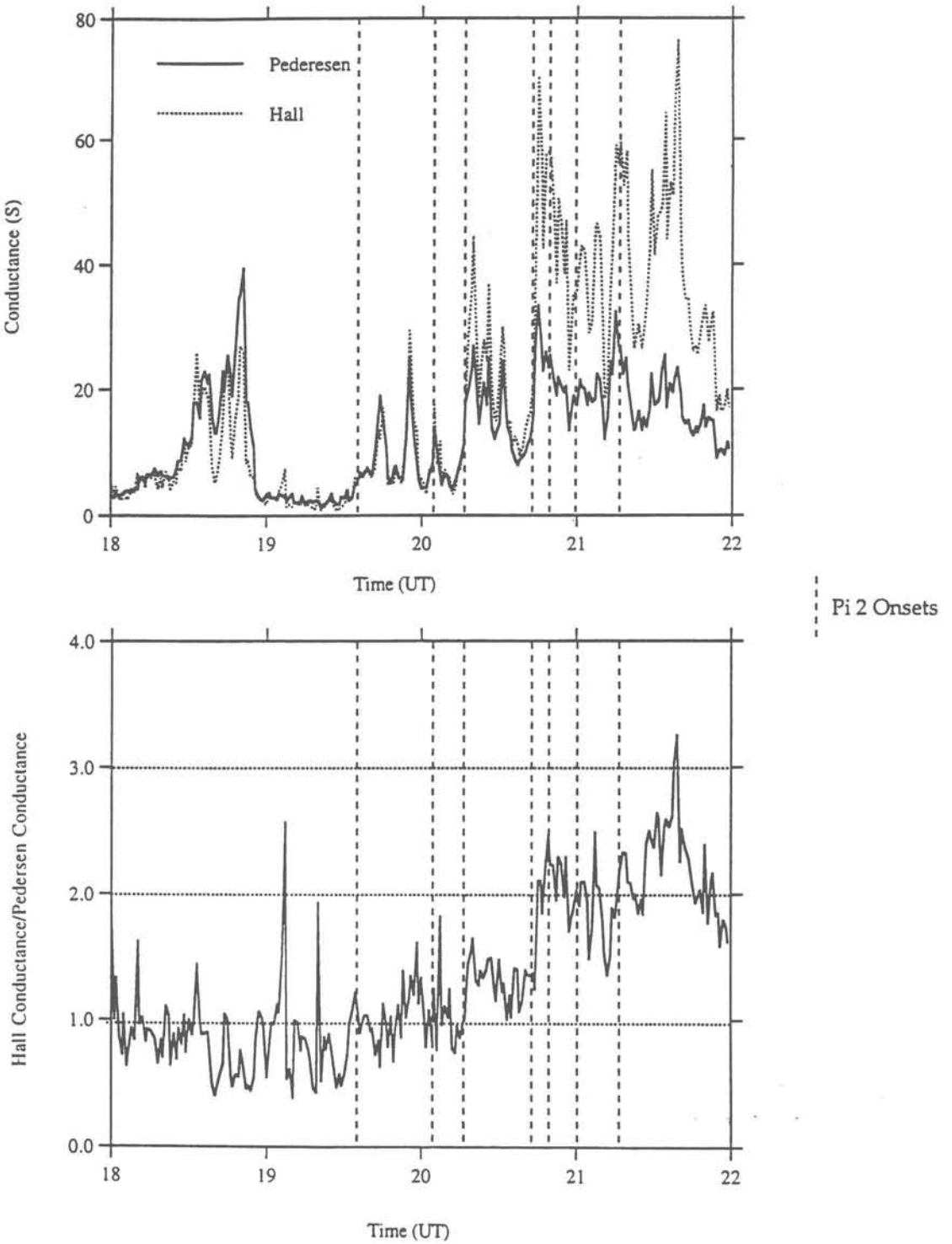

Fig. 37. In the top panel the Pedersen (solid line) and Hall (dotted line) Conductances are plotted as a function of UT from 18:00 to 22:00 UT. The lower panel shows the ratio of Hall to Pedersen Conductance for the same interval. The dashed vertical lines in each panel represent the times of Pi2 pulsations.

current density during this interval was 2.66 Am^{-1}, which occurred during the early part of the recovery phase of the substorm. At a number of intensifications, identified by Pi2 pulsations (Fig. 37), peaks in the current density were observed, for which the electric field was responsible in some cases and the Hall conductance in others (Lester and Davies).

Height profiles of the Pedersen, Hall, and Longitudinal conductivities have been calculated from nearly fifty sets of EISCAT UHF E-region data taken between 1985 and 1994 and covering a wide variety of geophysical conditions. Examples of results are shown in Fig. 38, the bottom three panels showing the longitudinal conductivity increasing with height, especially above 200 km, the Pedersen conductivity reaching a peak at around 125 km and the Hall conductivity at around 115 km. The quiet time variation of the Pedersen and Hall conductivities was generally evident, as were enhancements during disturbed conditions, for example around 01 UT and 21 UT in Fig. 38. One unexpected feature was that the Hall conductivity profile - but not the Pedersen conductivity profile - occasionally exhibited multiple peaks, as seen here around 13 UT. An investigation has been undertaken into the effect that the choice of different models of the neutral atmosphere, and hence of the ion-neutral collision frequency, have on the calculation of these conductivities. Four models of the ion-neutral collision frequency and two models providing neutral atmosphere parameters were examined, the latter being the well known Alcaydé-82 and MSIS-86 models. The separate use of these two models often gave noticeably different results.

The ionospheric Joule heating can be expressed as the product of the Pedersen conductance and the square of the electric field magnitude. The question naturally arises as to which has the greater effect. A study was therefore carried out in which these three parameters were calculated from EISCAT data taken at disturbed times on twenty-two days between 1987 and 1990. These were divided into two groups according to whether the data were taken during the daytime or at night, and, in both cases, a high correlation was found between the Joule heating and the electric field, but virtually none between the Joule heating and the Pedersen conductance. These results indicate that, for the set of data studied, the dominant factor controlling the time variation of Joule heating is the variation in the square of the electric field.

Several authors have proposed empirical or semi-empirical formulae for the solar control of quiet daytime ionospheric Pedersen and Hall conductance. A study was carried out in which these formulae were fitted to values of the two conductances calculated from EISCAT data taken at quiet times on the same twenty-two days during the period 1987 to 1990. Their validity was then assessed. Based on these results, further formulae were proposed to relate the conductances to the $S_{10.7}$ index and the solar zenith angle.

EISCAT has been employed to investigate an ionospheric conductivity gradient effect in Pc5 ULF waves (Chisham et al., 1995). Over 100 Pc5 events have been catalogued on the SAMNET magnetometer array, and the ground horizontal polarisation of these waves investigated. A far greater spread of polarisations is observed in the morning local time sector than in the afternoon. This difference between the two sectors is largely caused by Pc5 events which lie close to the dawn terminator having a variable polarisation pattern. The dusk terminator has little effect on the Pc5 waves, as the waves are mainly magnetosonic in nature in that

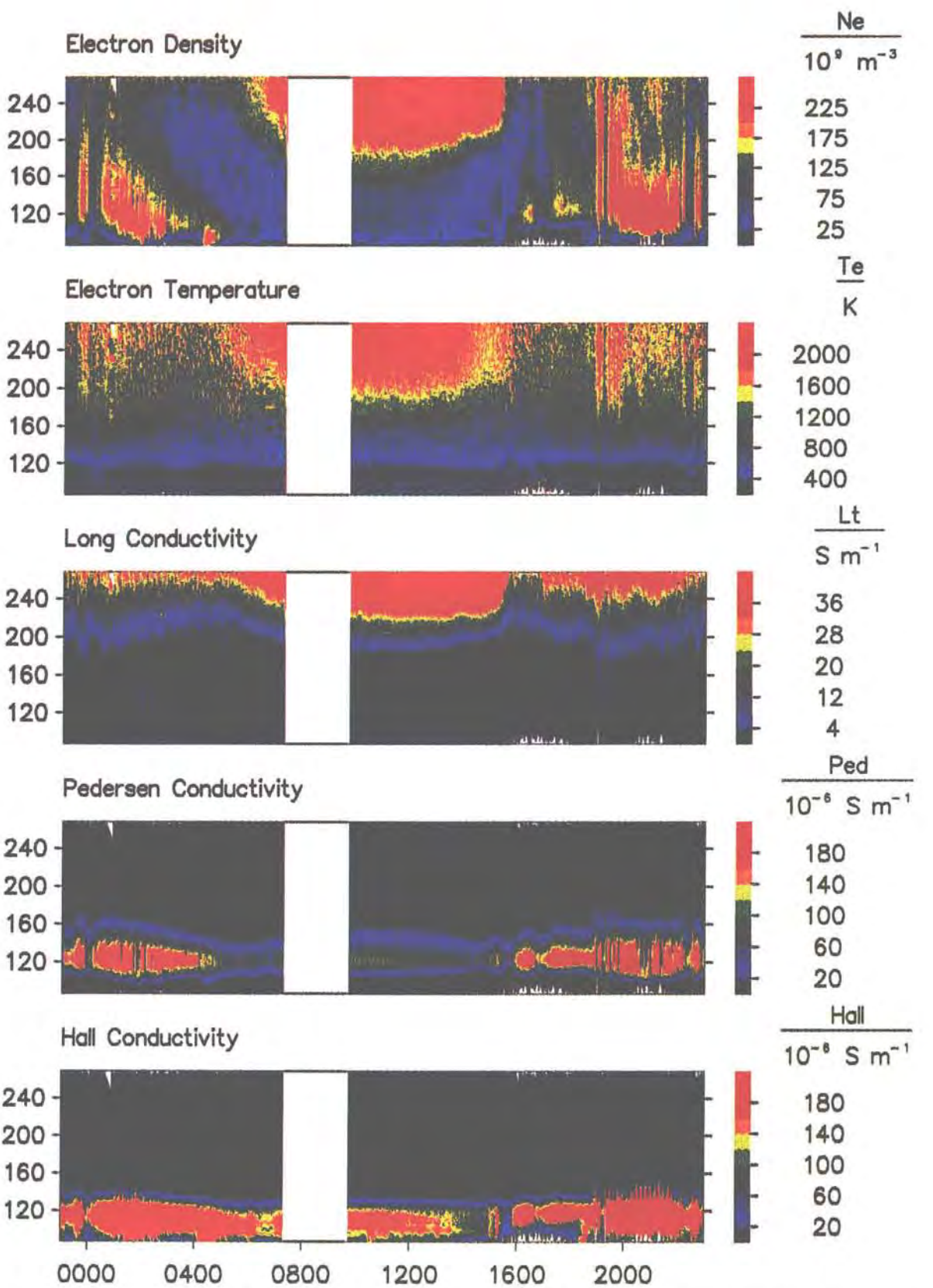

Fig. 38. Height-time plots showing ionospheric conductivities. As well as the diurnal quiet-time variation, the effects of disturbances are seen around 01 UT and 21 UT.

sector and are thus unaffected by ionospheric changes. Electron density profiles measured by EISCAT between 80 and 200 km have been combined with the IGRF model magnetic field and the MSIS neutral density and temperature models to evaluate height-integrated Hall and Pedersen conductivities. These data have confirmed the link between Pc5 polarisation and conductivity, demonstrating that changes in the Halland Pedersen conductivities associated with sunrise cause polarisation changes. It has also been demonstrated that changes in the Hall conductivity caused by energetic particle precipitation at other local times also influence the wave polarisation.

Auroral and Substorm Phenomena

During a coordinated EISCAT-optical campaign in January 1993 a substorm onset occurred south of Tromsø. The EISCAT radar made measurements of southward drifting arcs in the growth phase and of the westward travelling surge (WTS) in the expansion phase of the substorm. Fig. 39 shows the calculated Hall and Pedersen conductances with a time resolution of 3 s. The maximum value of the Hall conductance was as high as 214 S, obtained using a time resolution of 0.2 s. A schematic figure of the conductance distribution in and around the WTS based on the EISCAT measurements is shown in Fig. 40. It was concluded that the westward electrojet (WEJ) is latitudinally very inhomogenous and is concentrated near conductance enhancements, especially close to the head of the WTS (Aikio and Kaila).

The substorm events observed during the DYANA campaign from 11 January to 16 March 1990 were studied on the basis of riometer, rocket and EISCAT measurements. The EISCAT experiments were intended to measure all possible plasma parameters at heights from about 80 km to 250 km. In order to measure both the horizontal and vertical plasma drifts at these heights the UHF antenna was pointed in a sequence of positions. On 25/26 February the electron density was measured by EISCAT between 18 UT and 01 UT. The density was increased in the height region from 75 km to 120 km during the auroral electron precipitation. The electron density profiles measured covered the period of the substorm onset. The lower border of the increased electron density was quite variable. The electron density increase began between 75 km and 80 km and peaked at 110 km, corresponding to precipitating electrons of 3-4 keV energy. Electron density profiles were measured by EISCAT on 20 February between 0940 UT and 1120 UT. The energy spectrum of the precipitating electrons was generally harder than on the evening side. The electron density peaked at an altitude of 90 km, corresponding to the maximum energy flux into the atmosphere being by 20-30 keV electrons (H. Ranta, A. Ranta, Stauning, Rapoport, Sinelniv, Kirkwood, Lastovicka, Knyazev).

The extended optical and radar data set from the PULSE experiment has been used for a study of small-scale changes associated with auroral arcs. In one case, on January 18 1993, a system of auroral arcs moved toward the EISCAT viewing area, and a bright arc remained stationary for several seconds adjacent to the EISCAT beam. During this interval, electric fields were calculated at time resolutions of 3, 9 and 30 s. A number of dynamic features were seen, moving along the direction of the arc at speeds of several kms^{-1}. Associated with these were highly variable electric fields, measured in the region beside the arc, the existence of which was confirmed by high ion temperatures. It is difficult to estimate these fields accurately, as they occurred in a region of low electron density. In

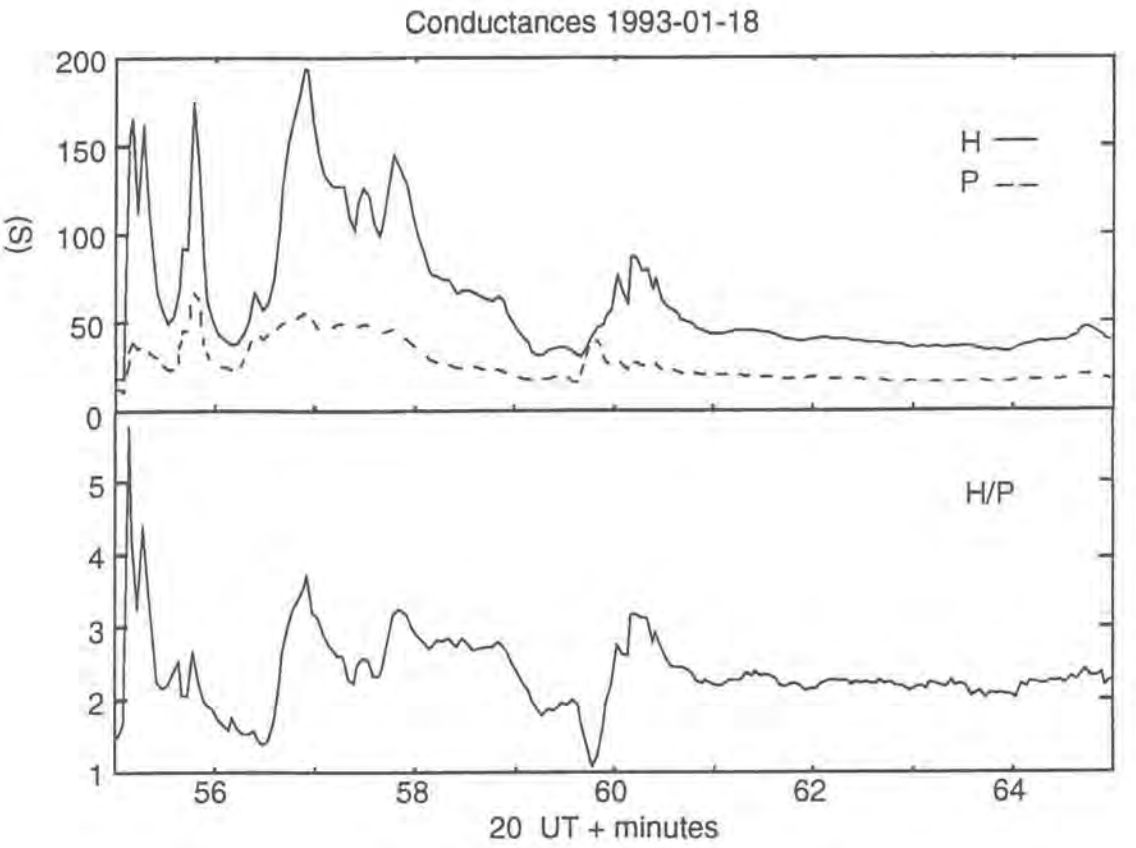

Fig. 39. Hall (solid line) and Pedersen (dashed line) conductances (top panel), and the Hall to Pedersen conductance ratio (bottom panel) obtained by 3 s integration during the expansion phase of a substorm. The highest conductances are observed at the edges and inside of a WTS.

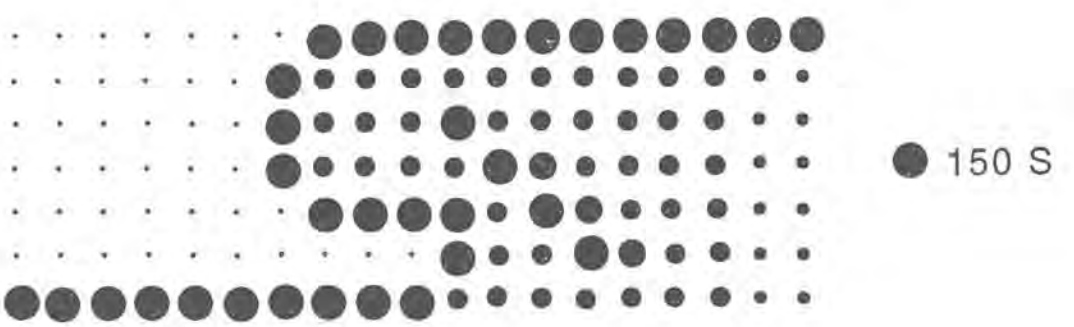

Fig. 40. A schematic model of the Hall conductance in the WTS. The regions of highest conductances contain a lot of fine structure not shown in the figure.

Fig. 41 are shown the horizontal electric field vectors from 21:24:30 UT to 21:25:00 UT superimposed on an average image (1 s, 25 frames) at 21:24:39 UT. The vectors are at 3 s resolution, and therefore have large errors. However, it is clear that the vectors point towards the highly variable optical features which move along the length of this arc. It was fortuitous that in this example the position of the arc was stationary, while the radar sampled the region only a few km away. The photometer field of view was larger (2°) than the EISCAT beam, and both are represented in the figure. The temporal variations measured by both radar and photometer over a 3 minute interval are shown in Fig. 42. Because of the larger field of view of the photometer (middle panel), it registered the optical variations (about 1-2 per second) during the 30 s represented in Fig. 41, whereas EISCAT measured very low electron densities (top panel) and high electric fields (bottom panel). Although it might appear from the electron density plot that the high electric fields occurred between two arcs, this was not the case. The TV images show that an arc element (here labelled 'arc 3') formed in the radar beam, moved slightly north, where it remains as shown in Fig. 41, then moved back southward into the beam for approximately 1 minute. The high fields were therefore measured on the poleward side of this arc, which was embedded in a southward background field (Lanchester, Kaila, McCrea).

An auroral model has been developed which can simulate different types of auroral events. It has as input a neutral atmosphere and an electron flux and energy distribution of the precipitating electrons. Using an electron transport model it computes the degraded electron spectra, folding in the ion chemistry, either time dependently or in steady state. The resulting height profiles of ionization rate, electron density and photon emission rates can be compared with the measured values, and the model then iterates on these parameters. The resulting values of energy flux, measured in the narrow and bright arcs, are extremely large. With the excellent images of the optical features in the radar and photometer fields of view, it is possible to investigate the difference in response time of the optical signatures of the aurora, which are prompt, and the radar measured densities, which are determined by the time dependent continuity equation. The rate of change of electron density is controlled by the time history of the ionization function, as well as the loss rate. Depending on the production function used, the delay between the optical and radar response, seen here to be greater than 1 second, can be explained, Fig. 43 (Lanchester).

A systematic survey of the data-base from EISCAT common-programmes CP-1 and CP-2 and from the Finnish network of all-sky cameras has indicated all occasions where a simple auroral arc, or the boundary of an omega band, has drifted steadily through the EISCAT beam. The E-region electron concentration centred at 110 km was measured directly by EISCAT while the vector of electric field at one height in the F region was determined directly from tristatic measurements of plasma velocity. In addition, the strength of the electric field at different heights along the EISCAT beam was estimated by measuring the ion frictional heating, and making the appropriate corrections for neutral velocity and non-Maxwellian ion-velocity distribution. When the EISCAT beam was pointing away from the direction of the local magnetic field the variation of electric field with height could be mapped down to a reference height of 110 km. The relative horizontal locations of all measured parameters at this height were normalised with respect to the leading edge of the drifting arc or the boundary of

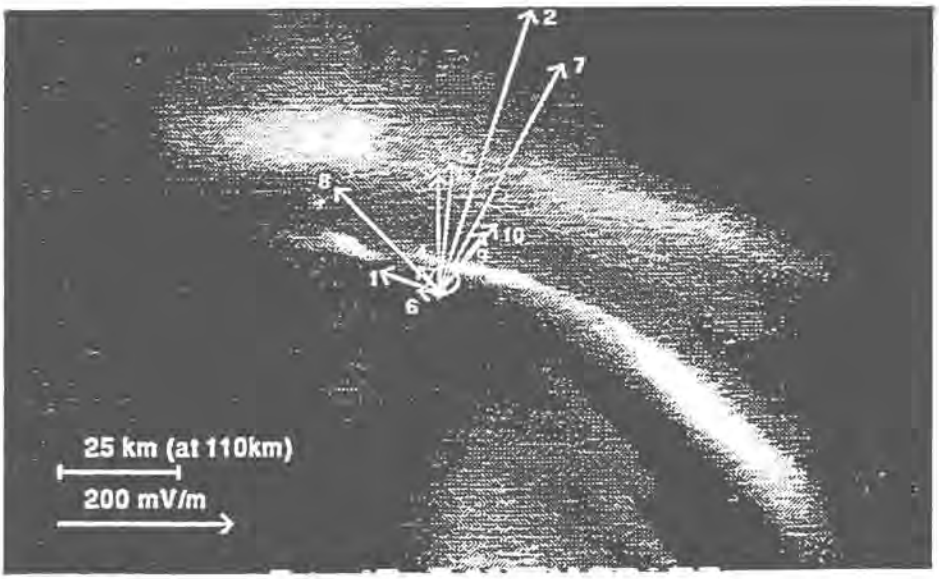

Fig. 41. Field of view of narrow angle camera looking field-aligned at Tromsø at 21:24:39 UT. The radar position is shown at the source of the electric field vectors. These are 3s measurements during the 30s of activity along the length of the arc from 21:24:30 to 21:25:00 UT. The larger circle is the photometer field of view.

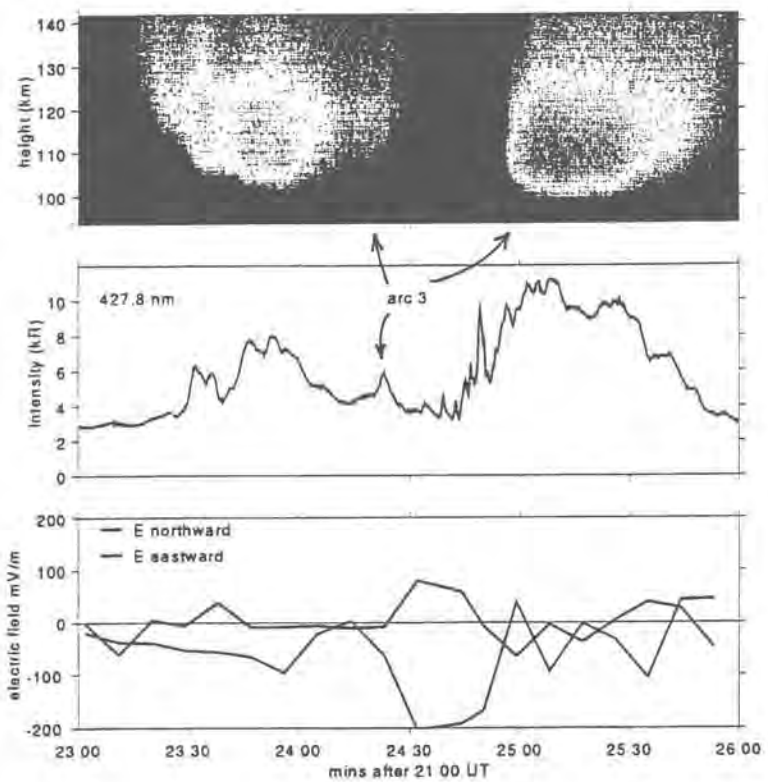

Fig. 42. EISCAT electron density profiles at 0.2 s resolution with maximum density greater than 10^{12} m^{-3} (top panel). Photometer measurements with wider field of view than EISCAT, showing the fast temporal variation at 21:24:30 in 'arc 3' (middle panel). Horizontal electric field measurements at 9 s resolution (bottom panel).

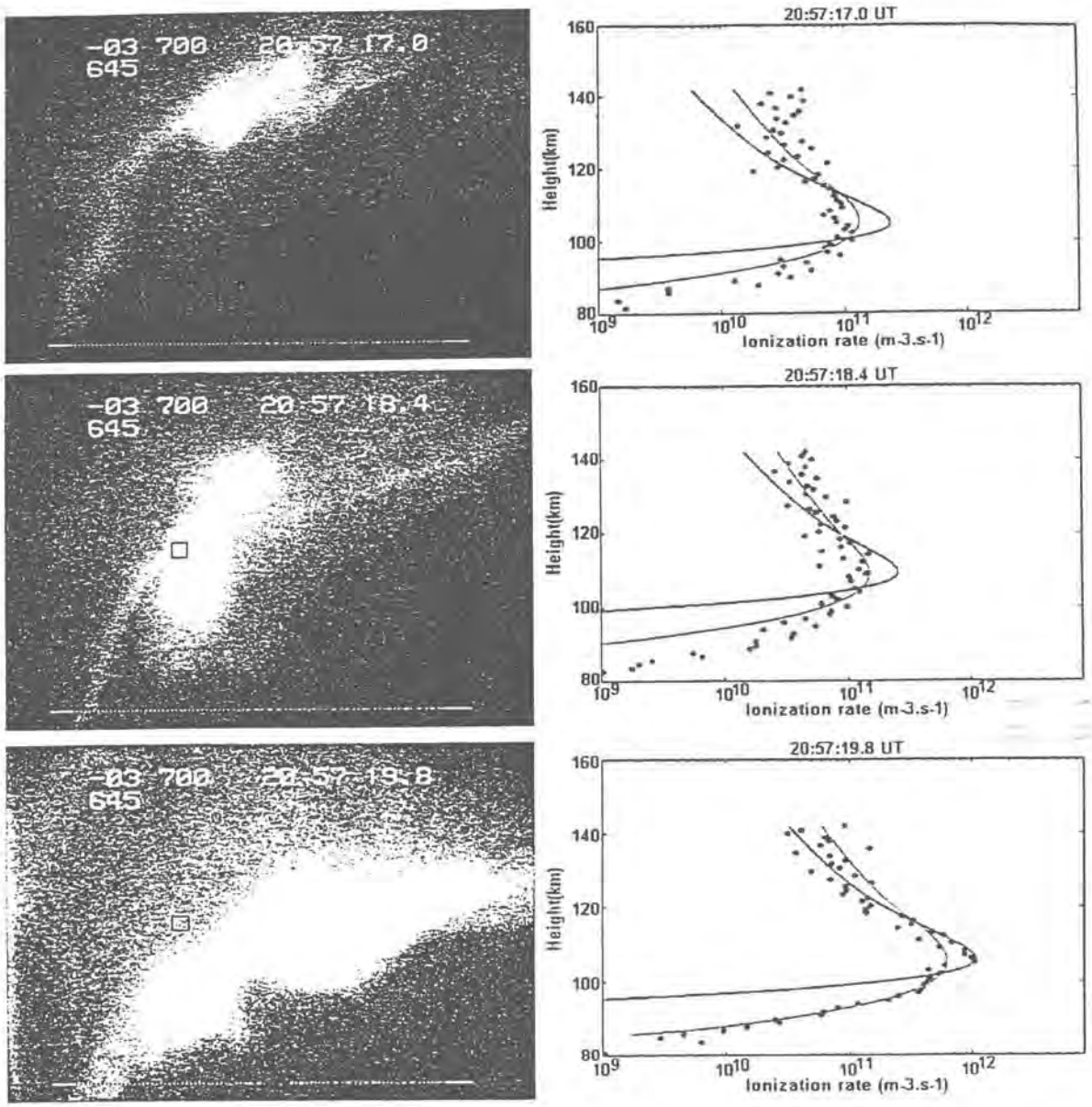

Fig. 43. Figure made up of three images from the narrow angle camera, each 1.4s apart. Beside these are fits between the observed plasma profiles and modelled results. The sequence shows a narrow arc element moving into the radar beam (marked with a box) between 17.0 and 18.4s after 20:57 UT, and on through the radar beam by 19.8s. The corresponding plasma profiles do not respond until more than a second after the instantaneous production of light, and it can be seen that the shape of the profile changes from a Maxwellian fit to a mono-energetic fit, as the energy flux increases from 25 mWm^{-2} to 100 mWm^{-2} in this instance.

the omega band. In the case of auroral arcs, a band of enhanced electric field and reduced electron concentration was always observed on one side of the arc, offset from the arc in the direction opposite to the prevailing convection field. This pattern is consistent with a double-layer of field-aligned currents completing a circuit through the region of depleted electron concentration and low conductivity adjacent to the arc. A similar pattern is observed near the boundaries of omega bands (Fig. 44).

In most cases the drift velocity of the arc or omega-band boundary was approximately equal to the average component convection velocity perpendicular to the arc or the boundary, but in a few cases, co-inciding with the onset of auroral activity, these velocities were very different. The selection of quiet features drifting steadily over EISCAT tended to exclude most examples occurring near substorm onset, which might explain this result (Williams et al.).

The study of Taylor et al. (1994) employed EISCAT flow vectors in conjunction with data from four other radars and three digisondes to study the ionospheric response to the extreme solar wind conditions during the 20-21 March 1990 magnetic storm. This study demonstrated that the ionospheric response to a change in the IMF z-component at the subsolar magnetopause propagates at a higher velocity from the dayside to the nightside when the magnetosphere is also subjected to a pressure pulse from the solar wind (Fig. 45). This study was extended by Taylor (1994) to measure response times as a function of MLT to a southward turning of the IMF at the subsolar magnetopause at 1314 UT on 20-21 March 1990, during an interval of constant solar wind pressure. In this study ionospheric response times measured by radars were compared with response times deduced from ground magnetometer measurements. Response times ranging from ~20 minutes post midday to ~60 minutes near midnight were measured. In addition to data from 103 magnetometer stations, 5 radars, three digisondes and DMSP polar orbiting satellites, EISCAT velocity measurements for 21 March 1990 were included in the input data to calculate the northern polar ionospheric convection electric field employing the AMIE procedure. The results suggest a delay of order 20- 40 minutes between the onset of a substorm expansion phase and the loss of open flux resulting from tail reconnection.

A substorm sequence, driven by a period of exceptionally large southward IMF, has been studied using EISCAT in CP-4-B mode along with a wide variety of other data. The observations revealed that the convection reversal boundary was poleward of the poleward edge of the UV aurora in both the growth and late expansion phases, showing that the open-closed field line boundary is also poleward of it. Evidence from the Goose Bay radar and EISCAT suggests that the commencement of field-line closure in the tail is after substorm onset and the EISCAT and IMAGE data reveal a separate electric field and current system poleward of the main substorm electrojet and over Spitsbergen. Fig. 46 shows that a small electric field spike was seen to move polewards in both the ion temperatures seen by EISCAT and the magnetic deflections seen by IMAGE at the time when poleward flow, consistent with field line closure, was seen to begin near dusk by the Goose Bay radar. Subsequently a broader band of enhanced electric field was seen to migrate equatorwards. Cross correlation of the radar data from the two VHF beam directions and of the magnetometer deflections showed that both features are moving east, away from midnight at 2.5 kms^{-1}. Enhanced flows

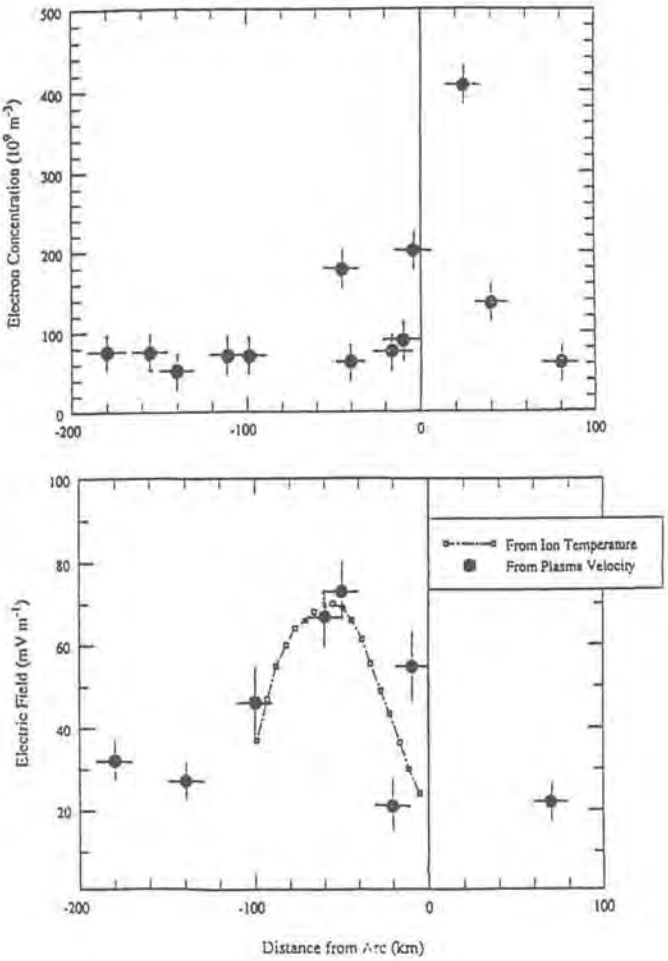

Fig. 44. Distribution of electric field strength and electron concentration in the vicinity of an auroral arc.

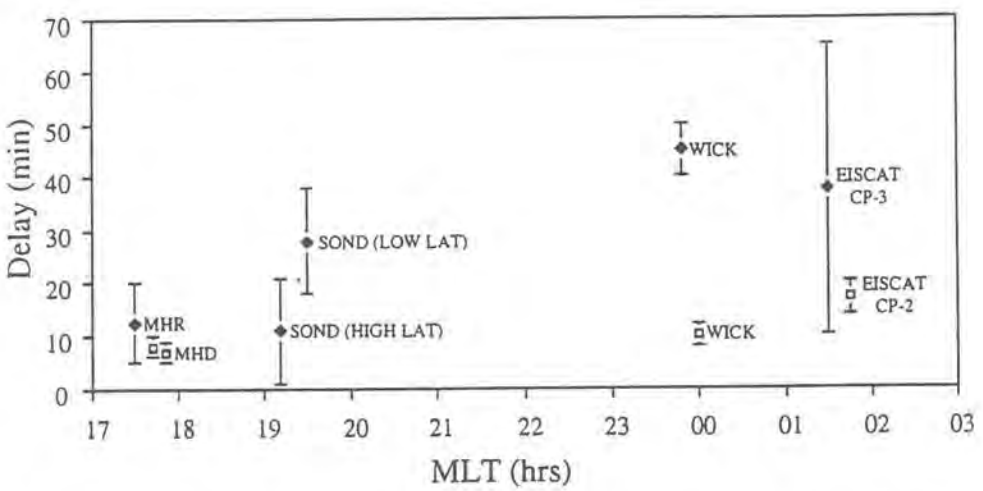

Fig. 45. Response times to changes at the subsolar magnetopause to a southward turning studied by Lester et al. (1993) at 22:22 UT (solid diamond plot symbol); and the southward turning associated with the SSC at 22:43 UT on 20 March 1990 (box symbol), with Millstone Hill radar (MHR) and digisonde (MHD), Sondrestrom (Sond) low and high latitude observations, Wick and EISCAT.

were seen for a considerable time after the expansion phase and the observed convection reversals migrated anti-sunward. The implication is that during this substorm cycle, the polar cap expanded sunward of its equilibrium position and flows were excited for an extended period while it relaxed back towards it.

A number of previous studies have shown that dayside ions can reach the substorm onset region. Previous work has also confirmed the build up of ions prior to onset. A recent study was aimed at establishing an experimental link between oxygen outflow on the nightside and oxygen injections into the magnetosphere as observed by a fortuitous pass of the CRRES satellite.

The study presented combined observations by the EISCAT radar, all-sky cameras and the CRRES satellite shortly before and during a substorm. In particular, a discrete equatorward-drifting arc was seen several degrees poleward of the onset region. The arc passed through the field-aligned beam of the radar and was seen to be associated with a considerable outflow of ionospheric plasma. During the substorm, CRRES observed two major injections 17 minutes apart, the second of which was dominated by O^+ ions. The study showed that the arc was in the required location in both latitude and MLT to have fed O^+ ions into the second injection and that the upward flux of ions associated with it was sufficient to explain the injection event. The interpretation was arcs in the nightside plasma

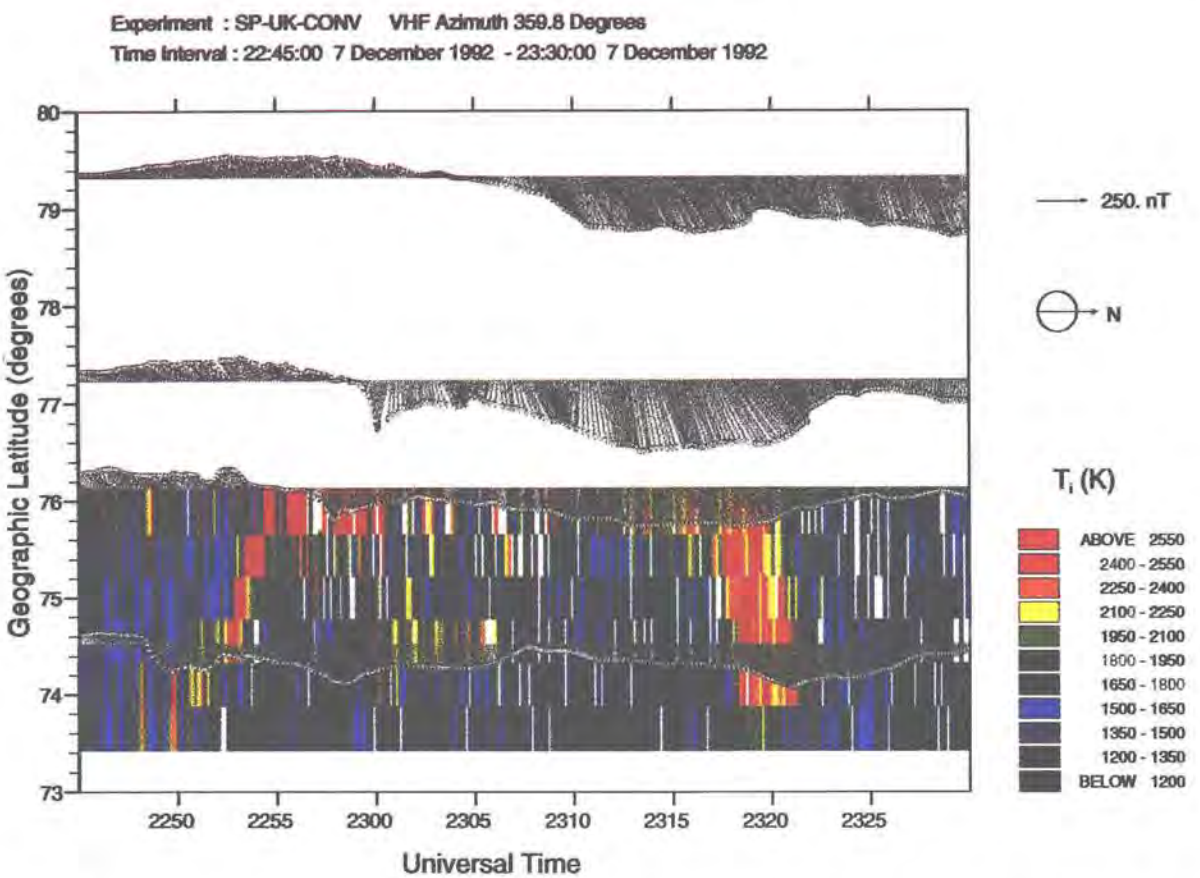

Fig. 46. EISCAT observations of ion temperatures and magnetic perturbations detected by local IMAGE magnetometers on Svalbard, observed in a major multi-instrument study of a substorm during the second Earth fly-by of the Galileo satellite. The data reveal a separate electric field and current system poleward of the main substorm electrojet.

sheet boundary layer are likely to be the source of O^+ ions energised by a dipolarisation of the mid- and near-earth tail, as opposed to ions ejected from the dayside ionosphere in the cleft ion fountain. The cleft ion fountain cannot, however, be ruled out as an important ion source, because the unusually long growth phase in this event would have allowed time for ions from the cleft to reach the onset region. This would have implied reconnection at the distant neutral line prior to onset, however. Growth phase reconnection would not be required if the southward drifting arc were the O^+ source, since the arc was on closed field lines and would thus have had direct access to the onset region (Gazey, Lockwood, Grande, Perry, Smith, Coles, Aylward, Bunting).

A careful analysis of EISCAT data from rare observations when the initial substorm onset took place directly overhead of the radar has revealed characteristic differences in the energy of substorm precipitation during the early and later phases of the substorm expansion. Two examples of overhead substorm onsets have been identified, occurring within the field-aligned beam of the UHF radar. In both cases magnetometer data and auroral data confirmed the observations of the western portion of the substorm current wedge. In Fig. 47 are shown the EISCAT electron density data for one such example of an overhead onset, on January 27, 1992. As a comparison, Fig. 47 includes a corresponding example for EISCAT observations during the passage of a westward travelling surge (WTS). This WTS started to the east of EISCAT during a substorm on January 25, 1993. The corresponding magnetograms from two longitudinally displaced stations (Kilpisjärvi, KIL, about 100 km southeast of EISCAT and Kevo, KEV, about 200 km to the east) are also displayed. The magnetograms in Fig. 47 clearly reveal the difference in ionospheric current flow during the WTS event (positive Y and Z component excursions progressing from east to west) as produced by the southward directed portion of an ionospheric Hall current loop ahead of the westward travelling surge. During the overhead onset case no such features could be identified, thus the magnetic disturbances stem from a locally developing, rather than expanding, current system, giving a true picture of the temporal development (Olsson, Persson, Opgenoorth, Uzan).

Neutral Atmosphere

Neutral winds in the E region (N-S, E-W and vertical components) were calculated for the two long CP-2 campaigns of October 1992 and January 1993. The winds were derived using simultaneously measured ion-neutral collision frequency. The tidal parameters of the horizontal winds were compared with models. The vertical component was determined in two independent ways. During the disturbed day of the October campaign very large vertical winds were obtained. Such large values are not reproduced in any model. EISCAT neutral winds were also compared with measurements obtained by the WINDII interferometer on board the UARS satellite during co-ordinated campaigns. A very good agreement was obtained as shown in Fig. 48 particularly for the meridional component at 100 and 170 km. These comparisons are part of the validation processes of the WINDII green line winds (Lathuillere, Gault et al.).

In the F-region, previous work has shown that ground optical measurements of the meridional wind compare well with the meridional wind deduced from the EISCAT experiments. But some questions remain unanswered. For example, the wind deduced from the radar oscillates around the optically measured one.

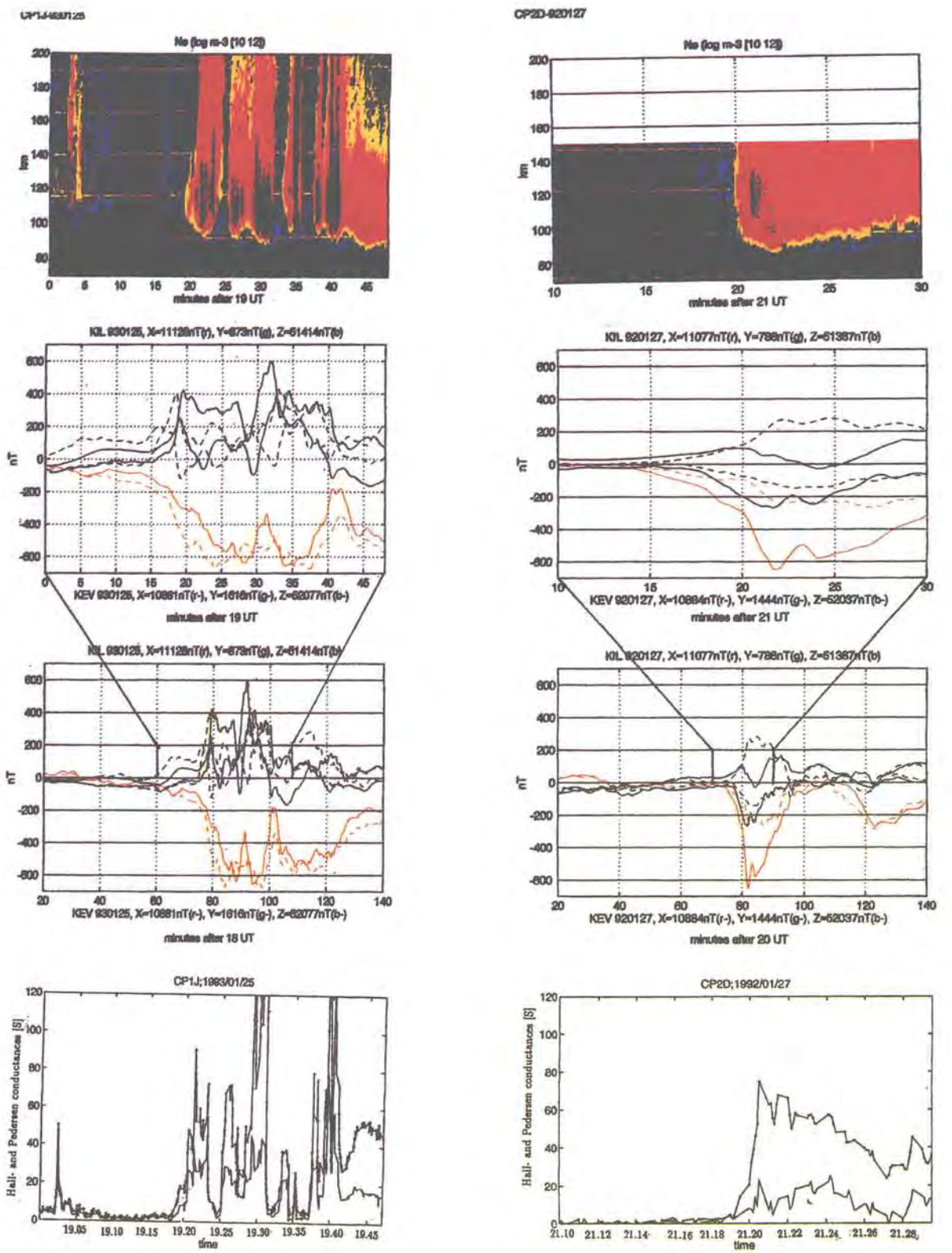

Fig. 47. Electron density in the E-region measured by EISCAT (top), nearby geomagnetic variations (centre two panels) and derived conductivities (bottom) for a local substorm onset (right column) and a westward travelling surge (left column).

Is this effect real, or due to ion drift effects not taken into account in the analysis of the radar data? What are really the amplitudes of the neutral atmosphere oscillations? To help answer these questions, the EISCAT deduced winds averaged over 2 hours were compared with different models; a very good agreement was found, giving good confidence in the EISCAT determination of the large scale wind (Lilensten and Lathuillere, 1995). Different EISCAT experiments were then analysed with various signal processing tools which showed that if some of the oscillations can be attributed to noise, a significant part of them can be related to gravity waves (Lilensten and Amblard). Finally, the EISCAT meridional wind was compared with the wind measured by the WINDII experiment using the red line emission. Again, the comparison was successful, showing that when oscillations are present in the EISCAT determination, the neutral atmosphere may well be oscillating also (Lathuillere, Lilensten, Gault, Thuillier).

CP-1 and CP-2 data from 10 years of operations have been analysed to determine the seasonal and solar cycle dependence of neutral densities and temperatures in the lower thermosphere. The results confirm earlier studies of the seasonal dependence but show, surprisingly, that winter temperatures decrease with increasing solar activity between 105 and 115 km altitudes. Summer temperatures, as expected, increase with solar activity (Fig. 49).

Work has continued on refining the determination of the O^+-O ion-neutral collision frequency using the EISCAT radar data and Fabry-Perot interferometers in Scandinavia. Having determined criteria for a better statistical evaluation of the significance of any result (Davis et al., 1995), refinements have been made to the analysis programs, and techniques revised, so that the complete joint database from 1981 to date (including Common Programme times when the FPIs were operating) is now being re-analysed. There is growing evidence that even for separations as small as 150 km there can be little or no correlation in vertical wind motions.

The INDI (Ion-Neutral Dynamics Investigation) work, comparing neutral winds derived from EISCAT with those measured directly by FPIs, continues, both developing the full statistical analysis described by Davis et al. (1995) and in a number of detailed studies looking at potential error sources in the FPI determinations. Besides the potential errors caused by insufficient knowledge of vertical winds and their horizontal scale sizes, other assumptions that have been examined include the effect of non-uniform emission in the viewing volume and the effects of partial cloud cover. EISCAT (averaged) data have been included in a study of the equinoctial asymmetry seen in the Kiruna FPI data to demonstrate a suggested mechanism due to different ion-neutral coupling patterns at the two equinoxes (Aruliah, Farmer, Rees, Steen, Fuller-Rowell, Wild, Hapgood).

Waves and Tides

Tides have been studied with the help of EISCAT using data from long runs. The fundamental 24-h tide was found in all four measured parameters, electron density, field-parallel ion velocity, ion temperature and electron temperature. In the electron density higher harmonics up to sixth order (4-hour period) have been detected. A remarkable result was the dominance of the terdiurnal tide in the temperature at E-region heights on various days as shown in Fig. 50. This finding is different from other observations of tides in the E-region and mesosphere at

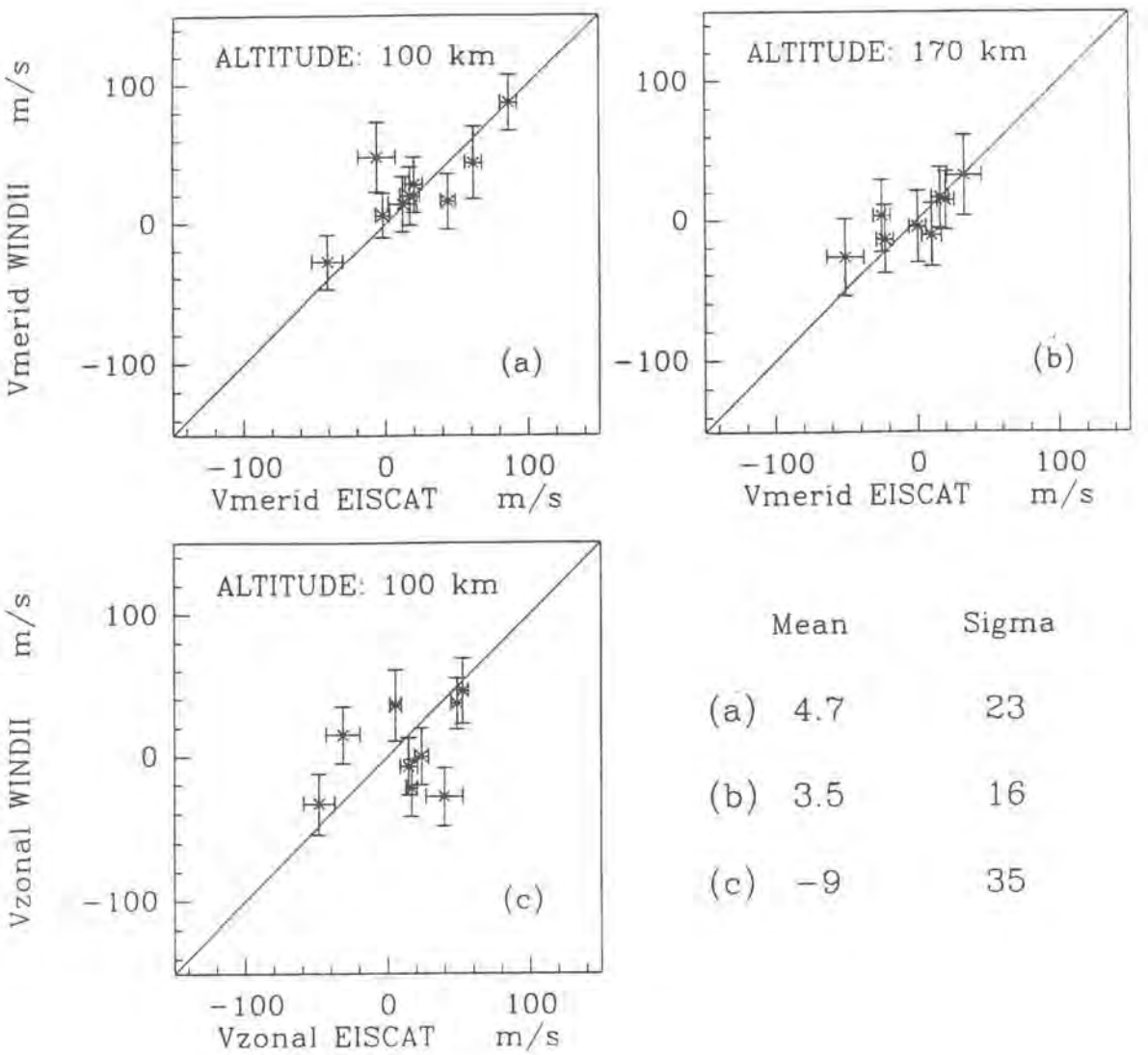

Fig. 48. Scatter plots for WINDII-EISCAT meridional (panels a and b) and zonal (panel c) winds comparisons. For each panel, the mean difference WINDII-EISCAT is indicated with its standard deviation.

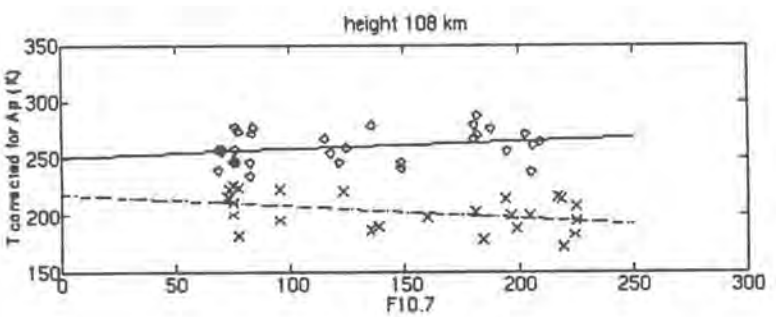

Fig. 49. Variation of daily average temperatures from EISCAT CP-1 and CP-2 experiments, at 108 km altitude, as a function of solar activity: o for summer, x for winter.

mid-latitudes where the semi-diurnal tide dominates (Hocke and Schlegel).

Atmospheric gravity waves are known to produce travelling ionospheric disturbances (TIDs) in the fundamental ionospheric parameters (i.e. electron density N_e, electron temperature T_e, ion temperature T_i, and ion drift velocity v_i). Gravity wave induced TID events from a digital filtering and frequency analysis of EISCAT CP-1 and CP-2 data have been compared with TIDs calculated by using a revised version of the quite realistic and compact model developed by Clark et al. (1971). The modelling of the TID and the underlying gravity wave takes into account a non-isothermal atmosphere and thermal conductivity, viscosity (by approximation) and ion drag as the general sources for gravity wave dissipation at thermospheric heights. The selected time ranges of EISCAT data correspond to magnetically very quiet conditions ($Kp < 2$) and low horizontal ion drift in order to avoid TID events induced e.g. by particle precipitation. An example of measurements and model results with respect to the electron density fluctuations is shown in Fig. 51. The wave period of this TID was estimated to $T = 50$ min. The model gives a good prediction of the tilting (forward propagation of phase) of the measured contours indicating a gravity wave caused TID. The density amplitudes agree quite well between 200 and 280 km whereas at greater heights the experimental values exhibit a stronger damping than the modelled values which is probably due to the imperfect modelling of the viscosity effects. The comparisons show that the model allows a quick check of the parameters of a gravity wave causing a measured TID (Hocke, Schlegel, Kirchengast). This model has also been used for parametric studies to explore the behaviour of gravity waves under a variety of conditions (Cierpka and Schlegel).

Topics like thermosphere-ionosphere weather modelling call for routine acquisition of information on important regional-scale phenomena in the upper atmosphere like AGWs and their ionospheric signatures, the TIDs. Measuring AGWs directly is difficult, however, so they are usually traced by the TIDs which can be routinely observed by IS radars like EISCAT even in all fundamental ionospheric parameters. Thus, an important problem is how to infer, as comprehensively as possible, AGW information from measured TIDs.

Kirchengast et al. (1995) introduced a new approach to AGW retrieval from TIDs: realistic modelling of AGW/TID physics, constrained by TIDs measured by the IS technique. The method was applied to several TID events in EISCAT data, which covered different seasons and solar activities during quiet magnetic conditions. It was found that the AGW-TID relationship can be quantitatively understood by means of careful physical modelling and that the method is capable of yielding comprehensive AGW information (the full polarization and dispersion information, i.e., amplitude and phase behaviour of AGW quantities and AGW wave-number vector and frequency). The method has further the potential to discriminate between TIDs from AGWs and non-AGW sources.

Fig. 52 shows, for an event considered, a comparison of TID modelling results, using the GIFTS model, and EISCAT data. Fig. 53 illustrates, for another event studied, the 'best-fit' agreement of model TID amplitudes with measured TID amplitudes and the corresponding amplitude and vertical wave-number profiles obtained for the associated AGW (using one more simple and one more elaborate AGW model). The method might be automated for routine processing of IS data with respect to AGWs, which could

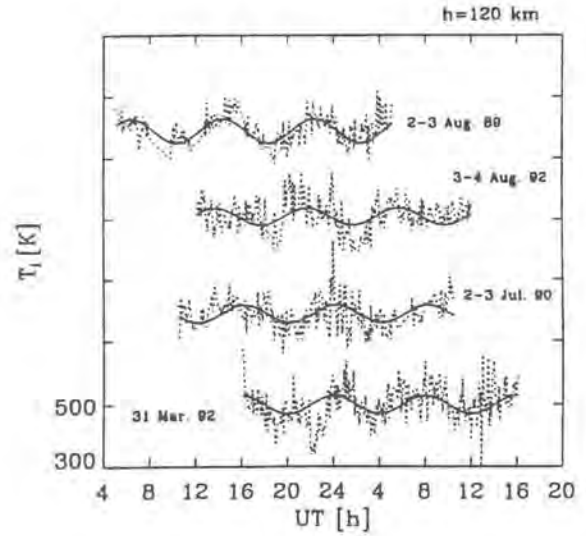

Fig. 50. Time series of ion temperature (dashed lines) in comparison with computed terdiurnal tides at 120 km altitudes for several days.

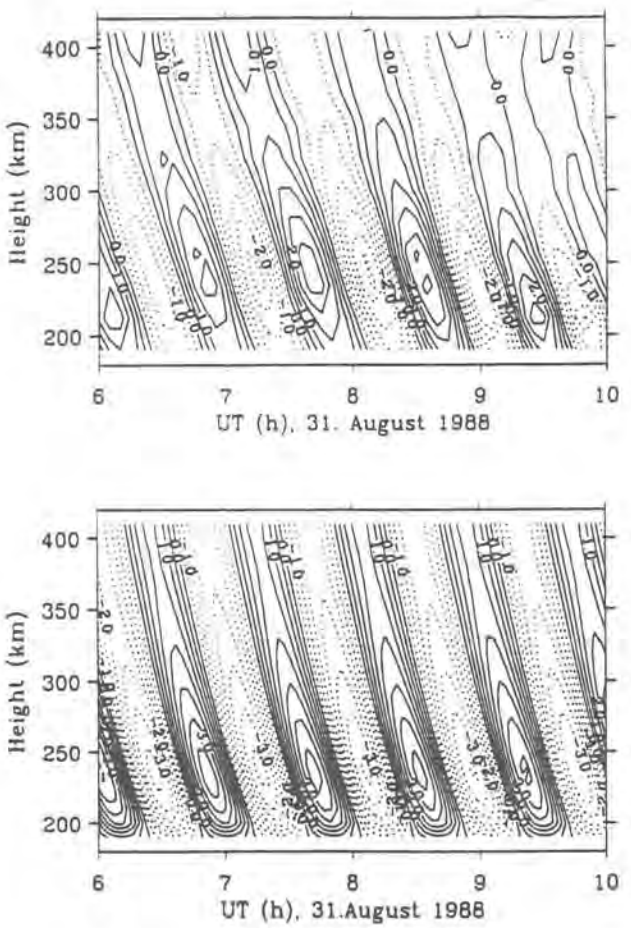

Fig. 51. Height-time amplitude contours of the TID quantity dNe/Ne_0 [%]. The modelled Ne-TID (lower panel) is compared with the Ne-TID in EISCAT data measured at August 31, 1988 (upper panel; bandpass filtered with a central period of 50 min.)

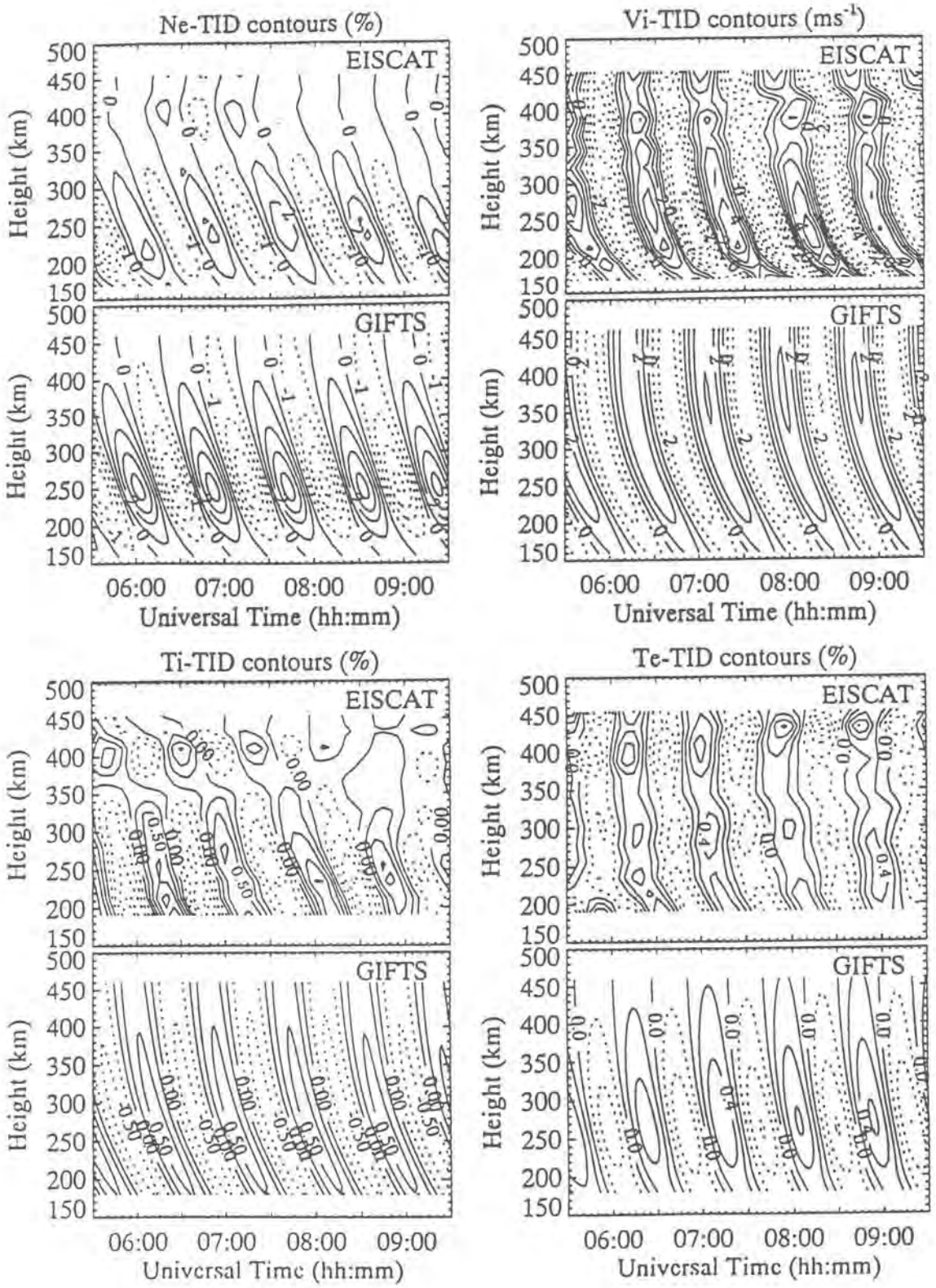

Fig. 52. One-to-one comparison of modelling results (labelled 'GIFTS') to EISCAT data (labelled 'EISCAT') for a TID event on August 31, 1988. Comparisons for the set of TID quantities (dNe/Ne_0, dVi, dTi/Ti_0, dTe/Te_0) are shown.

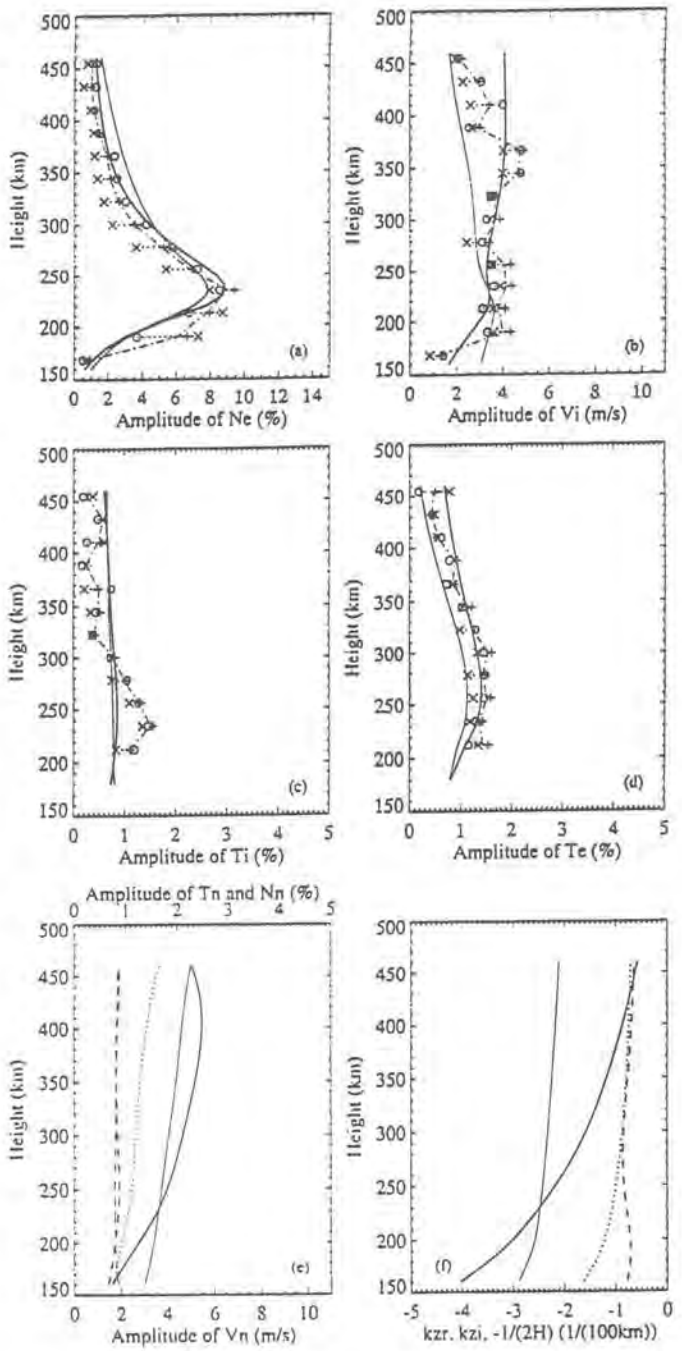

Fig. 53. Amplitude profiles illustrating an AGW/TID event on September 6, 1988. (a)-(d) Amplitude profiles of the TID set (dNe/Ne_0, dVi, dTi/Ti_0, dTe/Te_0) for a more simple (light solid lines) AGW model, a more elaborate (heavy solid lines) AGW model, and the experimental TID (dashed-dotted lines). In order to show that especially the quantities of the latter exhibit some variation around their mean (dashed-dotted) profile in the course of the event, amplitude profiles of three subsequent event sub-intervals are added in this case (o, +, x). *(e) Amplitude profiles of the corresponding AGW set (dV_n [solid lines], dNn/Nn_0 [dotted lines], dTn/Tn_0 [dashed lines]) for the simple (light lines) and elaborate (heavy lines) AGW model. (f) Real part, kzr (solid lines; light, simple AGW; heavy, elaborate AGW), and imaginary part, kzi (heavy dashed line; exists only for elaborate AGW), of the vertical AGW wave-number Kz, and the factor -1/(2H) (heavy dotted line; independent of AGW model).*

provide valuable AGW information for other research. Also, EISCAT could be used in future AGW Study campaigns to provide almost real-time information on AGW activity for the benefit of mid-latitude monitoring stations (Kirchengast, Hocke, Schlegel).

Mesosphere and D-region

A careful study of the main data-base of EISCAT observations of Polar Mesosphere Summer Echoes has demonstrated that the frequency of occurrence of PMSEs with time of day follows a semi-diurnal variation with minima at 8 and 20 h LT. PMSE layers observed for more than 30 minutes showed an average rate of descent of 2 kmh^{-1}. These characteristics suggest the influence of tidal winds. When the observed steady wind and diurnal and semi-diurnal tides at EISCAT were added, the overall magnitude showed a time-variation which matched the occurrence of PMSEs (Fig. 54), and the observed rate of descent, approximately 2 kmh^{-1}. Atmospheric gravity waves also contribute to the velocity of the neutral wind. When the wave reinforces the background wind, the PMSEs are stronger and descend more rapidly, but when the wave-related velocity opposes the background wind the PMSE is weaker and it descends more slowly (Williams et al., 1995; Palmer, Rishbeth, Jones, Williams).

PMSE have become well-known features of radar research of the high latitude middle atmosphere. These unusually strong echoes typically occur between the end of May and the middle of August at altitudes between 80 km and 90 km. They have been studied regularly with the EISCAT VHF and UHF radars. During recent years, doubts, expressed since the initial observations of the PMSE in the early 1980's, have been advanced that these echoes are not caused by intense active turbulence in the mesopause region. The assumption that layers of aerosols and ice particles, which form in the very cold polar summer mesopause, play the major role to increase the radar scatter cross section been supported by further radar as well as in-situ measurements with rockets and by new theories.

The EISCAT VHF radar can be used as an interferometer, since the antenna can be split into sectors. Radar interferometer measurements allow the study of details of the spatial structure of layer structures of scattering irregularities causing the PMSE. This permits discrimination between turbulent and stable laminar patterns in these layers, and is an essential criterion to test the assumption that the PMSE are not caused by classical turbulence scatter.

In Fig. 55 (upper panel) is shown a height-time-intensity diagram representing the temporal development of a thin PMSE layer. The initially stratified layer was lifted by about 500 m shortly before 09:40 UT. Thereafter it descended by about 1000 m during a short period of about 2 minutes, and then developed some kind of a cat's eye structure, which is typical for active turbulence. These observations indicate the existence of a thin and stable PMSE layer, which is turbulently disrupted by a Kelvin-Helmholtz Instability (KHI) occurring in the neutral atmosphere. The PMSE layer, detected here, is indisputably observed before the commencement of the KHI induced turbulence.

This interpretation is supported by the results of cross- spectral analyses, which are shown in the two lower panels of Fig. 55. The spectrogram in the centre panel shows a very narrow spectrum, which is consistent with remarkably weak turbulence. It also proves the vertical motion of the layer as seen in the upper

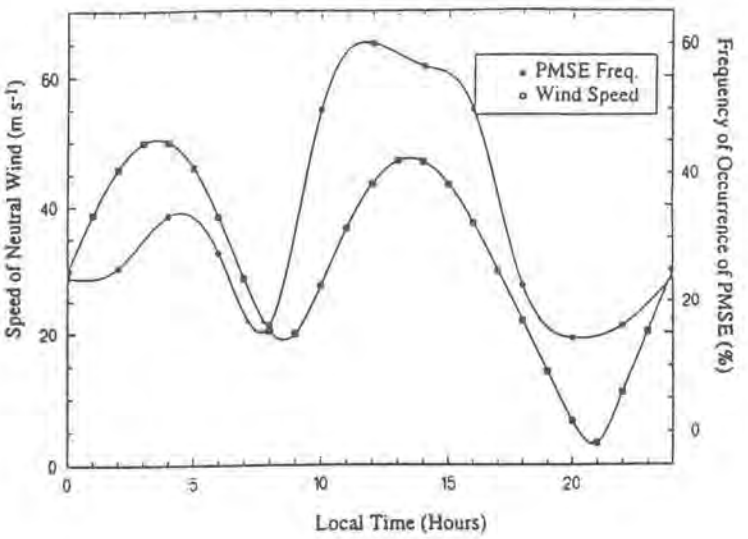

Fig. 54. Frequency of occurrence of PMSE and the magnitude of the neutral wind as functions of local time.

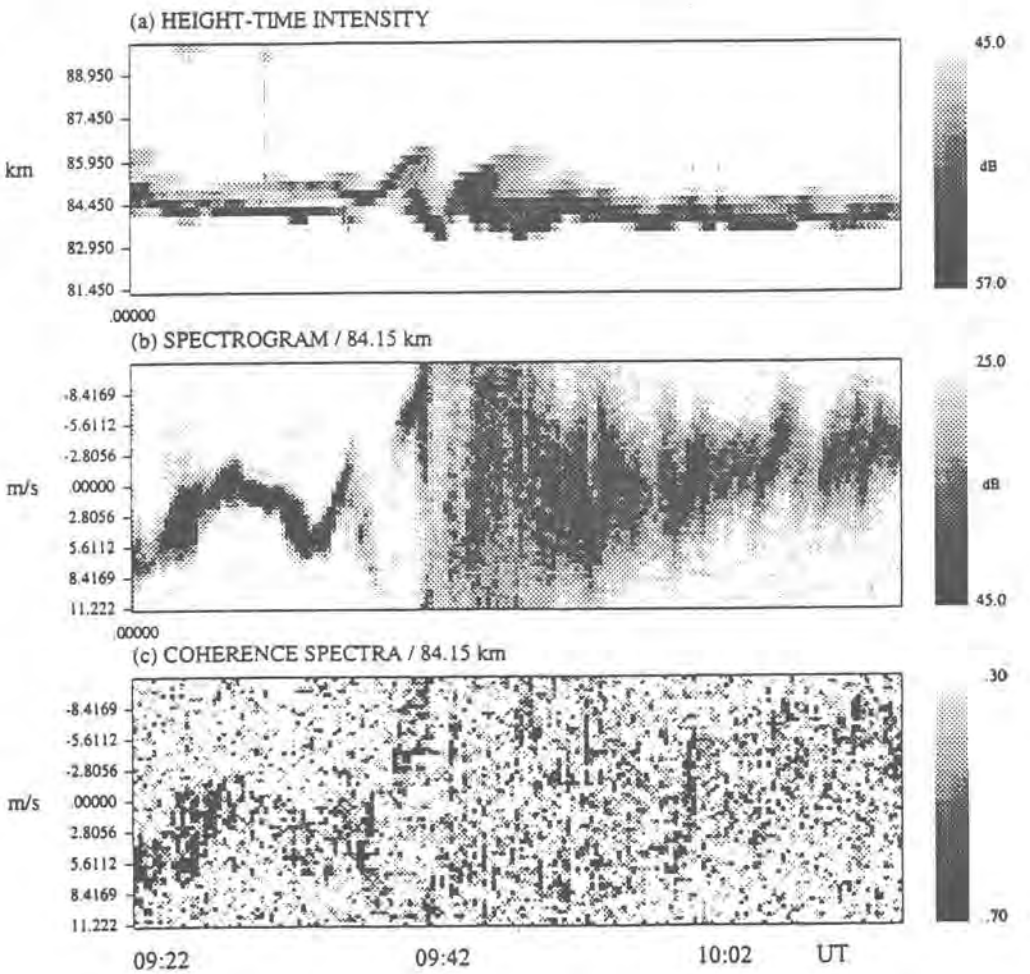

Fig. 55. Polar Mesosphere Summer Echoes observed with the EISCAT VHF Radar Interferometer on 16 June 1994.

panel. The spatial coherence, deduced with the interferometer technique and displayed in the lower panel, supports this finding: a high spatial coherence is consistent with a stable and stratified layer. Also the phase of the cross spectrum (not shown here) is consistent with this conclusion as well as with the observation (also by means of the spatial interferometer method) of a large change in the horizontal wind direction. When the PMSE layer is distorted by the KHI (around 09:40 UT), the spectrum gets dramatically widened and the spatial coherence becomes small. However, even after this turbulent break-up of the PMSE layer a high spatial coherence is still observed during short periods in certain narrow Doppler frequency bins.

These observations show that the PMSE layer pre-exists before active turbulence sets in. This turbulence just breaks the pre-existing layer into smaller pieces. The conclusion is that active turbulence is not the initial cause of the PMSE. The irregularities forming the layer are of different origin than active turbulence in the neutral atmosphere. The layering can for instance be due to accumulation of aerosols or the formation of sub-visible ice particles in cold areas resulting from long-period disturbances or waves in the mesopause region. These charged impurities, but not active neutral turbulence, initially cause the backscatter cross section for VHF radars to increase. The active turbulence further enhances the radar scatter cross section by stirring up such irregularities, but it does not appear to be the initial cause of the scattering irregularities (Röttger and Pan).

An imaging riometer (IRIS) was installed at Kilpisjärvi in August 1994 with the primary purpose of supporting EISCAT measurements of the D- and E-regions. IRIS data have been examined for interesting events during EISCAT's CP operations. Several of the CPs include D-region power profile measurements with sufficient height and time resolution to allow detailed investigations of variations in electron density. CP-6 is especially valuable because of the spectral measurements that it makes at mesospheric heights. Two case studies have been examined in detail: a localised, co-rotating daytime absorption event and a night-time substorm with an absorption spike at the onset. In both cases, important aspects in the interpretation of the EISCAT data and of the associated geophysical conditions would have been impossible without the simultaneous IRIS data. The daytime event was rather featureless as observed by conventional broad-beam riometer, but was shown to be a spatially confined region moving slowly through the EISCAT beam and actually co-rotating with the Earth (Fig. 56). The night-time substorm event was observed using both the EISCAT UHF and VHF radars, pointing in different directions. The onset was preceded by a weak arc-like absorption feature that reached the UHF beam but not the VHF, and the progression and development of the spike itself could be monitored through both radar beams. These observations took place in daylight, but displayed many analogies with the dynamical development of visible aurora during substorms: a drifting pre-onset arc, fading just prior to onset and a westward travelling intense feature at the onset itself (Collis and Hargreaves).

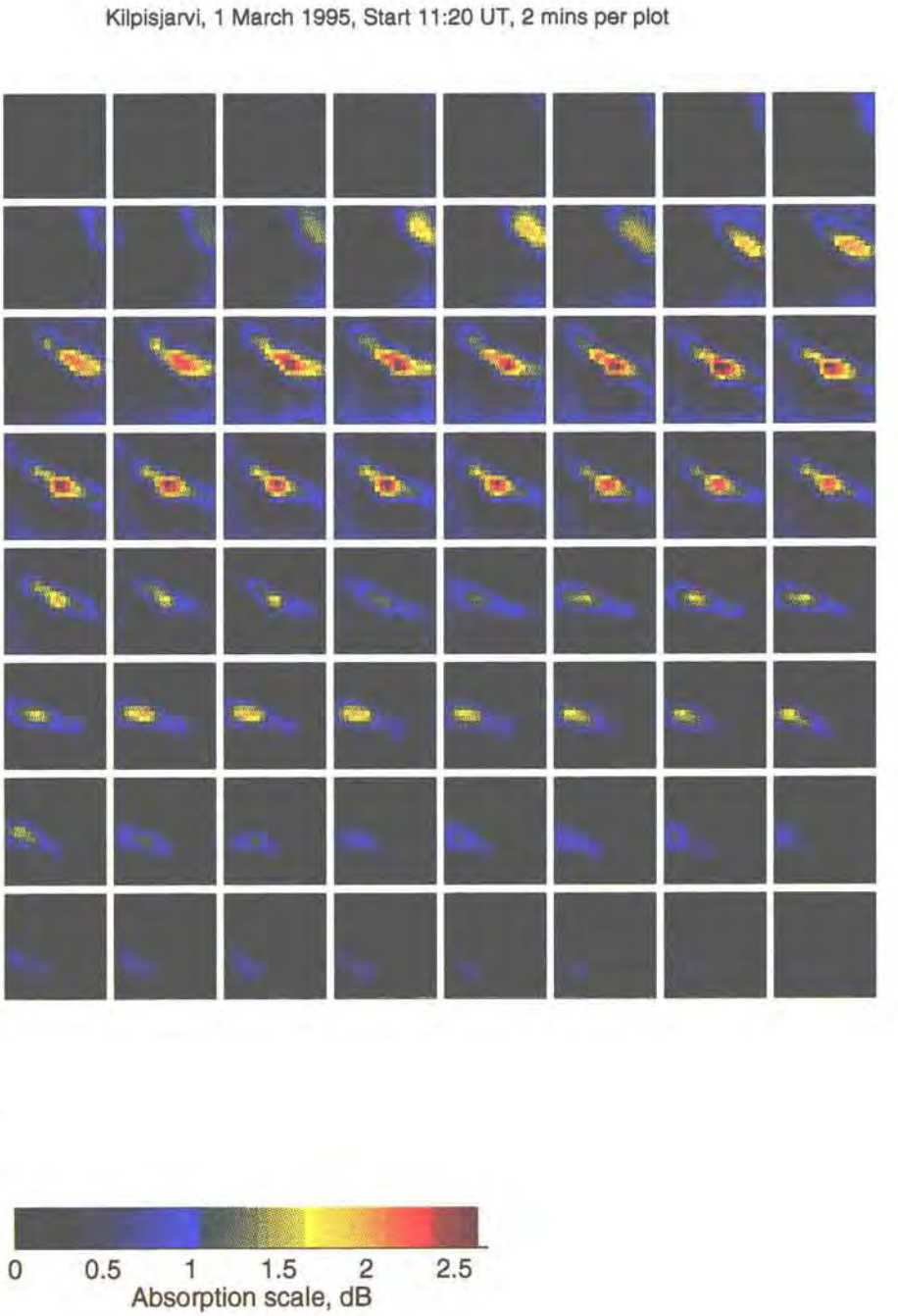

Fig. 56 (a). Horizontal distribution of radio absorption derived from the Kilpisjärvi IRIS observations on 1 March, 1995. Each plot extends over 240 km in both the N-S (vertical) and E-W (horizontal) directions by projecting each IRIS beam to 90 km altitude, looking down on the ionosphere. The top left image corresponds to 1050 UT; successive 2-min. averages run from left to right along each row, progressively from top to bottom. EISCAT's location is midway between the centre and the top left corner of each image. The absorption feature moved slowly equatorwards and westwards with respect to Kilpisjärvi from 11:30 UT onwards (the last image is 12:58-13:00 UT). As the local time span across the array is only 20 minutes, these observations indicate that the structure was effectively co-rotating with the Earth.

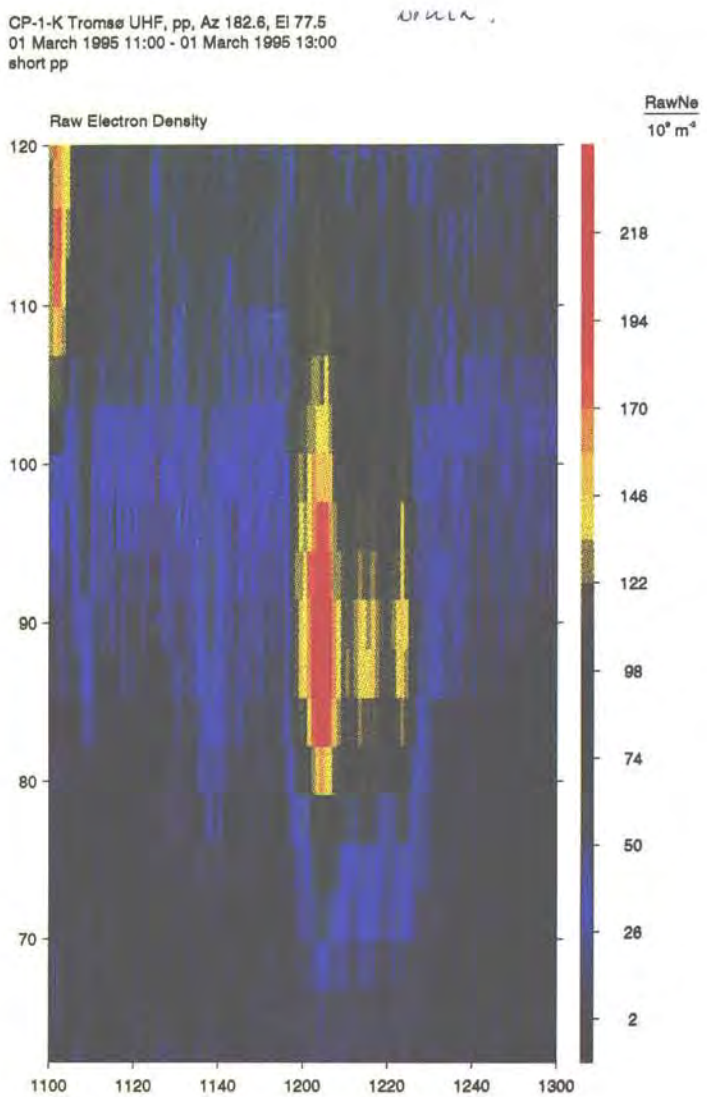

Fig. 56(b) Colour representation of EISCAT electron densities from CP-1 power profile measurements on 1 March 1995 as the absorption event shown in Fig. 56(a) crossed the radar beam. Note the low altitude of the peak (about 88 km) and that a density increase was seen even in the lowest range gate (62.2-65.3 km altitude), indicating the presence of electrons with energies of at least 300 keV.

PUBLICATIONS

Journals and Books, 1994

Blelly, P.-L. and D. Alcaydé, Electron heat flow in the auroral ionosphere inferred from EISCAT VHF observations, J. geophys. Res., 99, 13181-13188, 1994.

Blix, T.A., E.V. Thrane, S. Kirkwood and K. Schlegel, Plasma instabilities in the lower E-region observed during the DYANA campaign, J. atmos. terr. Phys., 56, 1853-1870, 1994.

Breen, A.R. and P.J.S. Williams, Theoretical model of electron density and electron temperature: comparisons with IRI and MSIS, Adv. Space Res., 14, (12)115-(12)118, 1994.

Brekke, A., S. Nozawa and T. Sparr, Studies of the E region neutral wind in the quiet auroral ionosphere, J. geophys. Res., 99, 8801-8825, 1994.

Collis, P.N., M.T. Rietveld and A.P. van Eyken, Dual-beam observations by the EISCAT radars during PMSE conditions, Adv. Space Res., 14, (9)149-(9)152, 1994.

Djuth, F., P. Stubbe, M.P. Sulzer, H. Kohl, M.T. Rietveld, J.H. Elder, Altitude characteristics of plasma turbulence excited with the Tromsø superheater, J. geophys. Res., 99, 333-339, 1994.

Fox, N.J., M. Lockwood, S.W.H. Cowley, M.P. Freeman, E. Friis-Christensen, D.K. Milling, M. Pinnock and G.D. Reeves, EISCAT observations of unusual flows in the morning sector associated with weak substorm activity, Ann. Geophys., 12, 541-553, 1994.

Gonzalez, N., A. Hauchecorne, S. Kirkwood, F.J. Lübken, A.H. Manson, A. Mourier, F.J. Schmidlin, R. Schminder, W. Singer and H.U. Widdel, Intercomparison of simultaneous remote and in situ wind measurements, J. Atmos. terr. Phys., 56, 1985-2001, 1994.

Hoppe, U.-P., T.A. Blix, E. Thrane, F.-J. Lübken, J.Y.N. Cho and W.E. Swartz, Studies of polar mesospheric summer echoes by VHF radar and rocket probes, Adv. Space Res., 14, 139-148, 1994.

Kersley, L. and S.E. Pryse, The development of experimental ionospheric tomography, Int. J. Image Syst. Technol., 5, 141-147, 1994.

Khudukon, B.Z., E.D. Tereshchenko, A.V. Galinov, A.A. Popov and T. Nygren, Determination of drift velocity and anisotropy of irregularities in the auroral ionosphere using radio source scintillation, J. atmos. terr. Phys., 56, 93-102, 1994.

Kimura, I., P. Stubbe, M.T. Rietveld, R. Barr, K. Ishida, Y. Kasahara, S. Yagtani and I. Nagano, Collaborative experiments by Akebono satellite, Tromsø ionospheric heater, and European incoherent scatter radar, Radio Sci., 29, 23-37, 1994.

Lanchester, B.S., J.R. Palmer, M.H. Rees, D. Lummerzheim, K. Kaila and T. Turunen, Energy flux and characteristic energy of an elemental auroral structure, Geophys. Res., Lett., 21, 2789-2792, 1994.

Lewis, R.V., P.J.S. Williams, G.O.L. Jones, H.J. Opgenoorth and M.A.L. Persson, The electrodynamics of a drifting auroral arc, Ann. Geophys., 12, 478-480, 1994.

Lockwood, M. and H.C. Carlson, Jr., Reply: ionospheric effects of transient magnetopause reconnection, Geophys. Res. Lett., 21, 2337-2338, 1994.

Lockwood, M., S.W.H. Cowley and M.F. Smith, Comment on "By fluctuations in the magnetosheath and azimuthal flow velocity transients in the dayside ionosphere" by Newell and Sibeck, Geophys. Res. Lett., 21, 1819-1820, 1994.

Lu, G., A.D. Richmond, B.A. Emery, P.H. Reiff, O. de la Beaujardiere, F.J. Rich, W.F. Denig, H.W. Kroehl, L.R. Lyons, J.M. Ruohoniemi, E. Friis-Christensen, H. Opgenoorth, M.A.L. Persson, R.P. Lepping, A.S. Rodger, T. Hughes, A. McEwin, S. Dennis, R. Morris, G. Burns and L. Tomlinson, Interhemispheric asymmetry of the high-latitude ionospheric convection pattern, J. geophys. Res., 99, 6491-6510, 1994.

Lühr, H. and K. Schlegel: Combined measurements of EISCAT and the EISCAT magnetometer cross to study Omega bands, J. geophys. Res., 99, 8951-8959, 1994.

Ma, Shu-ying, Xu Ji-sheng and K. Schlegel: Nonlinear evolution of TID's spectra in the auroral ionosphere, Chinese J. geophys. 36, 447-457, 1994.

Mishin, E.V. and K. Schlegel, On incoherent scatter plasma lines in aurorae, J. geophys. Res., 99, 11,391-11,399, 1994.

Moen, J., P.E. Sandholt, M. Lockwood, A. Egeland and K. Fukui, Multiple discrete arcs on sunward convecting field lines in the 14-15 MLT region, J. geophys. Res., 99, 6113-6123, 1994.

Opgenoorth, H.J., M.A.L. Persson, T.I. Pulkkinen, and R.J. Pellinen, The recovery phase of magnetospheric substorms and its association with morning-sector aurora, J. geophys. Res., 99, 4115-4129, 1994.

Pellinen-Wannberg, A., and G. Wannberg, Meteor observations with the European incoherent scatter UHF radar, J. geophys. Res., 99, 11 379-11390, 1994.

Persson, M.A.L., H.J. Opgenoorth, T.I. Pulkkinen, A.T. Eriksson, P.O. Dovner, G.D. Reeves, R.D. Belian, M. Andre, L.G. Blomberg, N.E. Erlandson, M.H. Boehm, A. Aikio, and I. Häggström, Near-Earth substorm onset; a co-ordinated study, Geophys. Res. Lett., 21, 1875-1878, 1994.

Peymirat, C. and D. Fontaine, Numerical simulation of the magnetospheric convection including the effect of field-aligned currents and electron precipitation, J. geophys. Res., 99, 11155-11176, 1994.

Peymirat, C. and D. Fontaine, Relationships between field-aligned currents and convection observed by EISCAT and implications concerning the mechanism that produces region 2 currents: Statistical study, Ann. Geophys., 12, 304-315, 1994.

del Pozo, C.F., Polarization electric field and Farley-Buneman instability during a precipitation event, J. atmos. terr. Phys., 56, 509-523, 1994.

Ranta, H., A. Ranta, P. Stauning, Z. Rapoport, S. Kirkwood, J. Lastovicka, A.K. Knyazev, Morphology of the D and E regions at high latitudes in the northern hemisphere during the campaign DYANA in 1990, J. atmos. terr. Phys., 56, 1933-1946, 1994.

Robinson, T.R., The role of natural E-region plasma turbulence in the enhanced absorption of high frequency radio waves in the auroral ionosphere: Implications for RF Heating of the auroral electrojet, Ann. Geophys., 12, 316-332, 1994.

Röttger, J., Polar mesosphere summer echoes: dynamics and aeronomy of the mesosphere, Adv. Space Res., 14, (9)123-(9)137, 1994.

Röttger, J., Middle atmosphere and lower thermosphere processes at high latitudes studied with the EISCAT radars, J. atmos. terr. Phys., 56, 1173-1195, 1994.

Röttger, J., STEP ground-based projects, in Solar-Terrestrial Energy Program; The Initial Results from STEP Facilities and Theory Campaigns, Proc. 199?, STEP Symposium/5th COSPAR Colloquium, Laurel, USA, ed. D.N. Baker, V.O. Papitashvili and M.J. Teague, Elsevier, 29-42, 1994.

Röttger, J., Solar proton events: a source for long-period gravity waves in the polar mesosphere, in Solar-Terrestrial Energy Program; The Initial Results from STEP Facilities and Theory Campaigns, Proc. 1992 STEP Symposium/5th COSPAR Colloquium, Laurel, USA, ed. D.N. Baker, V.O. Papitashvili and M.J. Teague, Elsevier, 473-476, 1994.

Sato, M., Y. Kamide, A.D. Richmond, A. Brekke and S. Nozawa, Regional estimation of electric fields and currents in the polar ionosphere, Geophys. Res. Lett., 22, 283-286, 1994.

Stubbe, P., A.J. Stocker, F. Honary, T.R. Robinson, and T.B. Jones, Stimulated electromagnetic emissions and anomalous HF wave absorption near electron gyroharmonics, J. geophys. Res., 99, 6233-6246, 1994.

Taylor, J.R., T.K. Yeoman, M. Lester, M.J. Buonsanto, J.L. Scali, J.M. Ruohoniemi and J.D. Kelly, Ionospheric convection during the magnetic storm of 20-21 March 1990, Ann. Geophys., 12, 1174-1191, 1994.

Widdel, H.-U., M. Bittner and U.-P. Hoppe, Vertical velocities measured at Biscarrosse (44N) and by EISCAT at Tromsø (66.9N) during the DYANA campaign, J. atmos. terr. Phys., 56, 1779-1796, 1994.

Williams, P.J.S., Movements in the ionosphere, J. atmos. terr. Phys, 56, 815-818, 1994.

Williams P.J.S., T.S. Virdi, G.O.L. Jones and A. Huuskonen, A comparison of three methods of measuring tidal oscillations in the lower thermosphere using EISCAT common programmes, J. atmos. terr. Phys., 56, 1347-1359, 1994.

Theses, 1994

Eglitis, P.E., Radar studies of small-scale E-region plasma irregularities, Ph.D. thesis, University of Leicester, UK, 1994.

Forme, F., Etude de la turbulence acoustique ionique observee dans l'ionosphere terrestre des hautes latitudes a partir du radar EISCAT, These de Doctorat de l'Universite Paris 6, France, 1994.

Freeman, K.S.C., Measurements of Joule heating in the auroral ionosphere. Ph.D. thesis, University of Wales, UK, 1994.

Gazey, N.G.J., Radar studies of auroral phenomena, Ph.D. thesis, University of Sussex, UK, 1994.

Hocke, K., Untersuchung des Phasen- und Amplitudenverhaltens von Travelling Ionospheric Disturbances mit Hilfe von EISCAT-Daten, Ph.D. thesis, University of Göttingen, Germany, 1994.

Lewis, R.V., Flow bursts in the auroral electrojet, Ph.D. thesis, University of Wales, UK, 1994.

Stalder, W., Radarbeobachtungen kuenstlich angeregter Langmuirinstabilitaeten in der Ionosphaere: Hoehenkorrelation und zeitliche Entwicklung, Diploma, Georg-August-Universitaet, Göttingen, Germany, 1994.

Taylor, J.R., The cause of magnetic disturbance in the Earth's ionosphere, Ph.D. thesis, University of Leicester, UK, 1994.

Proceedings, Reports, etc., 1994

Alcaydé, D., P-L. Blelly, and J. Lilensten, GIVEME: General Ionosphere Visualisation and Extraction from a Model for the EISCAT Svalbard Radar, EISCAT Technical Note, 94/52, 1994.

Bosinger, T. and L. Kalliopuska (eds), 3rd European Heating Seminar, Murmansk, Russia, May 24-26, 1994, Extended Abstracts, Report No. 125 (1994) Department of Physics, University of Oulu, Finland, 1994.

Brekke, A., EISCAT Svalbard Radar, in Proceedings of the joint Japanese-Norwegian Workshop on Arctic Research, University of Tokyo, 7-8 October 1993, STEL, Nagoya University, 55-64, 1994.

Bremer, J., W. Singer, D. Keuer, P. Hoffman, J. Röttger, J. Cho and W.E. Swartz, PMSE observations with EISCAT during summer 1991, in Proc. 6th Workshop on Technical and Scientific Aspects of MST Radar, Chung-Li, Taiwan, 1993, ed. B. Edwards. SCOSTEP Secret., Boulder, USA, 83-87, 1994.

Fox, N.J., M. Lockwood, S.W.H. Cowley, V.N. Davda, G. Enno, E. Friis-Christensen, R.A. Greenwald, M. Kivelson, M. Lester, H. Lühr, D.K. Milling, J.S. Murphree, M. Pinnock and G.D. Reeves, A comparison of Freja auroral images with substorm cycle observations, Proc. 2nd International Conference on Substorms, Fairbanks, Alaska, March 7-11, 1994, ed. by J.R. Kan, J.D. Craven and S.-I. Akasofu, Geophysical Institute, University of Alaska, Fairbanks, 421-428, 1994.

Goncharov, N.P., M.T. Rietveld, and J. Röttger, Creation of artificial periodic inhomogeneities for studies of the middle atmosphere and lower thermosphere, in Proc. 6th Workshop on Technical Aspects of MST Radar, Chung-Li, Taiwan, 1993, ed. B. Edwards, 436-440, 1994.

Kersley, L., D.L. Rice, C.D. Russell and C. Wilson, Observations of patches in the polar-cap ionosphere, Proc. Beacon Satellites Symposium, Aberystwyth, UK, 180-183, 1994.

Kirkwood, S. and U. von Zahn, Formation mechanisms for low-altitude sporadic-E layers - results from the METAL campaign, Proc. 11th ESA Symposium, Montreux, May 1993, ESA SP-355, 51-56, 1994.

Kofman, W., Propagation electromagnetique (1ere partie) (rapport CEPHAG n° 42) 1994.

Kofman, W. and J. Lilensten, EISCAT: Que cachent les aurores boréales?, Ciel et Espace, pp58-63, Décembre 1994.

Lockwood, M., Ionospheric signatures of pulsed magnetopause reconnection. in Physical signatures of magnetopause boundary layer processes, ed. J.A. Holtet and A. Egeland, NATO ASI Series C, Vol. 425, Kluwar, 229-243, 1994.

Mitchell, C.N., D.G. Jones, L. Kersley, S.E. Pryse and I.W. Walker, Imaging of field-aligned structures in the auroral ionosphere, Proc. Beacon Satellites Symposium, Aberystwyth, UK, 72-75, 1994.

Pan, C.J., C.H. Liu and J. Röttger, Refined method of frequency domain interferometry for the MST radar, in Proc. 6th Workshop on Technical Aspects of MST Radar, Chung-Li, Taiwan, 1993, ed. B. Edwards, 239-241, 1994.

Persson, M.A.L., A.T. Aikio and H.J. Opgenoorth, Satellite-groundbased co-ordination; Late growth and early expansion phase of a substorm, Proc. 2nd International Conference on Substorms, Fairbanks, Alaska, March 7-11, 1994, ed. by J.R. Kan, J.D. Craven and S.-I. Akasofu, Geophysical Institute, University of Alaska Fairbanks, 157-164, 1994.

Röttger, J., Scattering properties of mesopause irregularities causing PMSE at wide spatial scales, in Proc. 6th Workshop on Technical Aspects of MST Radar, Chung-Li, Taiwan, 1993, ed. B. Edwards, SCOSTEP Secret., Boulder, USA, 76-82, 1994.

Röttger, J., EISCAT stratosphere-troposphere experiment performance, in Proc. 6th Workshop on Technical Aspects of MST Radar, Chung-Li, Taiwan, 1993, ed. B. Edwards, SCOSTEP Secret., Boulder, USA, 340-345, 1994.

Röttger, J. and C. Alcala, Spatial interferometer applications to study PMSE and transient velocity features with the EISCAT VHF radar, in Proc. 6th Workshop on Technical Aspects of MST Radar, Chung-Li, Taiwan, 1993, ed. B. Edwards, SCOSTEP Secret., Boulder, USA, 289-293, 1994.

Röttger, J., U.G. Wannberg, A.P. van Eyken, and M T. Rietveld, The development of EISCAT as MST/ST radar, in Proc. 6th Workshop on Technical Aspects of MST Radar, Chung-Li, Taiwan, 1993, ed. B. Edwards, SCOSTEP Secret., Boulder, USA, 376-379, 1994.

Sato, M., Y. Kamide, A. Brekke and S. Nozawa, The altitude profile of ionospheric currents and conductivities deduced from EISCAT observations, Proc. NIPR Symp. Upper Atmos. Phys., 7, 18-25, 1994.

Yeoman, T.K., H. Lühr, R.W.H. Freidel, S. Coles, M. Grandé, C.H. Perry, M. Lester, P.M Smith, H.J. Singer and D. Orr CRRES/Ground-based multi-instrument observations of an interval of substorm activity. Proc. 2nd International Conference on Substorms, Fairbanks, Alaska, March 7-11, 1994, ed. by J.R. Kan, J.D. Craven and S.-I. Akasofu, Geophysical Institute, University of Alaska, Fairbanks, 627-633, 1994.

Aikio, A.T., G.T. Marklund, J. Woch and T. Potemra, Small scale structures in the high-altitude auroral electric field, Ann. Geophys., 13, 84-94, 1995.

Alcala, C., J. Röttger and M.C. Kelley, Spatial interferometry measurements of polar mesosphere summer echoes with the EISCAT VHF radar, Radio Sci., 30, 1205-1218, 1995.

Brekke, A., S. Nozawa and M. Sato, Samples of auroral E-region parameters derived from EISCAT experiments, J. geomag. Geoelectr., 47, 889-909, 1995.

Bremer, J., W. Singer, D. Keuer, P. Hoffman, J. Röttger, J.Y.N. Cho and W.E. Swartz, Observations of polar mesosphere summer echoes at EISCAT during summer 1991, Radio Sci., 30, 1219-1228, 1995.

Chisham, G., D. Orr, T.K. Yeoman, D.K. Milling, M. Lester and J.A. Davies, The polarization of Pc5 ULF waves around dawn: A possible ionospheric conductivity gradient effect, Ann. Geophys., 13, 159-167, 1995.

Collis, P.N., EISCAT data base for ionospheric modelling: F-region and topside ionosphere, Adv. Space Res., 16, (1)37-(1)46, 1995.

Davis, C.J., A.D. Farmer and A. Aruliah, An optimised method for calculating the O+ -O collision parameter from aeronomical measurements, Ann. Geophys., 13, 541-550, 1995.

Davies, J.A., M. Lester, B. Jenkins and R.J. Moffett, Dayside ion frictional heating: EISCAT observations and comparison with model results, J. atmos. terr. Phys., 57, 775-793, 1995.

Eglitis, P., T.R. Robinson, I.W. McCrea, K. Schlegel, T. Nygren and A.S. Rodger, Doppler spectrum statistics obtained from three different-frequency radar auroral experiments, Ann. Geophys., 13, 56-65, 1995.

Fontaine, D. and F. Forme, Ionospheric small-scale structures and turbulence inferred from EISCAT observations: a review, J. geomag. Geoelectr., 47, 869-878, 1995.

Forme, F.R.E., D. Fontaine and J. E. Wahlund, Two different types of enhanced ion acoustic fluctuations observed in the upper atmosphere, J. geophys. Res., 100, 14625, 1995.

Fritts, D.C. and U.-P. Hoppe, High-resolution measurements of vertical velocity with the European incoherent scatter VHF radar. 2: Spectral observations and model comparisons, J. geophys. Res. 100 16827-16838, 1995.

Fujii, R., S. Nozawa, M. Sato, N. Matuura, T. Ono, A. Brekke, C. Hall and T.L. Hansen, Comparison between electron spectra calculated from EISCAT electron density profiles and those observed by the DMSP satellites, J. geomag. Geoelectr., 47, 771-782, 1995.

Gavrilov, N.M., Distributions of the intensity of ion temperature perturbations in the thermosphere, J. geophys. Res., 100, 23835-23843, 1995.

Gazey, N.G.J., M. Lockwood, P.N. Smith, S.A. Coles, R.J. Bunting, M. Lester, and A.D. Aylward, The development of substorm cross-tail current disruption as seen from the ground, J. geophys. Res., 100, 9633-9648, 1995.

Hall, C., On the occurrence of Polar Mesosphere Summer Echoes, Geophys. Res. Lett., 22, 3469-3472, 1995.

Heaton, J.A.T., S.E. Pryse and L. Kersley, Improved background representation, ionosonde input and independent verification in experimental ionospheric tomography, Ann. Geophys., 13, 1297-1302, 1995.

Honary, F, A.J. Stocker, T.R. Robinson, T.B. Jones and P. Stubbe, Ionospheric plasma response to HF radio waves operating at frequencies close to electron gyroharmonics, J. geophys. Res., 100, 21489-21501, 1995.

Hoppe, U.-P. and D.C. Fritts, High-resolution measurements of vertical velocity with the European incoherent scatter VHF radar. 1: Motion field characteristics and measurement biases, J. geophys. Res., 100, 16813-16825, 1995.

Hoppe, U.-P. and D.C. Fritts, On the downward bias in vertical velocity measurements by VHF radars, Geophys. Res. Lett., 22, 619-622, 1995.

Kagan, L.M., E.N. Myasnikov, V.I. Kosolapenko, V.A. Kryazhev, V.A. Cheremnyj, and M.A.L. Persson, F-layer irregularities' formation at auroral latitudes: Radio wave scintillation and EISCAT observations, J. atmos. terr. Phys., 57, 917-928, 1995.

Kamide, Y. and A. Brekke, The importance of incoherent scatter radars in substorm studies, J. geomag. Geoelectr., 47, 813-822, 1995.

Kauristie, K., T.I. Pulkkinen, R.J. Pellinen, P. Janhunen, A. Huuskonen, A. Viljanen, H.J. Opgenoorth, W.J. Heikkila and D.N. Baker, Analysis of the substorm trigger phase using multiple ground-based instrumentation, Geophys. Res. Lett., 22, 2065-2068, 1995.

Kirchengast, G., K. Hocke and K. Schlegel: Gravity waves determined by modeling of travelling ionospheric disturbances in incoherent-scatter radar measurements, Radio Sci. 30, 1551-1567, 1995.

Kirkwood, S., J. Cho, C.M. Hall, U.-P. Hoppe,, D.P. Murtagh, J. Stegman, W.E. Swartz, A.P. van Eyken, U.G. Wannberg and G. Witt, A comparison of PMSE and other ground-based observations during the NLC-91 campaign, J. atmos. terr. Phys. 57, 35-44, 1995.

Kirkwood, S., H. Nilsson, J. Lilensten and M. Galand, Strongly enhanced incoherent scatter plasma lines in aurora. J. geophys. Res., 100, 21343-21356, 1995.

Kirkwood, S. and A. Osepian, Quantitative studies of energetic particle precipitation using incoherent scatter radar, J. geomag. Geoelectr., 47, 783-799, 1995.

Lathuillere, C., D. Fontaine, P. Gaimard and D. Hubert, Analysis of F-region incoherent scatter spectra during periods of high electric fields, J. geomag. Geoelectr., 47, 861-868, 1995.

Lester, M., M. Lockwood, T.K. Yeoman, S.W.H. Cowley, H. Lühr, R. Bunting and C.J. Farrugia, The response of ionospheric convection in the polar cap to substorm activity, Ann. Geophys., 13, 147-158, 1995.

Lilensten, J. and C. Lathuillere, The meridional thermosphere neutral wind measured by the EISCAT radar, J. geomag. Geoelectr., 47, 911-920, 1995.

Lockwood, M., Large-scale fields and flows in the magnetosphere-ionosphere system, Surveys in Geophysics, 16, 389-441, 1995.

Lockwood, M., S.W.H. Cowley, P.E. Sandholt and U.P. Løvhaug, Causes of plasma flow bursts and dayside auroral transients: an evaluation of two models invoking reconnection pulses and changes in the Y-component of the magnetosheath field, J. geophys. Res., 100, 7613-7626, 1995.

Lockwood, M., C.J. Davis, M.F. Smith, T.G. Onsager and W.F. Denig, The location and characteristics of the reconnection X-line deduced from low-altitude satellite and ground-based observations: 2. DMSP and EISCAT radar data, J. geophys. Res., 100, 21803-21814, 1995.

Lockwood, M. and H.J. Opgenoorth, Opportunities for magnetospheric research using EISCAT/ESR and CLUSTER, J. geomag. Geoelectr., 47, 699-721, 1995.

Lu, G., L.R. Lyons, P.H. Reiff, W.F. Denig, O. de la Beaujardiere, H.W. Kroehl, F.J. Rich, H. Opgenoorth, M.A.L. Persson, J.M. Ruohoniemi, E. Friis-Christensen, L. Tomlinson, R. Morris, G. Burns and A. McEwin, Characteristics of ionospheric convection and field-aligned current in the dayside cusp region, J. geophys. Res., 100, 11.845-11861, 1995.

Luo Yi, Chen Pei-ren and K. Schlegel, The observation on the ionospheric Hall conductivity in the auroral zone and its behaviour and E-region electron heating, Chin. J. Sp. Sci., 15, 273-279, 1995.

Mandeville, J.C., F. Riboni and P.-L. Blelly, Interpretation of EISCAT radar data for orbital debris study, Adv. Space Res., 11, 29-33, 1995.

Markkanen, M., M. Lehtinen, T. Nygrén, J. Pirttilä, P. Henelius, E. Vilenius, E.D. Tereshchenko and B.Z. Khudukon, Bayesian approach to satellite radiotomography with applications in the Scandinavian sector, Ann. Geophys., 13, 1277-1287, 1995.

Matuura, N., Mechanisms on the solar wind-magnetosphere interactions: importance of the Svalbard radar, J. geomag. Geoelectr., 721-733, 1995.

Matuura, N., R. Fujii, Y. Kamide, S. Kokubun and T Oguti, Japan-EISCAT collaboration on the Svalbard radar: scientific significance, J. geomag. Geoelectr., 681-684, 1995.

McCrea, I.W., G.O.L. Jones, and M. Lester, The BEAN experiment - an EISCAT study of ion temperature anisotropies, Ann. Geophys., 13, 177-188, 1995.

Mitchell, C.N., D.G. Jones, L. Kersley, S.E. Pryse and I.K. Walker, Imaging of field-aligned structures in the auroral ionosphere, Ann. Geophys., 13, 1311-1319, 1995.

Moen, J., P.E. Sandholt, M. Lockwood, W.F. Denig, U.P. Løvhaug, B. Lybekk, A. Egeland, D. Opsvik, and E. Friis-Christensen, Events of enhanced convection and related dayside auroral activity, J. geophys. Res., 100, 23917-23934, 1995.

Morelli, J.P., R.J. Bunting, S.W.H. Cowley, C.J. Farrugia, M.P. Freeman, E. Friis-Christensen, G.O.L. Jones, M. Lester, R.V. Lewis, H. Luhr, D. Orr, M. Pinnock, G.D. Reeves, P.J.S. Williams and T.K. Yeoman, Radar observations of auroral zone flows during a multiple-onset substorm, Ann. Geophys., 13, 1144-1163, 1995.

Nozawa, S. and A. Brekke, Studies of the E region neutral wind in the disturbed auroral ionosphere, J. geophys. Res., 100, 14717-14734, 1995.

Pellinen, R.J., T.I. Pulkkinen, A. Huuskonen, K. Kauristie, W.J. Heikkila, H.J. Opgenoorth and M. Pudovkin, The trigger phase of magnetospheric substorms, Geomag. Aeron. (English version), 34, 725-730, 1995.

Robineau, A, P.-L. Blelly, D. Alcaydé and J. Fontanari, Plasma transports in the ionosphere, EISCAT-VHF observations and numerical models, J. geomag. Geoelectr., 47, 847-859, 1995.

Robinson, T.R., F. Honary, A.J. Stocker and T.B. Jones, Factors influencing the heating of the auroral electrojet by high power radio waves, Adv. Space Res., 15, (12), 1241-1244, 1995.

Röttger, J. and T. Tsuda, Studies of the polar middle and lower atmosphere by an MST radar on Svalbard, J. geomag. Geoelectr., 47, 929-942, 1995

Röttger, J., U.G. Wannberg and A.P. van Eyken, The EISCAT Scientific Association and the EISCAT Svalbard Radar Project, J. geomag. Geoelectr., 47, 669-679, 1995.

Sato, M. and Y. Kamide, Estimate of global and regional distributions of ionospheric electrodynamic quantities from EISCAT radar and ground magnetometer data, J. geomag. Geoelectr., 47, 759-770, 1995.

Sato, M. and Y. Kamide, A.D. Richmond, A. Brekke and S. Nozawa, Regional estimates of electric fields and currents in the polar ionosphere, Geophys. Res. Lett., 22, 282-286, 1995.

Schlegel, K., EISCAT and the EISCAT data base - A tool for ionospheric modeling (E- and D-region), Adv. Space Res., 16, (1)147-(1)154, 1995.

Shibata, T., K. Inoue and K. Schlegel, Ion composition in the lower F-region inferred from residuals of ion temperature profile measured with the EISCAT CP1 experiments, J. geomag. Geoelectr. 47, 879-888, 1995.

Weiss, L.A., P.H. Reiff, H.C. Carlson, E.J. Weber, M. Lockwood and W.K. Peterson, Flow-aligned jets in the magnetospheric cusp: results from the GEM pilot programme, J. geophys. Res., 100, 7649-7660, 1995.

Westman, A., T. Leyser, G. Wannberg, and M. Rietveld, Tristatic EISCAT-UHF measurements of the HF modified ionosphere for low background electron temperatures, J. geophys. Res., 100, 9717-9728, 1995.

Williams, P.J.S., A multi-antenna capability for the EISCAT Svalbard radar, J. geomag. Geoelectr., 47, 685-698, 1995.

Williams, P.J.S. G.O.L. Jones, J.R. Palmer and H. Rishbeth, The association of polar mesosphere summer echoes with tidal modes, Ann. Geophys., 13, 454-457, 1995.

Yahnin, A., E. Titova, A. Lubchich, T. Bosinger, J. Manninen, T. Turunen and T.L. Hansen, Dayside high latitude magnetic impulsive events: Their characteristics and relation to the sudden impulses, J. atmos. terr. Phys., 57, 1569-1582, 1995.

Theses, 1995

Aikio, A., Studies on the electrodynamics of the auroral oval, Doctoral thesis, University of Oulu, Finland, 1995.

Fox, N.J., Ionospheric convection during substorms, Ph.D. thesis, Imperial College, London, UK, 1995.

Palmer, J.R, Plasma density variations in the aurora. Ph.D. thesis, Southampton University, UK, 1995.

Pellinen-Wannberg, A., Auroral and meteor applications of the EISCAT incoherent scatter radar, Ph.D. thesis, IRF Scientific Report 225, Sweden, 1995.

Proceedings, Reports, etc., 1995

Gamet, Ph., L'ionosphere aurorale: Comparaison de methodes d'analyse des donnees EISCAT et etude des performances des programmes d'integration, Rapport de stage DEA AGTS et fin d'etude Sup-Aero, Universite Paul Sabatier - Toulouse III, 1995.

Goumault, P., Calcul du vent meridional a partir des donnees d'EISCAT, Rapport de stage, CEPHAG, 1995.

Lathuillere, C., Inter comparison between wind and temperatures measurements by WINDII (O^1S) observations and EISCAT incoherent scatter radar, in Proc. Workshop on Wind Observations in the Middle Atmosphere, 15-18 Nov., 1994, CNES-HQ, Paris, session 2, paper 2, 1995.

Osepian, A., S. Kirkwood and N. Smirnova, Effective recombination coefficients in the D and E regions during auroral absorption events, ESA-SP 370, 263-268, 1995, Proc. 12th ESA Symposium, Lillehammer, May 1995.

Poulenard, O., Realisation d'un logiciel de visualisation EISCAT-ESR, CLUSTER, Rapport de stage d'Ecole d'Ingenieur E.S.I., CETP, 1995.

Rietveld, M. and L. Kalliopuska (eds), 4th European Heating Seminar, Ramfjordmoen, Norway, May 16-19, 1995, Extended Abstracts, Report No. 126 (1995) Department of Physics, University of Oulu, Finland, 1995.

Röttger, J., Incoherent scatter radar measurements of middle atmosphere winds, in Proc. Workshop on Wind Observations in the Middle Atmosphere, 15-18 Nov., 1994, CNES-HQ, Paris, session 1, paper 6, 1995.

Smirnova, N., S. Kirkwood and A. Osepian, Anomalous E-region ion layers in twilight conditions, experiment and model, ESA-SP 370, 269-272 1995, Proc. 12th ESA Symposium, Lillehammer, May 1995.

Svenes, K. and J Moen, Opportunities for correlated ground and satellite observations during the NISSE mission, ESA SP-370, 279-284, 1995.

Søraas, F., K. Aarsnes, J. Bjordal, J. Stadsnes, K. Måseide, M. Smith and U.P. Løvhaug, PULSAUR II: Rocket and ground-based measurements in pulsating aurora, Proc 12th ESA Symposium on rocket and balloon programmes and related research, 29 May- 1 June 1995, Lillehammer, Norway, ESA SP-370, 233-238, 1995.

Thuiller, G. and C. Lathuillere, La participation Francaise a UARS: Etudes specifiques et validation des observations, Rapport quadriennal 91-94 du CNFGG, 1995.

Supplement, 1993
(Journal publications)

Grassmann, V., The effect of different collision operators on EISCAT´s standard data analysis model, J. atmos. terr. Phys., 55, 567-571, 1993.

Grassmann, V., An incoherent scatter experiment for the measurement of particle collisions, J. atmos. terr. Phys., 55, 573-576.

Haerendel, G., S. Buchert, C. La Hoz, B. Raaf and E. Rieger, On the proper motion of auroral arcs, J. geophys. Res., 98, 6087-6099, 1993.

Khudukon, B.Z., E.D. Tereshchenko and V.M. Semenov, A VHF incoherent scatter receiving station at the Russian Polar Geophysical Institute: the current status and a brief description, J. atmos. terr. Phys., 55, 559-566, 1993.

Lester, M, A.J. Coates, R.A. Harrison, D. Rees, J.G. Roederer, M.J. Rycroft, and M.A. Saunders, International solar terrestrial energy programme and the UK participation, Surveys Geophys. 14, 555-583, 1993.

Rinnert, K., A case study of the reaction of the auroral atmosphere to local energy inputs, J. atmos. terr. Phys., 55, 615-622, 1993.

Shibata, T. and K. Schlegel, Vertical structure of AGW associated ionospheric fluctuations in the E- and lower F-region observed with EISCAT - a case study, J. atmos. terr. Phys., 55, 739-749.

Wannberg, G. The G2-system and general purpose alternating code experiments for EISCAT, J. atmos. terr. Phys., 55, 543-557, 1993.

EISCAT REPORTS AND MEETINGS

Reports 1994 - 1995:

EISCAT Annual Report 1993		
EISCAT Svalbard Radar	System Description Document	24 Feb. 1993 rev.: 20 Feb. 1994
EISCAT Meetings 94/18	Proceedings of the EISCAT Annual Review Meeting 1994	Oct. 1994
EISCAT Svalbard Radar	System Integration Document	25 Apr. 1995
EISCAT Technical Note 94/52	GIVEME: General Ionosphere Visualisation and Extraction from a Model for the EISCAT Svalbard Radar	D. Alcayde, P-L. Blelly and J. Lilensten

Brochure:

The EISCAT Svalbard Radar An evolutionary Step into EISCAT's Future		Second Edition May 1995

Meetings 1994:

COUNCIL	42nd meeting, 19/20 May	Copenhagen, Denmark
	43rd meeting, 28/29 Nov	Windsor, UK
SAC	46th meeting, 7/8 April	Copenhagen, Denmark
	47th meeting, 11/12 Oct	Paris, France
AFC	42nd meeting, 28/29 April	Tromsö, Norway
	43rd meeting, 20/21 Oct	Munich, Germany
EISCAT Annual Review and ESR Progress Analysis Meeting	4-7 March	Longyearbyen, Norway
ESR Mid-term Review Meeting (MRM)	14-17 June	Tromsö and Longyearbyen, Norway
ESR Software Project Group (ESPG)	2nd meeting , 13/14 May	Abingdon, UK
	3rd meeting, 25-28 Sept	Kiruna, Sweden

Meetings 1995:

COUNCIL	44th meeting, 22/23 May	Hamburg, Germany
	45th meeting, 27/28 Nov.	Paris, France
SAC	48th meeting, 2/3 April	Hamburg, Germany
	49th meeting, 7 Oct.	Corsica, France
AFC	44th meeting, 25/26 April	Tromsø, Norway
	45th meeting, 18/19 Oct.	Sodankylä, Finland
Long Term Planning Group (LTPG)	7/8 March	London, UK
	3/4 May	London, UK
Sub-committee on Restructuring	28/29 Sept.	Oslo, Norway

EISCAT Scientific Association

BALANCE SHEET 1994

As at 31.12.94

Values in SEK

Fixed Assets

	Book Value 31.12.93	Additions	Disposal	Depreciation	Book Value 31.12.94
KST					
Buildings	6 789 621			341 087	6 448 534
Tenancy	99 247	7 631	12 540	1 734	92 604
VSO	264 433			28 302	236 131
Transmitter	21 866 065	2 350 681		1 854 526	22 362 220
UHF Antenna	6 805 297			1 318 871	5 486 426
VHF Antenna	9 780 453			1 541 362	8 239 091
Computers	3 076 131	490 704		634 651	2 932 184
Vehicles	877 964			225 792	652 172
Office & Workshop	594 110	121 763		164 396	550 477
Instrumenation	1 056 624	8 011		402 053	662 582
	53 209 945	2 978 790	12 540	6 512 774	49 663 421
ESR					
Computers	694 623	205 276		99 396	800 503
Vehicles	196 640	224 156		39 328	381 468
Office & Workshop	64 413	417 977		13 191	470 199
Instrumentation	366 361	779 528	23 935	68 485	1 053 469
Transmitter	8 146 133	4 848 477			12 994 610
Antenna	6 186 884	22 683 041			28 869 925
Site Building	15 497 962	8 157 515			23 655 477
Testhall	179 677				179 677
Receiver		393 361			393 361
Data Acquisition		615 744			615 744
Controller		277 821			277 821
Peripheral		124 060			124 060
Housing		852 001			852 001
	31 332 693	39 578 957	23 935	220 400	70 667 315
KST + ESR Total	84 542 638	42 557 747	36 475	6 733 174	120 330 736

Current Assets

	Book Value 31.12.93	Book Value 31.12.94
EISCAT Total		
Debt. budget and uncalled contributions	1 108 763	
Site Advance	-1 303 976	539 018
Prepayments and accrued inc.	306 643	292 379
Consultant settlement account		-37 614
Petty Cash	1 000	1 659
Debtors:		
Value added tax	405 138	249 181
Others	21 050	75 442
Associate contribution		
Banks:		
Special Accounts	1 451 769	42 895
Ordinary Accounts	20 994 356	15 084 687
	22 984 743	16 247 647
Total Assets (Current + Fixed)	107 527 380	136 578 383

Capital and Liabilities

Capital

	1993	1994
Funds invested		
Pool	94 295 172	94 298 256
UHF Spare Klystron	671 814	3 019 411
Capital Operating	24 437 029	26 653 699
In Kind	25 123 200	25 123 200
Other	421 160	421 160
Heating	2 289 000	2 289 000
ESR	30 010 656	67 962 676
(gross)	177 248 031	219 767 402
Depreciation	-92 705 393	-99 436 666
(net)	84 542 637	120 330 736
Funds held on reserve		
Evolutionary Development fund	1 702 911	1 279 833
Evolutionary Interest fund	267 055	16 703
Klystron Fund	1 784 571	
Spare parts reserve	692 862	679 428
Capital Operating reserve	4 537 533	6 185 091
KST surplus previous year	2 463 169	990 651
ESR Construction Project Fund		
	11 548 101	9 151 706
Special Accounts	1 451 769	42 896
Total Capital	97 542 507	129 525 338

Liabilities

Liabilities		
Creditors	1 253 867	1 088 653
Provisions	688 700	999 607
Liability to Sites	-7 300	
Unused ESR-contribution	6 779 223	4 964 785
Liability to Associates	1 270 383	
	9 984 873	7 053 045
Total (Capital + Liabilities)	107 527 380	136 578 383

Values in MSEK

Recurrent Expenditure 1994

	Outcome	*Budget*
Personnel	11 678	*11 596*
Administration	5 172	*4 755*
Operation	4 284	*4 515*
Total (KST)	21 134	*20 866*
ESR Project	5 257	*4 450*

EISCAT Scientific Association

BALANCE SHEET 1995

As at 31.12.95

Values in SEK

Fixed Assets

	Book Value 31.12.94	Additions	Disposal	Depreciation	Book Value 31.12.95
KST					
Buildings	8 448 534			341 087	8 107 447
Tenancy	92 604	2 400		1 887	93 117
VSQ	236 131			28 302	207 830
Transmitter	22 362 220			2 005 497	20 356 723
UHF Antenna	5 486 426			1 318 871	4 167 554
VHF Antenna	8 239 091			1 541 362	6 697 729
Computers	2 932 184	184 152		654 467	2 461 869
Vehicles	652 172	320 880	119	107 204	747 260
Office & Workshop	550 477	391 372	59	108 049	775 213
Instrumenation	662 582	234 575		289 024	808 132
	49 662 421	1 133 379	177 175	6 395 749	44 222 875
ESR					
Computers	800 503	1 086 303		132 186	1 754 620
Vehicles	381 468			84 159	297 309
Office & Workshop	470 199	203 461	4 684	95 849	573 127
Instrumentation	1 053 469	15 021		224 391	844 098
Transmitter	12 994 610	625 794			13 620 404
Antenna	28 869 925	4 453 159			33 323 085
Site Building	23 655 477	1 466 592			25 122 069
Testhall	179 677			17 968	161 709
Receiver	393 361	346 544			739 906
Data Acquisition	615 744	849 550			1 465 293
Controller	277 821	22 974			300 795
Peripheral	124 060				124 060
Housing	852 001	1 023 217		85 200	1 790 018
	70 668 315	10 092 616	4 684	639 753	80 116 494
KST + ESR Total	120 330 736	11 225 995	181 859	7 035 503	124 339 369

Current Assets

	Book Value 31.12.94	Book Value 31.12.95
EISCAT Total		
Site Advance	539 018	1 004 842
Prepayments and accrued inc.	292 379	386 639
Consultant settlement account	-37 614	
Petty Cash	1 659	3 130
Debtors:		
Value added tax	249 181	545 397
Others	75 442	10 554
Associate contribution		5 559 436
Banks:		
Special Accounts	42 895	4 424 828
Ordinary Accounts	15 084 687	25 793 767
	16 247 647	37 728 596
Total Assets (Current + Fixed)	136 578 383	162 067 965

Capital and Liabilities

Capital

	1994	1995
Funds invested		
Pool	94 298 256	94 298 256
UHF Spare Klystron	3 019 411	3 019 411
Capital Operating	26 653 699	27 609 903
In Kind	25 123 200	25 123 200
Other	421 160	421 160
Heating	2 289 000	2 289 000
ESR	67 962 676	78 050 606
(gross)	219 767 402	230 811 538
Depreciation	-99 436 666	-106 472 169
(net)	120 330 736	124 339 369
Funds held on reserve		
Evolutionary Development fund	1 279 833	1 296 536
Evolutionary Interest fund	16 703	67
Klystron Fund		
Spare parts reserve	679 428	611 462
Capital Operating reserve	6 185 091	7 401 716
KST surplus previous year	990 651	
ESR Construction Project Fund		18 126 378
	9 151 706	27 436 159
Special Account CNRS	42 896	4 424 828
Total Capital	129 525 338	156 200 356

Liabilities

Liabilities		
Creditors	1 088 653	2 092 812
Provisions	999 607	447 011
Liability to Sites		
Unused ESR-contribution	4 964 785	
Associate contribution prepayment		3 327 787
	7 053 045	5 867 610
Total (Capital + Liabilities)	136 578 383	162 067 965

Values in MSEK

Recurrent Expenditure 1995

	Outcome	Budget
Personnel	12 176	*12 289*
Administration	5 314	*4 991*
Operation	4 012	*4 650*
Total (KST)	21 502	*21 492*
ESR Project	5 902	*6 695*

EISCAT SCIENTIFIC ASSOCIATION
Dec. 1994

	Finland	France	Germany	Norway	Sweden	United Kingdom
COUNCIL	J. Kangas A. Siivola	M. Aubry W. Kofman	G. Haerendel T. Hagfors M. Meinecke	A. Brekke* B. Benterud	B. Hultqvist J. Gustavsson	S.W.H. Cowley T.B. Jones R.L.T. Street
SAC	M. Lehtinen	D. Fontaine D. Alcaydé*	W. Baumjohann K. Rinnert	C. La Hoz	H. Opgenoorth	M. Lockwood P.J.S. Williams
AFC	E. Ikonen	D. Alloin *	C. Löw	A. Andersen	F. Karlsson	D.J. Morrell

SAC = Scientific Advisory Committee AFC = Administrative and Finance Committee * = Chairperson

EISCAT Senior Staff:

Director: J. Röttger (on secondment from MPG)
Deputy Director Technical: U. G. Wannberg
Deputy Director Science: A.P. van Eyken
Executive Assistant: H. Andersson

Site Leaders:
Kiruna: I Wolf
Sodankylä: M. Postila
Tromsø Radar: R. Jacobsen
Tromsø Heating: M. Rietveld

Non-Associate members of SAC were R. Fujii (Japan), J. Holt (USA) and P. Hoeg (Denmark)

EISCAT SCIENTIFIC ASSOCIATION
Dec. 1995

	Finland	France	Germany	Norway	Sweden	United Kingdom
COUNCIL	J. Kangas T. Turunen	M. Aubry W. Kofman	G. Haerendel T. Hagfors* M. Meinecke	A. Brekke B. Benterud	J. Gustavsson H. Opgenoorth	M. Lockwood T. B. Jones R.L.T. Street
SAC	M. Lehtinen	D. Fontaine D. Alcaydé	W. Baumjohann K. Rinnert	C. La Hoz	S. Kirkwood	M. Lockwood P.J.S. Williams*
AFC	E. Ikonen*	G. Leliévre	A.E. Röhr	A. Andersen	F. Karlsson	G. Brooks

SAC = Scientific Advisory Committee AFC = Administrative and Finance Committee * = Chairperson

EISCAT Senior Staff:

Director: J. Röttger (on secondment from MPG)
Deputy Director Technical: U. G. Wannberg
Deputy Director Science: A.P. van Eyken
Executive Assistant: H. Andersson

Site Leaders:
Kiruna: I Wolf
Sodankylä: M. Postila
Tromsø Radar: R. Jacobsen
Tromsø Heating: M.T. Rietveld

Non-Associate members of SAC were Y. Kamide (Japan) and A.D. Richmond (USA)

The front cover of this Annual Report shows a photo of the EISCAT Svalbard Radar

Annual Report 1994-1995 of the EISCAT Scientific Association

EISCAT Headquarters
P.O. Box 812, S-981 28 Kiruna, Sweden

Scientific contributions: EISCAT Associates and staff
Photos and graphics: Barlindhaug, EISCAT, NOTSA,
SGO, STEL, S.-E. Thunberg/Kvaerner-Kamfab
Editing and lay-out: EISCAT Headquarters (PNC, JR et al.)
Finishing and printing: IRF, Fabricii Kiruna

ISSN 0349-2710, July 1996

THE EISCAT ASSOCIATES

December 1995

SA
Suomen Akatemia
Finland

CNRS
Centre National de la Recherche Scientifique
France

MPG
Max-Planck-Gesellschaft
Germany

RCN
Research Council of Norway
(Norges forskningsråd)
Norway

NFR
Naturvetenskapliga forskningsrådet
Sweden

PPARC
Particle Physics and Astronomy Research Council
United Kingdom

From 1 April 1996:
NIPR
National Institute of Polar Research
Japan

EISCAT Scientific Association

HEADQUARTERS

EISCAT Scientific Association
Box 812
S-981 28 KIRUNA, Sweden
Phone +46-980-79153
Fax +46-980-79161
email: eiscat@eiscathq.irf.se

SITES

Kiruna

EISCAT
Swedish Institute of Space Physics
Box 812
S-981 28 KIRUNA, Sweden
Phone +46-980-79136
Fax +46-980-79161
email: eiscat@k2.irf.se

Sodankylä

EISCAT
Geophysical Observatory
FIN-99600 SODANKYLÄ, Finland
Phone +358-16-619880
Fax +358-16-610375
email: eiscat@sgo.fi

Tromsø

EISCAT
Ramfjordmoen
N-9027 RAMFJORDBOTN, Norway
Phone +47-776-92166
Fax +47-776-92380
email: eiscat@eiscat.no

Longyearbyen

EISCAT Svalbard Radar
P.O. Box 432
N-9170 LONGYEARBYEN, Norway
Phone +47-79 02 12 36
Fax +47-79 02 17 51
email: eiscat@esr.eiscat.no